MULTI-GNSS PRECISE POINT POSITIONING SOFTWARE ARCHITECTURE AND ANALYSIS OF GLONASS PSEUDORANGE BIASES

JOHN EGYIR AGGREY

A THESIS SUBMITTED TO THE FACULTY OF GRADUATE STUDIES
IN PARTIAL FULFILLMENT OF THE REQUIREMENTS FOR THE DEGREE OF
MASTER OF SCIENCE

GRADUATE PROGRAMME IN EARTH AND SPACE SCIENCE
YORK UNIVERSITY
TORONTO, ONTARIO

NOVEMBER 2014

Abstract

With expanding satellite-based navigation systems, multi-Global Navigation Satellite System (GNSS) Precise Point Positioning (PPP) presents an advantage over a single navigation system, which improves position accuracy and enhances availability of satellites and signals. The York GNSS PPP software was developed using C++ in the Microsoft.Net platform to utilize the existing multi-GNSS satellite constellations based on the software processor used by the Natural Resources Canada (NRCan) PPP online service. The software was built as a robust, scalable, modular tool that meets the highest of scientific standards compared to existing online PPP engines. There exists a correlation between receiver stations from heterogeneous networks, such as the IGS, in GNSS PPP processing and the increase in magnitude of the pseudorange and carrier-phase biases in both GPS + GLONASS and GLONASS-only PPP solutions. The correlation is due to mixed receiver and antenna hardware as well as firmware versions. Unlike GPS, GLONASS observations are affected by the Frequency Division Multiple Access (FDMA) satellite signal structure, which introduces inter-frequency channel biases and other system biases.

The GLONASS pseudorange inter-channel frequency biases show a strong correlation with different receiver types, firmware versions and antenna types. This research estimated the GLONASS pseudorange inter-frequency channel biases using 350 IGS stations, based on 32 receiver types and 4 antenna types over a period of one week. An improvement of 19% was observed after calibrating for the pseudorange ICBs, in the horizontal components respectively, considering a 20 minutes convergence period.

Acknowledgements

I thank God for His grace from the beginning of this thesis to the end.

I would like to express the deepest appreciation to my supervisor Professor Sunil Bisnath, who has shown the attitude and the substance of a great mentor. He continually and persuasively conveyed a spirit of adventure in regard to research and scholarship, and an excitement in regard to teaching. He kept a sense of humour when I had lost mine. Without his supervision and constant help this thesis would not have been possible.

I would also like to thank Professor Jian-Guo Wang, Professor Robert Allison and Professor Spiros Pagiatakis for serving as my Examination Committee members. I also want to thank them for allowing my defence be an enjoyable moment, and for their brilliant comments and suggestions. Professor Bisnath and Professor Wang served as my supervisory committee and my deep appreciation again goes to them.

Further appreciation is extended to NSERC for the financial support necessary to make this research possible. I acknowledge NRCan for the provision of the base PPP Fortran code.

I am also grateful for my family and fiancée for being there for me in so many ways with their support. It would have been impossible without you. Thanks so much.

Table of Contents

List of Tables

List of Figures

List of Acronyms

AC	Analysis Centers
ANTEX	Antenna Exchange Format
ASPRS	American Society for Photogrammetry and Remote sensing
C/A code	Coarse/Acquisition code
CDMA	Code Division Multiple Access
BeiDou	China's satellite system
CSRS-PPP	Canadian Spatial Reference System-Precise Point Positioning
DCB	Differential Code Bias
ECEF	Earth Centred Earth Fixed
FCB	Fractional Code Bias
FDMA	Frequency Division Multiple Access
Galileo	European satellite navigation system
GLONASS	Russian satellite navigation system
GNSS	Global Navigation Satellite System
GPS	Global Positioning System
GPST	GPS Time
ICB	Inter-frequency Channel Bias
IGS	International GNSS Service
IHO	International Hydrographic Organization
INS	Inertial Navigation System
IRC	Integer Recovery Clocks
ITRF	International Terrestrial Reference System
NRCan	Natural Resources of Canada
NRTK	Network RTK
ppm	parts per million
PPP	Precise Point Positioning
PPP-RTK	PPP and Real-Time Kinematic Integration
RF	Radio frequency
RHCP	Right Hand Circularly Polarized
RINEX	Receiver INdependent EXchange
RMS	root mean square
RTK	Real-Time Kinematic
S/N	Signal-to-noise Ratio
ZPD	Zenith path delay

Chapter 1
Introduction to GNSS Precise Point Positioning

Precise Point Positioning (PPP) is one of a handful of algorithmic techniques to estimate position and time using a Global Navigation Satellite System (GNSS) receiver. PPP processing requires the collection of observations from a single receiver through the process of trilateration to determine the axial coordinate components and time, while applying correction parameters such as atmospheric refraction delays, clock errors, earth rotation, code multipath, relativity, code biases, and noise.

In recent years, researchers, educators and engineers have adapted the PPP technique through modified and improved algorithms for various applications. PPP in commercial applications include precision farming in the agricultural industry, sensor positioning for seafloor mapping in marine applications, airborne mapping, land surveying, photogrammetry and remote sensing (Bisnath and Gao, 2007).

1.1 Brief Overview of GNSS and PPP

PPP is a standalone precise Global Positioning System (GPS) point positioning approach that uses un-differenced, dual-frequency pseudorange and carrier-phase observations along with precise satellite orbit and clock products to produce decimetre to sub-centimetre positioning in real-time and post-processing (Cai, 2009). Positioning techniques such as relative GPS positioning, Real-Time Kinematic (RTK) and Network RTK require the use of more than one

receiver. In contrast, PPP, as a cost-effective technique, requires a single user GNSS receiver with no additional local GNSS infrastructure, to achieve sub-centimetre horizontal and few centimetre vertical positioning accuracy. Static and kinematic data processing can be done using the PPP technique either in post-processing or real-time mode (Gao and Chen, 2005; Héroux *et al.*, 2004; Leandro, 2009).

Precise positioning and navigation becomes an asset in remote areas where reference stations are not available. In recent years, Collins *et al.* (2008) determined the plausibility of using real-time PPP technique in the determination and monitoring of seismic activities by resolving PPP non-integer ambiguities. By assessing the performance of PPP, it is possible to further extend to other scientific applications such as satellite clock error estimation, satellite pseudorange bias, pseudorange multipath estimation and ionospheric delay estimation (Leandro *et al.*, 2010). As more visible satellites and observations are made available by the advancement and modernization of various satellite constellations, a combined use of various satellite systems in PPP is expected to improve the positioning accuracy, reliability and solution convergence period.

Various satellite navigation constellations are in existence including GPS, GLONASS, BeiDou and Galileo. GPS was created and realized by the U.S. Department of Defense (DoD) and was originally operated with 24 satellites. It became fully operational in 1994. Each GPS satellite continuously transmits a microwave radio signal composed of two carriers, three to four codes, and a navigation message. GPS applies the code division multiple access (CDMA) principle, and as such, each GPS satellite emits a different Pseudo Random Noise (PRN) code. GPS was originally developed as a military system, but was made available to civilians as well. However,

to keep a military advantage, the U.S. DoD provides two levels of GPS positioning and timing services: the Precise Positioning Service (PPS) for military use and the Standard Positioning Service (SPS) for everyone (El-Rabbany, 2002). GPS is currently undergoing a system modernization which will result in the improvement of the performance of GPS services.

GLONASS is a radio-based satellite navigation system operated for the Russian government by the Russian Aerospace Defense Force. It complements and provides an alternative to GPS and is currently the only other fully-operational alternative navigation system in operation with global coverage and similar precision. Each satellite transmits the same PRN code but at different frequencies. GLONASS had achieved 100% global coverage with a full orbital constellation of 24 satellites. The GLONASS satellites' designs have undergone several upgrades, with the latest version being GLONASS-K (Reshetnev Company, 2010).

GALILEO is currently being built by the European Commission (EC) and European Space Agency (ESA). One aim of GALILEO is to provide a high-precision positioning system upon which European nations can rely on, independent from GPS and GLONASS that may be disabled in times of war or conflict. To achieve this independence, ten navigation signals have been defined in four frequency bands. To increase the reliability and capabilities of the signals, three different ranging codes will be used, namely the open-access ranging code, commercially encrypted ranging codes and government encrypted ranging codes. As with GPS, GALILEO's modulation scheme follows the CDMA principle (Hofmann-Wellenhof and Lichtenegger, 2008). Completion of the

30 satellite free service GALILEO system (27 operational + 3 active spares) is expected by 2019 (European Space Agency, 2011).

The Chinese government BeiDou navigation satellite system consists of five Geostationary Earth Orbit (GEO) and thirty Medium Earth Orbit (MEO) satellites transmitting on various ranges of carrier frequencies. The BeiDou ground segment consists of a master control station, upload station, and monitor station. BeiDou is intended to be compatible with GPS, GLONASS, and GALILEO receivers in terms of signal modulation and interoperability. Two kinds of services will be provided: an open service, designed to provide positioning accuracy within 10 metres, velocity accuracy within 0.2 metres per second and timing accuracy within 50 nanoseconds; and an "Authorized Service" which will also provide "safer" positioning, velocity, timing communication services, and integrity information for authorized users (Dou and O'Keefe, 2013).

Table 1.1 summarizes the major differences and similarities between the satellite navigation systems. The space segment is the main difference between the four navigation systems. GPS consists of 24 nominal active satellites in 6 orbital planes. GLONASS consists of 24 nominal satellites in three orbital planes. Galileo will consist of 30 satellites with 27 of them operational, and 3 as spare satellites spaced around the plane in three circular Medium Earth Orbit (MEO) orbital planes. BeiDou consists of 35 satellites including 5 Geostationary (GEO) satellites and 30 MEO satellites. GLONASS is different from the other navigation systems as each satellite transmits at its own frequency with the same code whereas GPS, Galileo, and BeiDou transmits at the same frequency but have different modulated codes.

Characteristics	GPS	GLONASS	GALILEO	BEIDOU
First launch	February 1978	October 1982	December 2005	April 2007
FOC	February 1995	January 1996 – December 2011	--	Up to 2020
Funding	public	public	public and private	public
Nominal SV number	24	24	27	27
Orbital planes	6	3	3	3
Orbital inclination	55°	64.8°	56°	55°
Semi-major	26,560 km	25,508 km	29,601 km	21,500 km
Orbital plane separation	60°	120°	120°	--
Revolution period	11h 57.96 min	11h 15.73 min	14h 4.75 min	12h 35 min
Geodetic reference	WGS-84	PZ-90	GTRF	CGS2000
Time system	GPS time, UTC (USNO)	GLONASS time, UTC(SU)	Galileo system time	BeiDou System Time (BDT)
Signal separation	CDMA	FDMA	CDMA	CDMA
Number of frequencies	3-L1,L2,L5	one per two antipodal SV	3(4)-E1,E6,E5(E5a,E5b)	3-B1,B2,B3
Frequency (MHz)	L1: 1,575.420	G1: 1,602.000	E1: 1,575.420	B1: 1,575.420
	L2: 1,227.600	G2: 1,246.000	E6: 1,278.750	B2: 1,191.795
	L5: 1,176.450	G3: 1,204.704	E5: 1,191.795	B3: 1,268.520
Number of ranging codes	11	6	10	--

Table 1.1: GPS, GLONASS, GALILEO and BeiDou comparison (Compiled from Hofmann-Wellenhof et al., 2007; Daly and Kitching, 1990; Dawoud, 2012)

Thus, GLONASS uses Frequency Division Multiple Access tecnique (FDMA) while GPS, Galileo and BeiDou use Code Division Multiple Access (CDMA) technique (Hofmann-Wellenhof et al., 2007; Daly and Kitching, 1990; Dawoud, 2012).

1.2 Current GNSS PPP research issues

This section discusses key current GNSS PPP research topics in the fields of ambiguity resolution, integration of other GNSS satellite constellations in PPP and real-time positioning. One common but relatively undiscussed issue which poses a hindrance in achieving improvements in the fields of research highlighted, is the mitigation of GNSS equipment biases. The quest for increased PPP performance has heighten the desire to examine possible ways to mitigate these GNSS equipment biases.

1.2.1 Integration of GPS and GLONASS in PPP

In environments such as urban canyons, mountainous areas and open-pit mines, the visibility of signals is hindered and available signals become insufficient. The integration of GPS and GLONASS constellations provides more signals, enhances satellite geometry and improves the quality of solutions in PPP processing (Shen and Gao, 2006; Li and Zhang, 2013).

By differencing out measurements between two receivers, satellite specific errors such as atmospheric errors, as well as clock and orbital errors, are mitigated. However, in PPP, only a single GNSS receiver is used which presents a challenge in mitigating the satellite specific errors. To estimate and correct for the atmospheric errors and satellite orbital and clock errors, precise satellite and clock corrections and satellite orbits are provided as a product by organizations to

enhance the accuracy of PPP solutions. The International GNSS Service (IGS) has been providing precise satellite clock and orbit products as well as atmospheric parameters since 1994. These products have different accuracy levels and latencies. The products are therefore grouped into the "ultra-rapid", "rapid" and "final" products, based on the needed accuracy, latency and sampling rate. Table 1.2 summarizes the GPS precise orbits and clocks produced by IGS.

Orbits and Clock products		Accuracy	Latency	Updates	Sampling
Broadcast	orbit	~100 cm	Real time	--	daily
	clock	~5 ns rms ~2.5 ns SDev			
Ultra-Rapid (predicted half)	orbit	~5 cm	Real time	Four times daily	15 min
	clock	~3 ns rms ~1.5 ns SDev			
Ultra-Rapid (observed half)	orbit	~3 cm	3 - 9 hours	Four times daily	15 min
	clock	~150 ps rms ~50 ps SDev			
IGS Rapid	orbit	~ 2.5 cm	17 - 41 hours	daily	15 min
	clock	~75 ps rms ~25 ps SDev			5 min
IGS Final	orbit	~2.5 cm	12 - 18 days	weekly	15 min
	clock	~75 ps rms ~20 ps SDev			5 min

*SDev (Standard Deviation) *rms (root mean square error)

Table 1.2: GPS Precise satellite orbit and clock products (IGS, 2013)

The introduction of the International GLONASS Experiment (IGEX-98) (Willis *et al.*, 1997) and GLONASS Service Pilot Project (IGLOS) (Weber and Slater, 2001) have made GLONASS precise orbit and clock products available to PPP end users. Four IGS Analysis Centres are currently providing GLONASS precise and clock products; CODE (University Berne,

Switzerland), IAC (Information-Analytical Centre), ESA/ESOC (European Space Agency / European Space Operations Centre, Germany) and BKG (Bundesamt für Kartographie und Geodäsie, Germany). Table 1.3 summarizes the accuracy, latency, updates and sampling rates from these Analysis Centres.

Orbit and Clock products		Accuracy	Latency	Updates	Sampling rate
IGS Final	orbits	~3 cm	12 – 18 days	weekly	15 min
IAC Rapid	orbit	--	1 day	--	15 min
	clock	--			5 min
IAC Final	orbit	~ 15 cm	5 days	--	15 min
	clock	~ 1.5 ns			5 min
ESA/ESOC Final	orbit	--	--	--	15 min
	clock	--			5 min

Table 1.3: GLONASS precise orbit and clock products (IGS, 2013)

It must be noted that there is a direct relation between the quality of the precise orbit and clock products and the positional accuracy of solutions in PPP. A level of agreement of 1.5 ns exists between IAC and ESA post-mission GLONASS clock values (Oleynik, *et al*., 2006).

In Figure 1.1, it can be observed that from GPS weeks 1720 to 1786, the solutions of the AC Final orbits were consistent at the 5 - 20 mm level (European Space Agency, 2011). As shown in the figure, the ESA final solution is comparable to the combined IGS Final solution in the order of a few millimetres in the weighted rms.

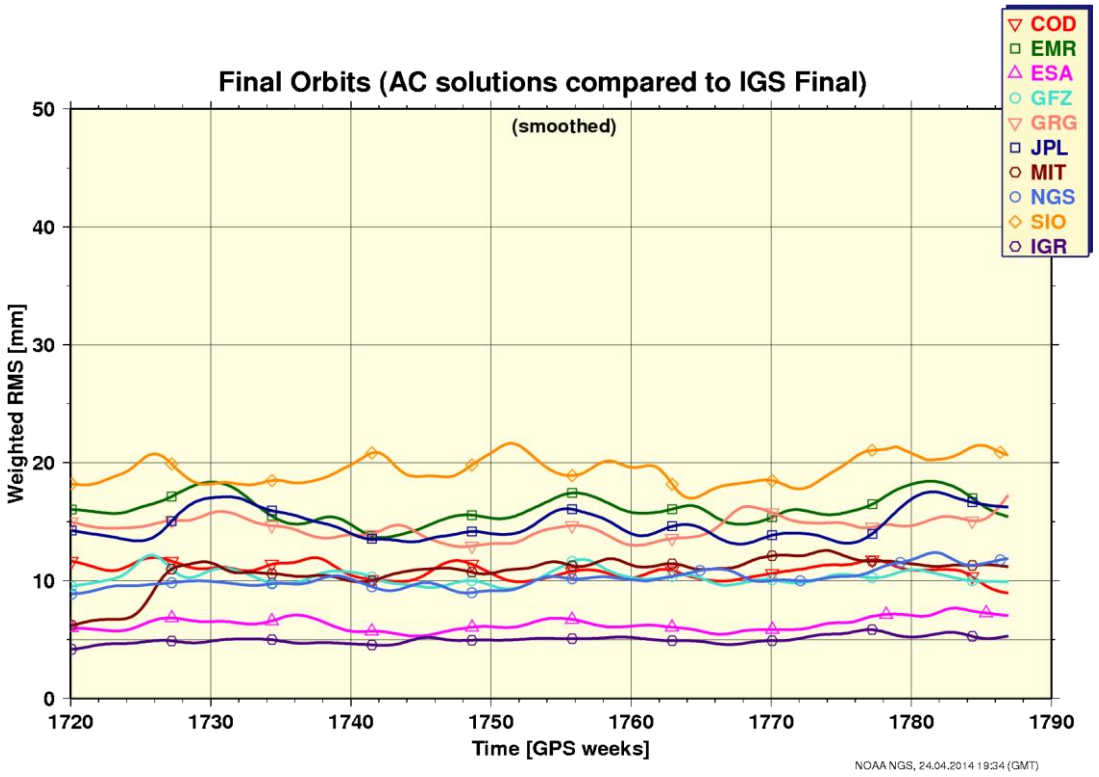

Figure 1.1: Weighted orbit RMS of the ESA products and AC Final orbits solutions between December 2012 and April 2014, with comparison to the IGS Final orbit products (European Space Agency, 2011)

Cai and Gao (2013) assessed the performance of GPS and GLONASS PPP by implementing a combined GPS and GLONASS PPP model. The results showed an improvement in the position accuracy from GPS-only solutions of 39%, 30% and 60% in the easting, northing and up components. The kinematic results also improved by more than 50%. Choy *et al.* (2013) compared the performance of GPS-only and combined GPS and GLONASS PPP for static and kinematic positioning modes. Using very few stations, the horizontal and vertical accuracy was within 1 cm and 2 cm, respectively, for GPS-only PPP in static processing. The addition of GLONASS did not improve the accuracy significantly. The performance of the combined GPS

and GLONASS PPP in kinematic mode, showed improvement of 43% and 25% in the horizontal and vertical components, respectively.

Wang *et al.* (2012) further investigated the trend and periodic residual characteristic of combined GPS and GLONASS observations. Their results showed that the positional accuracy of GPS was better than that of GLONASS by an improvement of 38%, 17% and 1.2% in the northing, easting and up components, respectively. Regular variations in the residuals including trend and periodic items were also investigated. To mitigate these trends and periodic characteristics, an error compensation model was proposed.

Tu *et al*. (2013) analyzed PPP convergence period using a combined GPS and GLONASS approach. The receiver's differential code biases (DCB), which is the pseudorange bias between the C/A-code and precise code observables, were estimated by treating them as unknowns. It was concluded that though there was not a significant improvement in the positional accuracy, there was a positive impact on the satellite availability and geometry. By estimating the receiver DCBs, there was a 20% reduction in convergence period, as well as an improvement in the Position Dilution of Precision (PDOP), which is a measure of the geometric strength of the solution. The horizontal error was better than 10 cm considering 10 minutes convergence period.

Li and Zhang (2013) further analyzed the integration of GPS and GLONASS observations with the aim of accelerating the convergence period in a combined GPS and GLONASS PPP static and kinematic processing. Using 178 IGS stations, the contribution of GLONASS measurements to ambiguity resolution in PPP, was investigated. GPS integer ambiguities were fixed while GLONASS ambiguities were left as "float" real values. The results indicated that the average

convergence time was reduced by 46% from 23 to 12 minutes in static mode and by 58 % from 41 to 18 minutes in kinematic mode, respectively, for ambiguity-float PPP. The convergence time was also reduced by 27% from 22 to 16 minutes in static mode and by 42% from 34 to 20 minutes in kinematic mode, respectively, for ambiguity-fixed PPP.

The coordinate and time reference frames for GPS and GLONASS are different. The difference in time is due to the different realizations of Coordinated Universal Time (UTC) used. Concerning coordinate reference differences, GPS adopts World Geodetic System (WGS) 84 while GLONASS adopts Parametry Zemli (PZ) 90. Differences are observed in the accuracy of the time and coordinate reference framework of GPS and GLONASS which constitutes inter-system biases (ISBs). These inter-system biases (ISB) were estimated by Chen *et al.* (2013) by analyzing the combined GPS and GLONASS system bias product of the Shanghai Astronomical Observatory (SHAO) GNSS Analysis Centre. The conclusions included the fact that receivers of the same type have similar ISBs, but the ISBs are different for different receiver types. The same pattern was observed with varying ISBs for all stations, which was indicative of the fact that the system time offset plays a role in the variations of the ISBs over a long time. The relationship between the ISBs and antenna types was investigated and it was concluded that the ISBs are influenced by different antenna types. The ambiguities however were found to absorb the ISBs and, as such, made no impact on the final positional accuracy of the solutions.

1.2.2 Ambiguity resolution in multi-GNSS PPP

It is well known that one of the problems PPP faces is a long initial solution convergence period. Though PPP takes full advantage of both the pseudorange and carrier-phase measurements, the ambiguity components in the carrier-phase measurements affect the final solution accuracy. The unresolved ambiguities are not integers due to the presence of so-called un-calibrated phase delays (UPDs) which are a function of the unknown cycles of the carrier waves (Collins *et al.*, 2010; Ge *et al.*, 2008; Geng *et al.*, 2010; Leandro *et al.*, 2006; Shi and Gao, 2010). It becomes imperative that the unknown cycle ambiguities are resolved as this is a key component to obtaining sub-centimetre to millimetre-level GNSS positioning.

In a generalized sense, GNSS ambiguity resolution can be looked at through a three step approach. First, a "float" solution is obtained through a least-squares adjustment while the integer component of the ambiguities is discarded. Second, the integer constraints are estimated by adjusting the real-valued float solution of the ambiguities. And third, the float solution of the position, satellite and receiver clock parameters, as well as any remaining parameters, are corrected for due to their correlation with the phase ambiguities, resulting in a centimetre to millimetre "fixed" solution (Teunnissen and Odijik, 1999).

One of the profound problems of GNSS carrier-phase positioning is that it requires real-time integer ambiguity resolution. The last twenty years have seen a plethora of research on GPS ambiguity resolution with different developed approaches. Some of these approaches include the Least-squares Ambiguity Decorrelation Adjustment (LAMBDA) (Teunissen and Verhagen, 2009a; Teunissen and Verhagen, 2009b; Teunissen, 2003), Fast Ambiguity Search Filter (FASF)

(Chen, 1994), Ambiguity Function Method (AFM) (Erickson, 1992), Three/Multiple Carrier Ambiguity Resolution (TCAR/MCAR) (Werner and Winkel, 2003), Fast Ambiguity Resolution Approach (FARA) (Hofmann-Wellenhoff *et al*., 2001), and Cascading Integer Resolution (CIR) (Jung *et al*., 2000). However, a challenge still remains with quickly fixing these ambiguities correctly (Liu *et al*., 2014).

Due to the Frequency Division Multiple Access (FDMA) signal structure of GLONASS satellites, ambiguity resolution for GLONASS is much more complicated compared to GPS. The GLONASS double-differenced carrier-phase observations can be significantly influenced by inter-frequency channel biases. It is a difficult task in estimating the inter-frequency channel biases for mixed receivers, as well as separating these biases from the ambiguity terms. It therefore becomes a daunting task for GNSS software applications to resolve and fix GLONASS ambiguities, especially if heterogeneous receiver types are used. Rather, the float estimates of the GLONASS ambiguities absorb the inter-frequency channel biases. Even though the ambiguity resolution integrity of GPS is improved by using this approach, it is expected that by fixing GLONASS ambiguities to integers, the full potential of GLONASS will be realized enhancing the solution accuracy in GNSS PPP (Takac, 2009).

1.2.3 Real-time PPP positioning

Over recent years, there has been a shift of focus from PPP post-processing to real-time positioning solutions. The IGS continues to develop real-time orbit and clock streaming since the introduction of the IGS Real-Time Project in 2007 (Ge *et al*., 2008). Since the launch of the Real

Time Service (RTS) in 2013, the IGS has freely distributed real-time GPS orbit and clock correction in the RTCM format. This service has made real-time PPP solutions possible despite a few seconds of delay (Grinter and Roberts, 2013).

With the expanding GNSS constellations, more signals are being introduced warranting new or improved receiver hardware and a growing real-time network. The advent of the IGS Multi-GNSS Experiment (M-GEX) offers innovative ways to improve the collection of measurements from tracking networks. However, a challenge is presented to both the IGS and GNSS communities regarding the streaming of real-time corrections from different satellite constellations: How to guarantee availability, accuracy and consistency from varying satellite constellations. Thus, the need for application-based and receiver hardware innovations becomes necessary (Caissy *et al*., 2012).

1.3 Problem statement and objectives

Given that GLONASS measurements are based on the FDMA satellite signal structure, inter-frequency channel biases (ICBs) and other system biases are introduced. The effects of these biases are visible in the pseudorange and carrier-phase residuals, which affect GLONASS PPP convergence period and un-differenced ambiguity resolution. Current research has shown the correlation between receiver stations from heterogeneous networks, such as the IGS, in PPP processing and the increase in magnitude of the pseudorange and carrier-phase ICBs in both GPS + GLONASS and GLONASS-only PPP solutions. Discounting other system biases which may be

present, the correlation is due to mixed receiver and antenna hardware types, differences in firmware versions, and irregularities in the updates of the receiver equipment at the stations.

With new and expanding satellite constellations, it is expected that PPP convergence period will decrease due to improved geometry, more observations and stronger signals. However, the inclusion of GLONASS has introduced additional biases that need to be accounted for in the data processing or else this relationship will not hold. So does the current performance of GLONASS PPP reflect the limits of the processing technique, or by accurate modelling of GLONASS biases can there be improvements in the solution accuracy and reliability? And can the behaviour of the ICBs help mitigate the effect of these biases that compromise the solution integrity of GPS + GLONASS and GLONASS-only PPP?

With an increasing number of receiver and antenna hardware types available, the error modelling for the pseudorange and carrier-phase biases becomes more complex. In the GNSS community, there is also a limited understanding of these equipment biases, which introduce varying magnitudes of observable error due to each receiver-antenna combination.

A strong correlation between the pseudorange ICBs and receiver firmware and antennas exists, which relates to the differences that exist in the estimated inter-channel biases and similar firmware of the same receiver types. Currently, there is no standard correction format for PPP users in relation to these biases given a specific receiver firmware or antenna type. This research proposes a possible GLONASS ICB correction using 350 IGS stations, based on 32 receiver types and 8 antenna types, by observing the unique trends observed in the bias estimates in relation to the GLONASS satellites.

The Multi-GNSS Experiment (MGEX) was established by the IGS for the tracking and analysis of available GNSS signals. Signals are from any space-based augmentation system (SBAS), as well as from GNSS systems such as GPS, GLONASS, BeiDou, Galileo and Quasi-Zenith Satellite System (QZSS). One of the roles of the Analysis Centres within the MGEX network involves the estimation of inter-system calibration biases (IGS, 2014). These biases include the derivation of DCBs for all available GNSS signals by differencing ionosphere-free pseudoranges (Montenbruck *et al.,* 2014). The derived MGEX DCB corrections were applied in this reseach in the estimation of the pseudorange ICBs.

While these pseudorange and carrier-phase equipment biases do not cause significant errors in GLONASS PPP positioning results, and have almost no effect on GPS PPP results, they impact float ambiguities and associated float covariance estimates in this processing. By improving these estimates, more accurate fixed PPP solutions can be produced and more quickly. Further analysis will be done to evaluate the realism of the associated float covariances with bias modelling, and the impact on PPP fixed solutions.

In summary, the research objectives mainly focus on developed algorithms and models for the combined PPP satellite navigation constellations using dual-frequency, un-differenced pseudorange and carrier-phase observations and assessing the performance of PPP by estimating, calibrating and proposing corrections for GLONASS pseudorange ICBs. As a result, the following objectives are intended to be achieved:

1. Implementation of GNSS PPP models and algorithms in software development. The GNSS PPP software is intended to be modular, scalable and capable of handling all constellations.

2. Assessment of the performance of PPP from combining data from multiple constellations in data processing with regards to the positional accuracy for static applications.
3. Estimation and analysis of GLONASS pseudorange ICBs and the residual characteristics of GPS-only and GPS + GLONASS PPP processing with respect to heterogeneous receiver and antenna type combinations.
4. A novel approach to correcting the pseudorange ICBs in GLONASS-only and GPS+GLONASS PPP by observing unique trends in the bias estimates in relation to the GLONASS satellites.

It is expected that by fulfilling the above objectives, some improvements to the positioning performance of PPP will be made, including:

1. The reduction of convergence period.
2. Increased positional accuracy with regards to static positioning and navigation modes.
3. The development of a PPP software suite implementing the various PPP algorithms and models for combined satellite constellations. This software is intended to be written with unmanaged ANSI C++ in the Microsoft.NET framework.

1.4 Thesis outline

Chapter 2 details on the development of the multi-GNSS PPP processor. A detailed description of the various namespaces, classes, functions and models are given. The chapter concludes with significant PPP performance results based on the processing from the York GNSS PPP software. Chapter 3 reviews GPS and GLONASS PPP residual characteristics. Focus is given

to the relationship between the GLONASS satellites' inter-frequency channel pseudorange biases and various receiver and antenna types. A correction format is proposed with respect to the GLONASS satellite PRN, frequency channel number, receiver and antenna types. Validation of the estimated biases is demonstrated with the improvement in GLONASS-only and GPS + GLONASS PPP solutions. Chapter 4 summarizes all the findings of this work and provides conclusions and recommendations for future work.

Chapter 2
Multi-GNSS PPP Software Design and Development

The York GNSS PPP software is a well-developed and sophisticated GNSS measurement processing tool that meets high-quality standards for geodetic and research applications. It was developed by the author based on the software processor used by the CSRS-PPP online service (NRCan, 2010) and is an extension of the GPS PPP processor developed by Seepersad *et al.* (2012). The following sections provide detailed aspects of GNSS data processing, and principles of the York GNSS PPP processor. The theoretical components of standard PPP processing are reviewed, followed by the architecture and functionalities of the software processor. The chapter concludes with results from the York GNSS PPP processor to verify that it meets the highest scientific standards of performance.

2.1 Brief introduction to GNSS data formats

A well-defined set of standards are followed in defining GNSS data sets. There are many advantages provided by standard GNSS data formats which include the ease of exchanging data. Two main formats exist: American Standard Code for Information Interchange (ASCII) and binary formats. ASCII is generally preferred over the binary formats because binary formats are computer operating system dependent (GAGE, 2010).

Building a software program to read a standard format description is a challenge. However, to process GNSS datasets, it is required for any GNSS data processing software to effectively read data in order to process. This section provides brief introduction to existing data formats used in GNSS data processing.

2.1.1 RINEX data format

Receiver Independent Exchange Format (RINEX) is data interchange format for raw satellite navigation system data. RINEX is an ASCII data format developed by the Astronomical Institute of the University of Berne for the easy exchange of GNSS data. RINEX is used as a post processing file format (static and kinematic) and is not suitable for real-time applications. RINEX format includes: GNSS observation data, navigation messages, meteorological data, geostationary satellite data, satellite and receiver clock files. Each RINEX file has a specific name convention which is essential for downloading and processing purposes (Gurtner, 1993; Astronomical Institute of University of Bern, 2007).

2.1.2 RTCM data format

The Radio Technical Commission for Maritime Services (RTCM) Special Committee developed a specific data format to satisfy industry standards for Real time differential data. This format is known as RTCM followed by a specific version number such as RTCM 2.3, RTCM 3.0, etc. RTCM standards were originally developed and are constantly being updated by Special Committee 104 which is concerned with Differential Global Navigation Satellite System (DGNSS). RTCM data are transmitted as a continuous binary data stream. Typically, a complete

RTCM data record is transmitted within one second. RTCM compresses the various contents of a data record in several message types. Every message within a data record comprises a message header and a message body. The message type, time information, the reference station ID, the length of the message and further information such as the monitoring status, are all coded in the header. The body comprises the relevant operational data for every data type. The length of a message depends on the data type (RTCM Special Committee No. 104, 2001).

2.1.3 SP3 data format

Precise orbital data (Satellite Position and Velocity), the associated satellite clock corrections, orbit accuracy exponents, correlation information between satellite coordinates and satellite clock are available in this format. This information can be observed or predicted simultaneously with those precise orbits. The structure of this format is different from the RINEX format explained earlier. To facilitate exchanging such precise orbital data**,** the U.S. National Geodetic Survey (NGS) developed the SP3 format, which later became the international standard. The SP3 file is an ASCII file that contains information about the precise orbital data (in the ITRF reference frame) and the associated satellite clock corrections (Spofford and Remondi, 1994).

2.1.4 ANTEX data format

The basic results from the absolute GNSS antenna calibration are GNSS carrier-phase center offsets and variations (PCV). ANTEX is the international exchange format for antennas' PCV. ANTEX describes all relevant antenna information. Different GNSS, offsets, pure elevation

dependent PCV and azimuth and elevation dependent PCV are available. GLONASS PCV are also provided in the ANTEX format (Schmid, 2011).

2.1.5 IONEX data format

The defined IONosphere map EXchange format (IONEX) is a data format to exchange, compare, or combine Total Electron Content (TEC) maps. TEC is a quantitative description for the total number of electrons in the ionosphere of the Earth. IONEX supports the exchange of 2- and 3-dimensional TEC maps given in a geographic grid. The IGS network is used to extract information about the TEC of the ionosphere on a global scale (Schaer *et al.,* 1998).

2.2 Standard GNSS PPP processing

PPP can generally be defined as a positioning technique where a single receiver's coordinates (and time) are determined using precise satellite orbit and clock products. Unlike network-based techniques where common errors cancel out, PPP requires that all errors introduced by the space segment, signal propagation and user segment, are accounted for. These errors can be mitigated either by elimination, estimation or modelling. The proper handling of these systematic and random error sources largely impact the solution integrity of PPP. It becomes imperative, in PPP, to mitigate these errors (Hofmann-Wellenhof *et al.*, 2001; Leick, 2004; Boehm and Werl *et al.,* 2007; Bisnath and Langley, 2001; Kouba *et al.*, 2001; Mader, 1999; Zhu *et al.*, 2002). Figure 2.1 shows the processing scheme used in PPP with the correction models needed to be implemented. Processing of GNSS data is performed in five main stages, which involve: reading of GNSS observations; data pre-processing; application of error correction models;

filtering; and output of estimated parameters. The GNSS observations include GNSS RINEX and RTCM observations, together with precise orbit and clock products. These observations undergo data pre-processing which involves the removal of cycle slips from carrier-phase data. Error correction models are applied to account for any possible error sources. Incorporating the corrected observables into a sequential least-squares filter and applying functional and stochastic PPP models, updated and predicted parameters such as coordinates and ambiguities, are estimated. The final output includes station coordinates, receiver clock offset, tropospheric delay and GNSS system time differences.

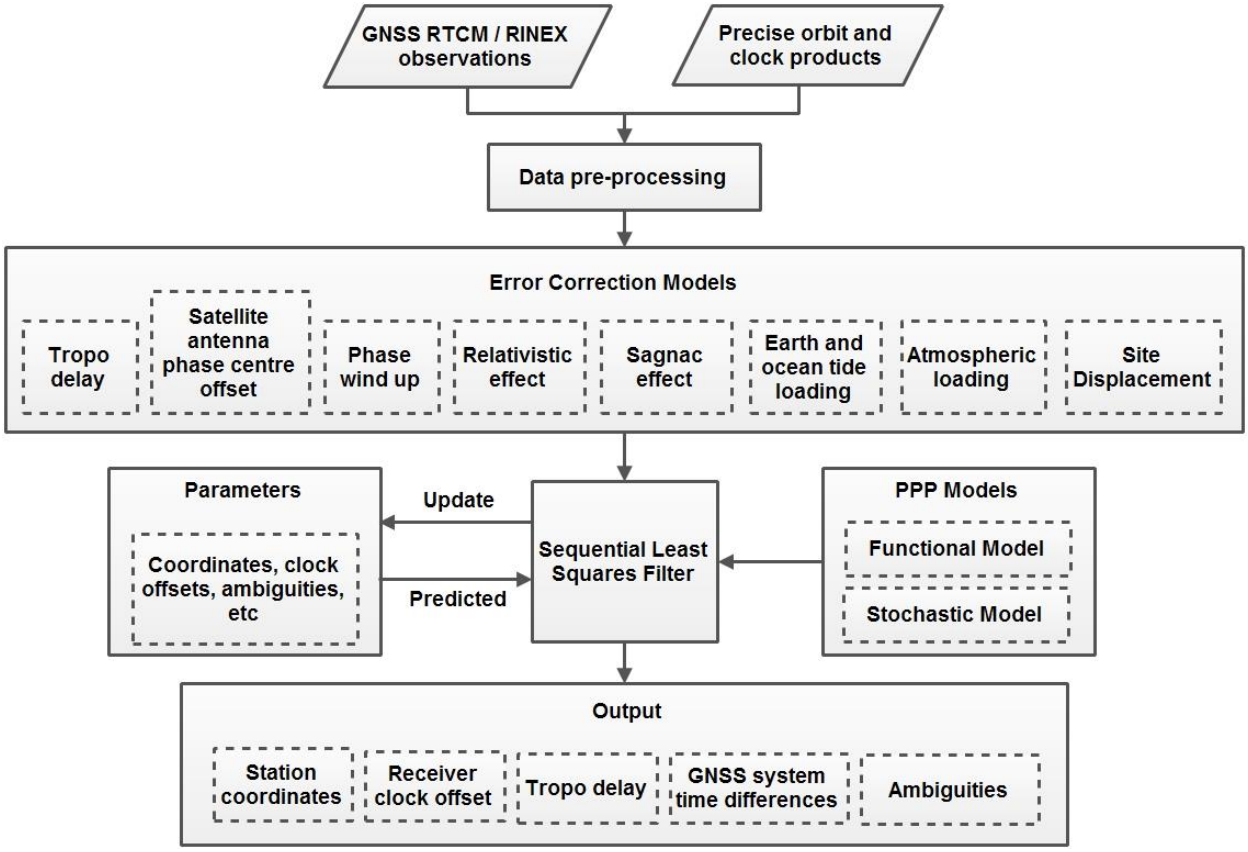

Figure 2.1: Flowchart showing the standard GNSS PPP processing scheme

Given that all relevant PPP errors have either been modelled or estimated, the conventional un-differenced observation equations can be written as (Wells *et al*., 1986):

$$P_{L_i}^{GNSS} = \rho^i + c(\partial t^s - \partial t_r) + d_{trop} + d_{ion,L_i} + b_{Pr_i}^{L_i} + b_P^{L_i,s_j} + d_{multi\left(P_{L_i}\right)} + \varepsilon\left(P_{L_i}^{GNSS}\right) \quad (2.1)$$

$$\Phi_{L_i}^{GNSS} = \rho^i + c(\partial t^s - \partial t_r) + d_{trop} - d_{ion,L_i} + b_{\Phi r_i}^{L_i} + b_\Phi^{L_i,s_j} + \lambda_{L_i}, N_{L_i} + d_{multi\left(\Phi_{L_i}\right)} + \varepsilon\left(\Phi_{L_i}^{GNSS}\right) \quad (2.2)$$

The terms in equation 2.1 and 2.2 are:

$P_{L_i}^{GNSS}$ - Pseudorange measurement on L1 or L2 (m)

$\Phi_{L_i}^{GNSS}$ - Carrier-phase measurement on L1 or L2 (m)

ρ^i - Geometric range (m)

c - Speed of light (m/s^{-1})

∂t^s - Satellite clock error (sec)

∂t_r - Receiver clock offset (sec)

d_{ion,L_i} - Ionospheric delay (m)

d_{trop} - Tropospheric delay (m)

$b_{Pr_i}^{L_i}, b_{\Phi r_i}^{L_i}$ - Receiver equipment bias for pseudorange and carrier-phase measurements, respectively (m)

$b_P^{L_i,s_j}, b_\Phi^{L_i,s_j}$ - Satellite equipment bias for pseudorange and carrier-phase measurements, respectively (m)

λ_{L_i} - Wavelength of L1 or L2 carrier waves (m)

N_{L_i} - Unknown cycle ambiguity term on L1 or L2 carrier-phases (cycles)

$d_{multi(\Phi_{L_i})}$ - Carrier-phase multipath on L1 or L2 (m)

$d_{multi(P_{L_i})}$ - Pseudorange multipath (m)

$\varepsilon(P_{L_i}^{GNSS})$ - Pseudorange measurement noise (m)

$\varepsilon(\Phi_{L_i}^{GNSS})$ - Carrier-phase measurement noise (m)

By linearizing equations 2.1 and 2.2 through the relation of the unknown quantities and the observations, equation 2.13 is obtained:

$$A\delta + W - V = 0 \tag{2.3}$$

Where

A - Design matrix

δ - Estimated corrections to unknown quantities

W - Pre-fit misclosure vector

V - Residual vector

The design matrix (A) is the partial derivatives of the observation equations with respect to the unknown parameters (x) which primarily are the receiver station 3D position (X, Y, Z), receiver clock offset (∂t_r), tropospheric zenith path delay (zpd), carrier-phase ambiguities and hardware biases. The design matrix is given as follows:

$$A = \begin{bmatrix} \frac{\partial \rho_i^{j=1}(t)}{\partial X_i^j} & \frac{\partial \rho_i^{j=1}(t)}{\partial Y_i^j} & \frac{\partial \rho_i^{j=1}(t)}{\partial Z_i^j} & \frac{\partial \rho_i^{j=1}(t)}{\partial t_i} & \frac{\partial \rho_i^{j=1}(t)}{\partial zpd} & 0 & 0 \ldots & 0 \\ \frac{\partial \Phi_i^{j=1}(t)}{\partial X_i^j} & \frac{\partial \Phi_i^{j=1}(t)}{\partial Y_i^j} & \frac{\partial \Phi_i^{j=1}(t)}{\partial Z_i^j} & \frac{\partial \Phi_i^{j=1}(t)}{\partial t_i} & \frac{\partial \Phi_i^{j=1}(t)}{\partial zpd} & \frac{\partial \Phi_i^{j=1}(t)}{\partial N_{if,1}} & 0 \ldots & 0 \\ \vdots & \vdots & \vdots & \vdots & \vdots & 0 & 0 \ldots & 0 \\ \frac{\partial \rho_i^{j=n}(t)}{\partial X_i^j} & \frac{\partial \rho_i^{j=n}(t)}{\partial Y_i^j} & \frac{\partial \rho_i^{j=n}(t)}{\partial Z_i^j} & \frac{\partial \rho_i^{j=n}(t)}{\partial t_i} & \frac{\partial \rho_i^{j=n}(t)}{\partial zpd} & 0 & 0 \ldots & 0 \\ \frac{\partial \Phi_i^{j=n}(t)}{\partial X_i^j} & \frac{\partial \Phi_i^{j=n}(t)}{\partial Y_i^j} & \frac{\partial \Phi_i^{j=n}(t)}{\partial Z_i^j} & \frac{\partial \Phi_i^{j=n}(t)}{\partial t_i} & \frac{\partial \Phi_i^{j=n}(t)}{\partial zpd} & 0 & 0 \ldots & \frac{\partial \Phi_i^{j=n}(t)}{\partial N_{if,n}} \end{bmatrix} \quad (2.4)$$

The misclosure vector represents the differences between the pseudorange or carrier-phase observations and the computed pseudoranges and carrier-phases determined through the functional model. The misclosure vector elements are determined by the following equations:

$$W_{P_{L_{if}}} = P_{L_{if}} - \rho_i - cdT^j + cdt_i - T_{zpd} \quad (2.5)$$

$$W_{\Phi_{L_{if}}} = \Phi_{L_{if}} - \rho_i - cdT^j + cdt_i - T_{zpd} - \lambda_{L_{if}} N_{L_{if}}^j \quad (2.6)$$

$$W = \begin{bmatrix} W_{P_{L_{if}}}^{j=1} \\ W_{\Phi_{L_{if}}}^{j=1} \\ \vdots \\ W_{P_{L_{if}}}^{j=n} \\ W_{\Phi_{L_{if}}}^{j=n} \end{bmatrix} \quad (2.7)$$

The weight matrix for stationary receivers is given as:

$$P_l = \begin{bmatrix} 1 & & & & \\ & 100^2 & & & \\ & & \ddots & & \\ & & & 1 & \\ & & & & 100^2 \end{bmatrix} \quad (2.8)$$

The weight coefficient matrix with respect to the estimated parameters is given as:

$$P_x = C_x^{-1} \tag{2.9}$$

where C_x is the a priori variance-covariance matrix.

$$X^T = \begin{bmatrix} x & y & z & dt & zpd & N_{j=1,nsat}^{j} \end{bmatrix} \tag{2.10}$$

$$\Delta x = (A^T P A + P_x)^{-1} A^T P W \tag{2.11}$$

$$\widehat{X} = x^o + \Delta x \tag{2.12}$$

Given that the carrier-phase observations are about 100 times more precise than the pseudorange measurements, the weight matrix of the observations (P_l) is applied as shown in equation 2.8. Using the sequential least-squares approach weighted with a priori weighted constraints (P_x), the unknown parameter estimates (Δx), as computed in equations 2.11 and 2.12.

2.3 York GNSS PPP software

The York GNSS PPP software is a scalable and modular GNSS PPP processor written in C++ using Visual Studio in the Microsoft.NET platform. Its entire design and development is within the purview of this thesis. The usage of C++ in developing the GNSS PPP processor makes it not only platform-independent but also enhances re-usability. A total of over 27,000 lines of C++ codes were written by the author, with 6 namespaces, over 100 classes, over 200 functions and over 4000 lines of MATLAB code for the analysis and plotting of results. The proceeding sections highlight the various development stages of the GNSS PPP software, detailed object-oriented structure in the terms of namespaces, classes and some core functions and present the software validation and performance.

Figure 2. 2 illustrates the software architecture of York GNSS PPP software. It consists of four main segments: the data input module; error correction, sequential least-squares module, and the parameter output module. The user is required to specify processing parameters and input files. All provided data are read and stored in internally defined structures before data-handling checks are performed. These data-handling checks constitute the data pre-processing module and involve making sure that all necessary satellite data are available, as well as bad data are rejected. The correction module depends on user-required data supplied in the form of an observation file, precise satellite orbits and clocks, ANTEX file and ocean loading coefficients. The corrected observation data goes through the sequential filtering module where position estimates as well as other parameters are obtained. The output parameter segment is intended for the purpose of evaluation and result analysis. The York GNSS PPP software currently supports post-processing using GPS and GLONASS data. However, it has been made modular and scalable to handle other data formats such as RTCM data. Future work would involve real-time processing and the addition of other GNSS navigation systems. The following sub-sections provide details in the development of the York GNSS PPP processor. Given that it was written in C++ in the Microsoft.NET platform, the proceeding sections provide the organizational structure of the entire software by describing key components which follow the same framework for all other components. The fundamental unit of the software is a function, which contains program code to execute a specific task depending on user-defined inputs. A group of functions constitute a class of functions aimed towards a particular task. A cluster of classes of functions finally constitute a namespace. Structuring the software enhances scalability, modularization and processing speed of the software.

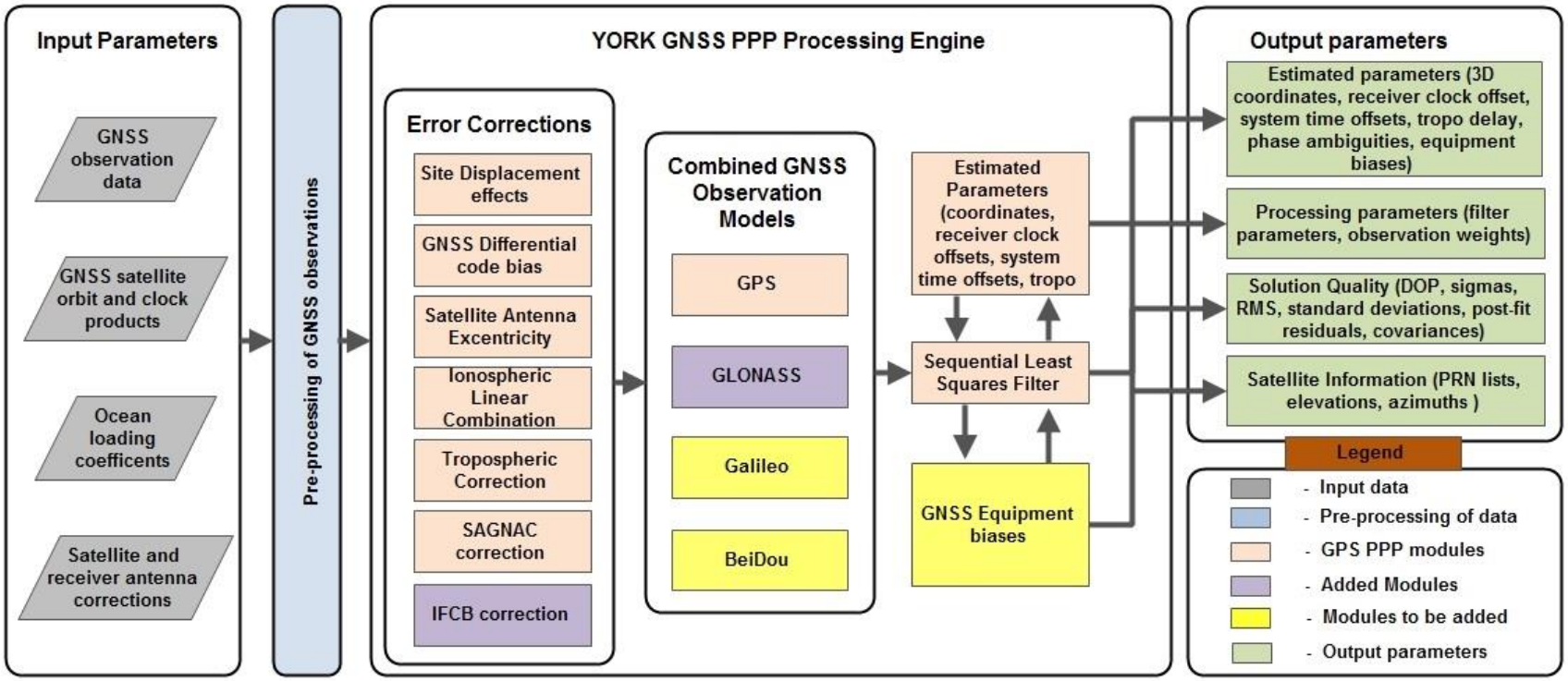

Figure 2.2: York GNSS PPP processing engine

Four key namespaces were created in the development of the software. Presented in the sub-sections are brief descriptions of the details of classes and functions that constitutes the namespaces.

2.3.1 File Readers Namespace

The File readers' namespace consists of various classes which are intended for RINEX and RTCM operations. These operations involve reading, updating and outputting RINEX and RTCM files. The various classes were developed:

- Class GNSS RINEX reader
- Class GNSS precise satellite orbits reader
- Class GNSS precise clock product reader
- Class GNSS IONEX reader
- Class GNSS RTCM reader
- Class GNSS ANTEX reader

The classes in this namespace contain functions for the purpose of reading various RINEX data formats. The main RINEX reader processes RINEX versions 2.11, 2.12 and 3.0. The GNSS RINEX reader is a sub-post-processing software package which does not support real-time data reading. Appendix A illustrates the RINEX reader design flowchart. The GNSS RINEX reader is divided into two sub-readers: one that reads RINEX observation files and another one that reads RINEX navigation files. Both of the sub-readers have identical software design. They begin by reading the header of a file and extracting header information. If any error occurs during the

reading and extraction process due to damage of the input file, the error information will be recorded in header error log. Once the end of header is reached, sub-readers start reading body of the file and extracting useful body information, outputting any errors into the body error log. The GNSS RINEX reader supports single or multiple observation and navigation files, as well as batch processing. Appendices B and C illustrate the RINEX observation and navigation file readers further.

Considering that the GNSS RINEX reader is intended to read RINEX data formats from GPS, GALILEO, BeiDou and QZSS navigation systems, it has been designed to cater to the intricacies of reading from these different GNSS systems. The complexity of handling different satellite constellations required conditions and switches for the appropriate GNSS data stream to be read and decoded as a number of possible combinations of the different GNSSs can occur. Appendix C and D provide the details and functionalities of how the combined GNSS observation and navigation data are decoded depending on the RINEX version being considered.

The GNSS RTCM reader is designed to process RTCM binary data for real-time processing. It processes transmitted GNSS corrections from GNSS reference stations to GNSS rover receivers. Versatility and robustness demanded that the reader be able to process different versions of the RTCM data formats which include:

- RTCM 2.0 (Code correction, mostly DGPS)
- RTCM 2.1 (Code + Phase correction, RTK)
- RTCM 2.2 (Code + Phase correction + GLONASS)
- RTCM 2.3 (Code + Phase correction + GLONASS + GPS Antenna Definition)

- RTCM 3.0 (Code + Phase correction + GLONASS + GPS Antenna Definition + Network RTK and GNSS)

The RTCM reader has been designed to process live streaming RTCM data in the above formats. Two ways were designed to achieve this capability; streaming data directly using GNSS receivers that support that option and an NTRIP software client, the GNSS Internet Radio which connects to one of the global broadcasting stations to stream continuous RTCM data. Both options are provided for, and Appendix E describes general design of the RTCM reader.

The Clock reader class contains various functions intended on reading and processing satellite and receiver clock information contained in the RINEX clock file. The satellite clock values from each input clock RINEX file are copied without any modifications into a York satellite clock format with the same name as the input file but in a different directory. An equidistant sampling of the epochs in the output clock file has been added as an option based on the decimation of the RINEX clock file. There is an alternative option for the user to specify a subset of clocks to be processed. All other clocks are skipped when reading the input clock RINEX files. The only exception is that the reference clocks from all input clock RINEX files are processed. Appendix F illustrates the general structure of the RINEX clock reader.

The GNSS IONEX reader has been designed for the exchange of ionosphere map information. The IONEX reader has various functions to read and write IONEX files when available. Other functionality has been included for date and time conversions, that is, date to Mean Julian Day conversion, Mean Julian Day to date conversions and day-fraction into hours-minutes-seconds conversions. Concerning the IONEX format 1.0, the reader processes the header section

which contains global information for the entire file. It reads all the header labels for each line. For the data section, it processes the data block of the TEC map for a given latitude and height. Given that after 16 values per latitude band, the values continue in the next record, the reader handles this complexity and reports any missing data or inconsistency in an error logging module. The reader is designed to handle any other optional labels which may not appear in other IONEX formats. The read information is parsed to output modules which writes the data in the defined York format. Appendix G illustrates the general structure of the IONEX reader.

The GNSS ANTEX reader is designed for the processing of receiver and satellite antenna information. The ANTEX reader processes ANTEX phase center offsets (PCO) and phase centre variations (PCV) for each antenna. Other functionalities which are included involve obtaining the PCO, PCV and total offsets from the ANTEX file, as well as error logging functionality. The reader processes the header and data section. It has been designed to handle any other optional labels which may not appear in other ANTEX formats. The read information is parsed to output modules which write the data in the defined York format. Appendix H illustrates the general structure of the ANTEX reader.

The GNSS precise reader has been designed for the processing of satellite clock corrections, which are computed simultaneously with the satellite orbits. The precise reader processes precise orbits, coordinates and velocities of the ground stations. The reader also processes the header and data section and is designed to handle any other optional labels which may not appear in other SP3 formats. Appendix I illustrates the general structure of the precise orbits and clock reader.

The GNSS Ocean loading reader has been designed for the processing and computation of time series of tidal displacements from an input file containing the ocean loading coefficients for a given station. The reader processes the header and data section. Appendix J describes the structure of the ocean loading reader together with functions which are utilized.

2.3.2 Error Correction Namespace

Since PPP uses undifferenced measurements, all errors caused by the space segment, propagation, environment and receiver need to be accounted for directly. Mitigation can be accomplished by modelling, estimation or elimination. Most of PPP errors, except for the troposphere, ionosphere and receiver clock can be mitigated to a certain extent, by modelling. The others are accounted for through parameter estimation and elimination through linear combinations.

This section discusses the various error models and the developed classes built for them. Various auxiliary functions were built and incorporated into the namespace. The classes include:

- Class Atmospheric refraction
- Class Relativistic effect
- Class Site displacement
- Class Satellite orbit and clock

Class Atmospheric refraction incorporates two correction models namely Tropospheric and Ionospheric models. The relativistic class contains that correct the relativistic effect imposed on the GNSS satellite. Class Site displacement encompasses five error correction models used in

PPP. These include antenna phase offsets, phase wind up, solid Earth tides, ocean loading and Earth rotation parameters. See Appendix K for further description of the functionality of the class.

2.3.3 Data Quality Control Namespace

One of the essential elements of navigation positioning systems is the ability to tolerate and detect any anomaly in observations. This sections deals with the detection of cycle slips from carrier-phase observations, inconsistent and missing satellite data, inconsistent pseudorange-carrier-phase jump detection, epoch decimation, pseudorange smoothing, residual testing and satellite rejection.

Various classes were developed for this namespace. These involved the cycle slip detection class which incorporated the geometry-free carrier-phase linear combination and L1-C1 cycle slip detection techniques.

2.3.4 Filters Namespace

The adjustment models developed in this namespace include the epoch-by-epoch least-squares and the sequential least-squares filters that adapt to varying user dynamics. The implementations of these filters consider the variations in the states of the parameters between observation epochs and uses appropriate stochastic processes to update their variances. The models involve four types of parameters: station position, receiver clock, troposphere zenith path delay and carrier-phase ambiguities. The station position may be constant or change over time depending on the user dynamics. These dynamics could vary from tens of metres per second in the case of a land vehicle to a few kilometres per second for a Low Earth Orbiter (LEO). The receiver clock

will drift according to the quality of its oscillator, e.g., several cm/sec in the case of an internal quartz clock with frequency stability of about 10^{-10}. Comparatively, the zenith path delay will vary in time by a relatively small amount, in the order of a few cm/hr. Finally, the non-integer carrier-phase ambiguities will remain constant as long as the carrier-phases are free of cycle-slips, a condition that requires close monitoring (Kouba *et al*., 2000).The sequential least-squares class was developed to be the engine of the GNSS PPP processor. Figure 2.3 illustrates the structure of the class. The core sequential least-squares function implements the procedural matrix manipulations of sequential least-squares estimation as described in the matrix manipulation block in Figure 2.3. Input parameters includes C++ structs for the various file readers and class objects for the various error correction models.

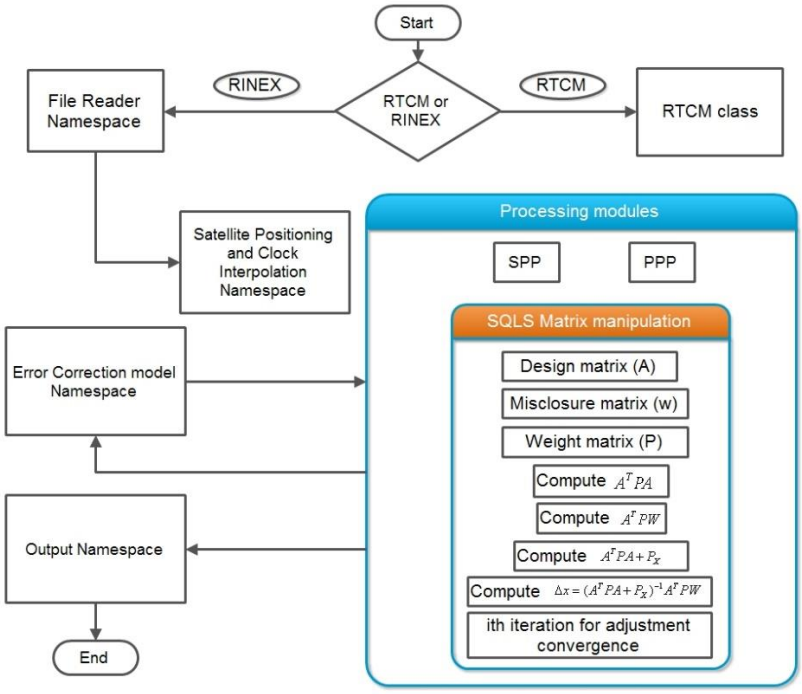

Figure 2.3: Sequential Least-squares class scheme for data processing in GNSS PPP

2.4 Software validation and performance

The performance and accuracy of the York GNSS PPP processing engine was compared to other online PPP services, namely the CSRS-PPP service by Natural Resources Canada (NRCan, 2010), GPS Analysis and Positioning Software (GAPS) by the University of New Brunswick (UNB) (Leandro *et al.*, 2010), Automatic Precise Positioning Service by Jet Propulsion Laboratory (Zumberge *et al.,* 1997) and Magic GNSS by GMV (GMV, 2013). 24-hour datasets from 40 globally-distributed IGS stations were processed using the developed PPP software and the online PPP services, for a one week period. The sites chosen were a subset of those processed regularly by most IGS ACs which represents a good global distribution.

Table 2.1 shows the similarities and differences between the online PPP engines and York GNSS PPP software engine. All the services process dual-frequency data in post-processing mode for static and kinematic datasets. APPS and GAPS currently process GPS-only solutions. Though GPS and GLONASS datasets were used for the analysis, only GPS PPP statistics are presented for uniformity. The York GNSS PPP engine provides similar functionalities as the existing PPP engines and the results are comparable to the highest scientific standards held by the other PPP services.

Referring to section 1.2.1, there are varying degrees of accuracy in the existing orbit and clock products from different organizations and product manufacturers. Given that each online PPP service compared to York GNSS PPP engine, used either internally generated or other satellite or clock products, there are differences in the positional errors and solutions.

	APPS	CSRS	GAPS	magicGNSS	York
Reference frame	ITRF08	ITRF08 (IGB08)/NAD83	IGB08	ITRF08/ETRS89	ITRF08 (IGB08)/NAD83
Coordinate format	LLH/XYZ	LLH/XYZ/UTM	LLH/XYZ	LLH/XYZ	LLH/XYZ/UTM
Quality information	Covariance matrix, std dev	Covariance matrix, std dev	std dev	--	Covariance matrix, std dev
Antenna corrections	IGS	IGS	IGS	IGS	IGS
Satellite orbits and clocks	JPL rapid/final	IGS	IGS	IGS or GMV	IGS/ESA
Elevation mask	Minimal 7.5°	Minimal 10°	Minimal 10°	Minimal 10°	Minimal 10°
GNSS system	GPS	GPS + GLONASS	GPS	GPS + GLONASS	GPS + GLONASS
File number for upload allowed	1- max size 10 MB	1 file	1 file	1 file	--
Observation data	Dual-frequency, static and kinematic	Dual-frequency, static and kinematic	Dual-frequency, static and kinematic	Dual-frequency, static and kinematic	Dual-frequency, static and kinematic
Data transfer	E-mail, web interface	E-mail	E-mail	E-mail, web interface	--
Data format	RINEX 2.0, 2.11 or Hatanaka	RINEX 2.0, 2.11 or Hatanaka	RINEX 2.0, 2.11 or Hatanaka	RINEX 2.0, 2.11 or Hatanaka	RINEX 2.0, 2.11 or 3
Troposphere modelling	GMF	Hydrostatic delay: Davis (GPT) Wet delay: Hopf (GPT) Mapping function	UNB-VMF1 (NCEP), UNB-VMF (CMC), VMF1 (ECMWF), UNB3m Mapping function: VMF1-	--	Hydrostatic delay: Davis (GPT) Wet delay: Hopf (GPT) Mapping function

Table 2.1: Similarities and differences in parameters that define the existing online PPP engines and York GNSS PPP software

The error models implemented in each PPP engine processing also contributes to the overall accuracy of the solutions. Table 2.2 shows the horizontal and 3D standard deviations and rms of the PPP engines. The proper modelling and estimation of errors significantly affects the position accuracy. However the results are comparable to the millimetre level.

	Std dev (mm)		rms (mm)	
PPP engine	**2d**	**3d**	**2d**	**3d**
APPS	6	15	12	29
CSRS-PPP	6	14	10	23
GAPS	8	16	15	34
MAGIC	8	17	13	32
York GNSS PPP	6	14	11	25

Table 2.2: Results of final solutions by existing PPP online services and the York GNSS PPP engine for combined GPS and GLONASS PPP processing for 40 IGS stations

Using a distribution of 350 IGS stations from DOY 195 to 201 in 2013 to further assess the performance of the York GNSS PPP processor, GNSS PPP solutions in the horizontal and vertical components, for GPS, GLONASS and GPS + GLONASS solutions, were compared. Only static solutions were considered though kinematic data can be processed. Figure 2.4 shows the global distribution of selected IGS stations used for the processing. A total of 2500 datasets were processed.

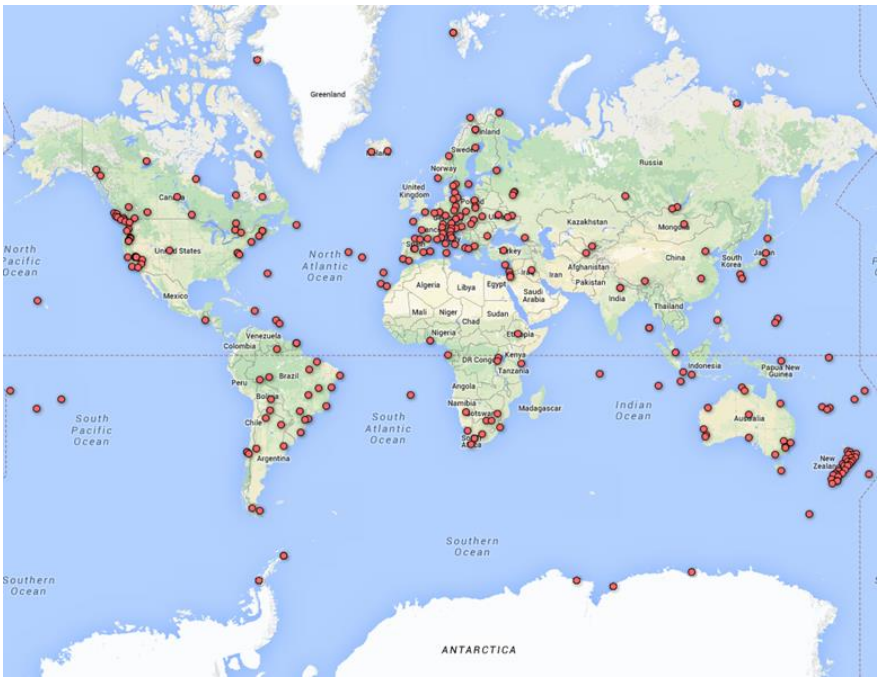

Figure 2.4: Map of selected 350 IGS GNSS stations used for static data post-processing

The York GNSS PPP GPS-only results, show that 98% of the data processed had an error in the horizontal component of less than or equal to 2 cm and that 69% of the results had a horizontal error of less than one centimetre. In the vertical component, 99% of the data processed had an error of 6 cm or less. However, 90% of the processed data had a vertical error of 3 cm or less. Due to the satellite geometry and limitations in the atmospheric and displacement models, the vertical component is expected to be less accurate than the horizontal component.

The GLONASS-only results, in Figures 2.5 and 2.6, show that 72% of the data processed had an error in the horizontal component of less than or equal to 2 cm and that 24% of the results had a horizontal error of less than 1 cm. 95% and 69% of the data processed had an error which was less or equal to 6 cm and 3 cm respectively, in the vertical component.

The GPS+GLONASS results, in Figures 2.7 and 2.8, also show that 99% of the data processed had an error in the horizontal component of less than or equal to 5 mm and that 95% of the results had a horizontal error of less than 2 mm. In the vertical component, 99% of the data processed had an error of 5 mm or less.

The GPS-only PPP results showed improvement over the GLONASS-only PPP solutions. In the horizontal component, an improvement of 26% is observed considering a horizontal error of 2 cm. The GPS PPP vertical component also improved over the GLONASS PPP solutions by 5 and 21% considering a vertical error of 6 cm and 3 cm, respectively.

The GPS + GLONASS PPP results also showed improvement over the GPS-only and GLONASS-only PPP solutions. Comparing the GPS + GLONASS PPP results with GPS-only PPP in the horizontal component, an improvement of 61% is observed considering a horizontal error of 5 mm. The GPS + GLONASS PPP vertical component also improved over the GPS PPP solutions by 80% considering a vertical error of 5 mm. Comparing GPS + GLONASS PPP results with GLONASS-only PPP in the horizontal component, an improvement of 73% is observed considering a horizontal error of 5 mm. The GPS + GLONASS PPP vertical component also improved over the GLONASS PPP solutions by 83% considering a vertical error of 5 mm.

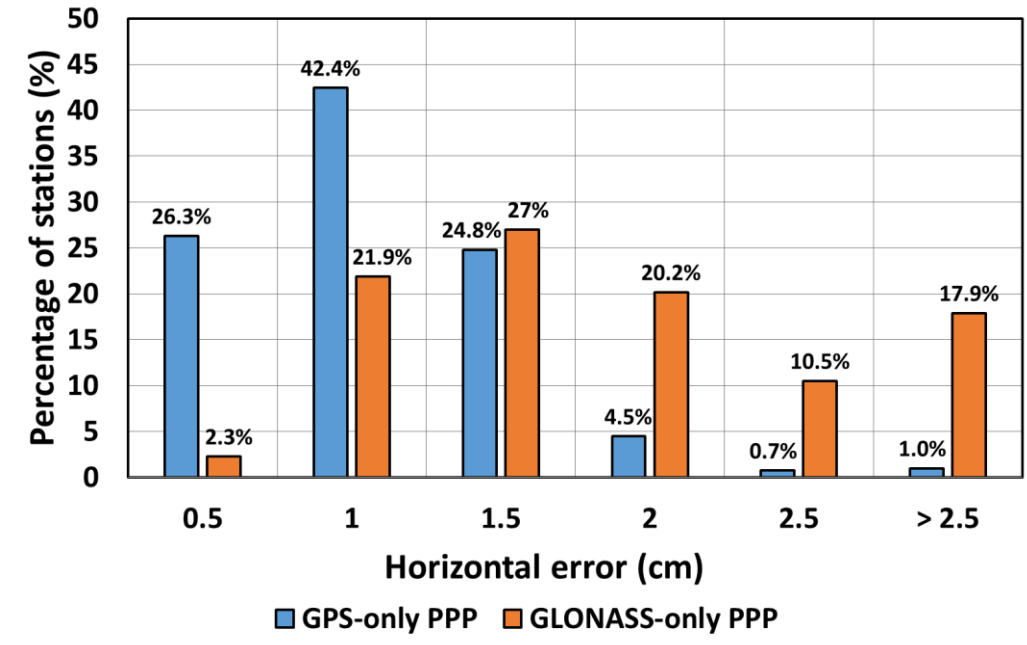

Figure 2.5: Horizontal error histogram for GPS-only and GLONASS-only 24 hour PPP solutions for 350 IGS stations processed in static mode

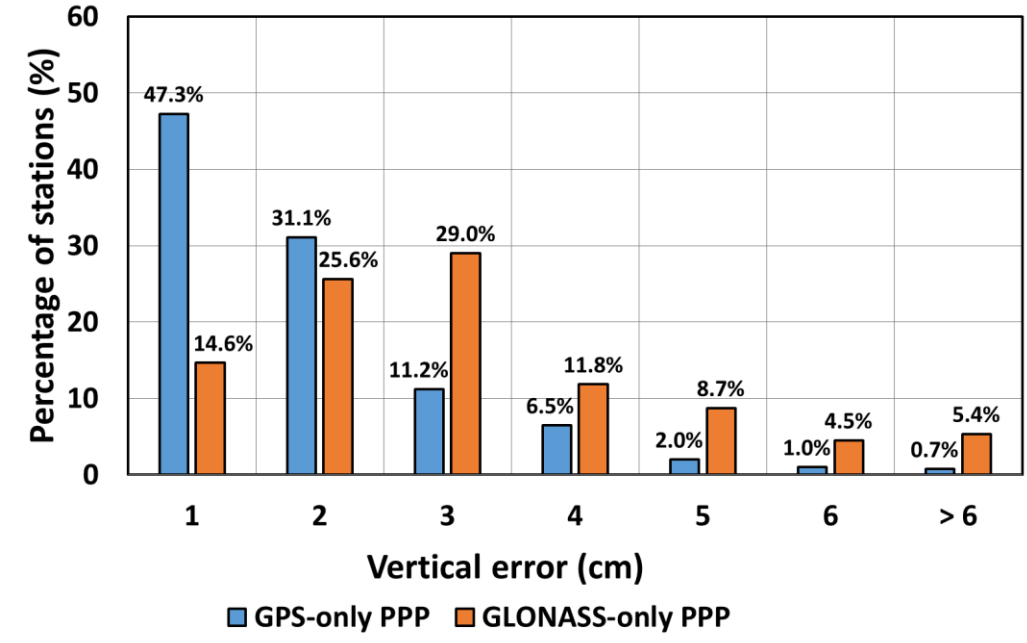

Figure 2.6: Vertical error histogram for GPS-only and GLONASS-only 24 hour PPP solutions for 350 IGS stations processed in static mode

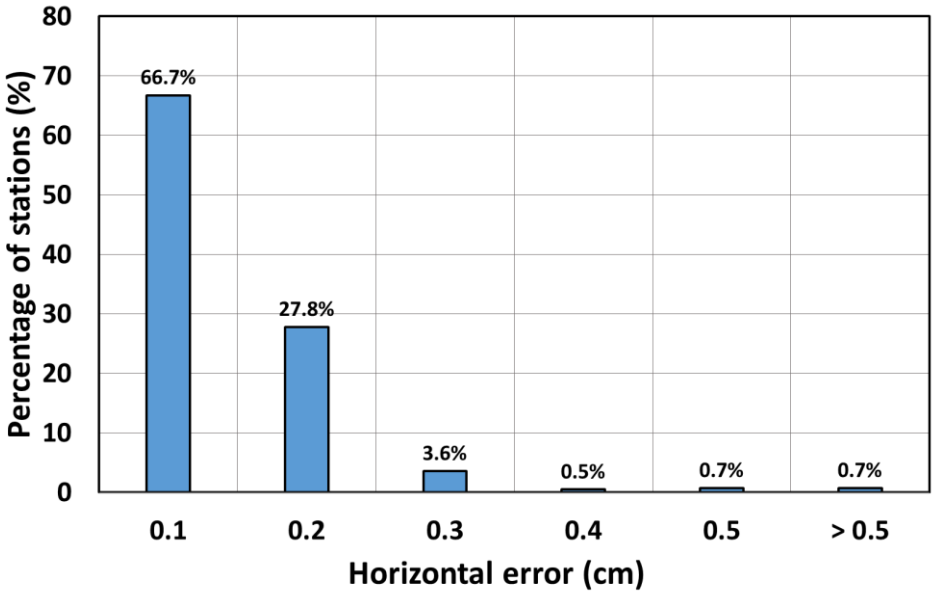

Figure 2.7: Horizontal error histogram for GPS + GLONASS 24 hour solutions for 350 IGS stations processed in static mode

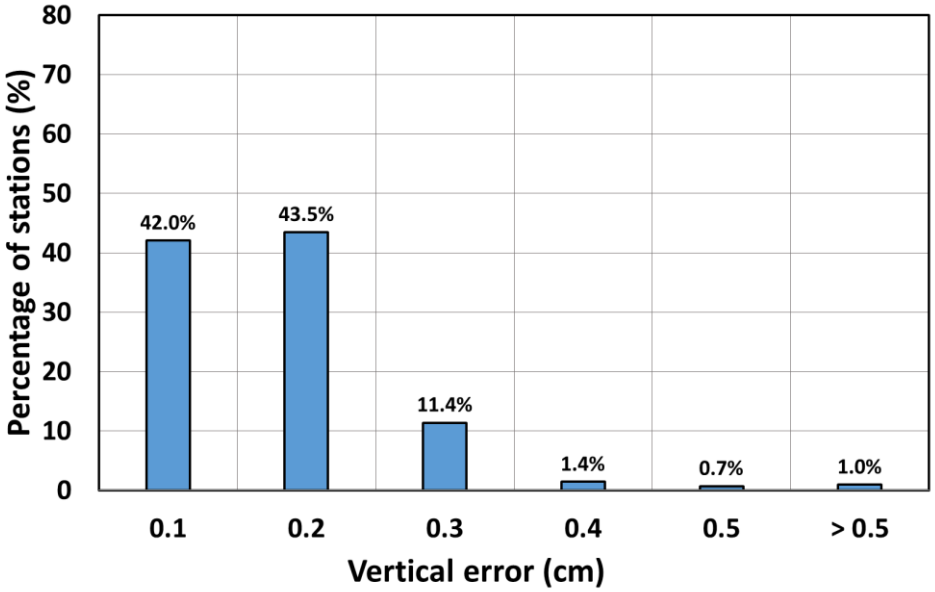

Figure 2.8: Vertical error histogram for GPS + GLONASS 24 hour solutions for 350 IGS stations processed in static mode

The results presented indicate that GPS + GLONASS PPP solutions significantly performed better over both GPS-only and GLONASS-only PPP. The availability of more observations from GLONASS satellites in a combined GPS and GLONASS PPP solution, enhances the solution quality, provides good geometry and strengthens the solution accuracy and integrity. The improvement of GPS PPP over GLONASS PPP solutions could be attributed to the fact that the GLONASS observations are much noisier than GPS. The quality of the satellite orbits and clocks is not a factor here because the same product was used for both GPS and GLONASS.

Table 2.3 shows the statistics of the positional components for GPS-only, GLONASS-only and GPS + GLONASS PPP processing for 350 stations over the period of one week for 24 hour datasets. The results show that the position errors for GPS-only and the combined GPS and GLONASS PPP solutions are quite similar, with the differences in the millimetre range in the East, North, Vertical, horizontal and 3D components.

A substantial conclusion that can be reached involves the fact that the addition of GLONASS to GPS in PPP processing does improve the positional accuracy. The solution quality gets better as GLONASS contributes more signals and satellites and improves the geometry of the satellites, leading to a stronger DOP. However, the position accuracy however, in a combined GPS and GLONASS solution, can be said to be driven by the GPS solution because of less weight given to the noisier GLONASS observations.

GNSS processed	Component	rms (mm)
GPS	**2D**	8
	3D	19
GLONASS	**2D**	18
	3D	34
GPS+ GLONASS	**2D**	1
	3D	2

Table 2.3: Results of final solutions by York GNSS PPP for GPS-only, GLONASS-only and combined GPS and GLONASS PPP for 350 stations over one week period.

The horizontal component of the GPS and GLONASS PPP solutions were comparable to the results presented by Choy *et al.,* (2013) and Cai and Gao (2013), with horizontal and 3D errors of 8 mm and 19 mm for the GPS PPP solutions, respectively. The GLONASS PPP solutions had horizontal and 3D errors of 18 mm and 34 mm, respectively. However, the GPS + GLONASS PPP results published by Choy *et al.,* (2013) and Cai and Gao (2013) were comparable to their GPS-only PPP solutions with 2 mm differences in the horizontal errors. The results presented in Table 2.3 for GPS + GLONASS PPP solutions however contradict the conclusions of Choy *et al.*, (2013) and Cai and Gao (2013), given that the GPS + GLONASS PPP results were better than GPS-only results with a difference of 7 mm and 17 mm for the horizontal and 3D components, respectively. It must be noted that MGEX DCB corrections for GPS and GLONASS systems were applied in the PPP processing. According to Jin *et al*., (2012), several metres of positioning error can occur if the effect of the DCBs are ignored, especially in the first few minutes of PPP data processing when the pseudorange measurements dominate the solution.

Chapter 3
GNSS Equipment Biases

The reliability and accuracy of PPP solutions depend on the number of satellites, satellite geometry, availability of signals, and quality of measurements. Though the GPS satellite constellation has reached full operational capability, poor satellite geometry due to obstructed environments still negatively impact the accuracy and reliability of solutions (Bisnath and Gao, 2008; Ge *et al*., 2008; Geng *et al.*, 2010; Héroux *et al*., 2004; Laurichesse *et al*., 2009). The integration of GPS and GLONASS constellations provides more signals, enhances good satellite geometry and improves the quality of solutions in PPP processing (Shen and Gao, 2006; Li and Zhang, 2013).

However, one of the challenges of integrating GPS and GLONASS in PPP processing is the fact that the GLONASS carrier-phase and pseudorange observations suffer from inter-frequency channel biases (ICBs). The ICBs originate from signal transmission through multiple frequency bands, each designated for a particular satellite. These pseudorange and carrier-phase biases are stable over time, but have no distinct pattern in terms of magnitude with respect to the GLONASS satellite frequencies. Various receiver and antenna types show varying characteristics with regards to these biases. To resolve GLONASS float ambiguities faster, the estimation and analysis of the GLONASS pseudorange and carrier-phase biases become a necessary step in GNSS PPP. With an increasing number of receiver and antenna hardware types, the error modelling for the pseudorange and carrier-phase biases become more complex, but is definitely warranted due

to the unique contribution of hardware biases coming from each receiver and antenna type. There is, in general, a limited understanding of these equipment biases, which introduce varying magnitudes of observable error due to each antenna-receiver-firmware combination.

The pseudorange and carrier-phase observations are affected by biases that can be categorized depending on the source of the bias. In general, the classification of GNSS biases can be made at the signal generation and user or receiver levels. Table 3.1 illustrates such a classification. A further categorization can be made when the pseudorange and carrier-phase measurements are considered, relative to the satellite and receiver GNSS segments. Finally, an inter-system classification of the GNSS biases exist when considering multiple constellations of satellites. It must be noted that the proper modelling of these biases become complex given that they originate both at the transmitter and receiver ends (Hefty and Gerhatova, 2012).

<table>
<tr><th colspan="2">SOURCE OF BIAS</th><th>GNSS BIASES</th></tr>
<tr><td rowspan="2">Satellite transmission and receiver level</td><td>Satellite related</td><td rowspan="2">Hardware biases
Firmware biases
Code measurement biases
Phase measurement biases</td></tr>
<tr><td>Receiver related</td></tr>
<tr><td rowspan="2">Code and carrier-phase observable</td><td>Satellite related</td><td rowspan="2">Inter-frequency biases
Differential code biases
Differential phase biases</td></tr>
<tr><td>Receiver related</td></tr>
<tr><td rowspan="2">Multi-constellations of satellites</td><td>Inter-system time system offset</td><td rowspan="2">GPS / GLONASS
GPS / Galileo
GPS / BeiDou</td></tr>
<tr><td>Inter-system coordinate system offset</td></tr>
</table>

Table 3.1: Classification of GNSS equipment biases with respect to their sources (Compiled from Takac, 2009; Schaer, 2012; Kozlov, 2000; Wanninger, 2011; Wanninger, 2012).

Table 3.1 intuitively shows that with the inclusion of BeiDou and Galileo satellites to GPS and GLONASS in PPP processing, the magnitude of the equipment biases originating from all the satellites can potentially deteriorate the solution. Wanninger (2011) and Banville (2013) show how ambiguity resolution is affected given the magnitude of the inter-frequency biases of GLONASS satellites in baseline processing. The problem is significantly worse when considering all equipment biases emanating from all satellite constellations, especially in terms of sub-centimetre accuracy for PPP solutions.

This chapter focuses on the estimation and calibration of the pseudorange ICBs in GLONASS-only PPP. The characteristics of GPS and GLONASS residuals are discussed, with emphasis on how the ICBs become inherent in the GLONASS residuals due to its FDMA signal structure. Finally, the effect of the calibration of the pseudorange ICBs, depending on the satellite PRN, receiver and antenna types, are analyzed with respect to PPP data processing.

3.1 Combined GPS and GLONASS PPP and residual characteristics

To fully analyze and assess the performance of GNSS PPP, the processing of GPS-only, GLONASS-only and GPS + GLONASS PPP based on a static receiver station, were investigated. For example, the IGS station NRC1's 24 hour dataset for DOY 196 in 2013, illustrates the expected processing results of a typical GPS, GLONASS and GPS + GLONASS PPP. NRC1 is located in Ottawa, Canada and it is part of the Canadian Active Control System (CACS), as well as the IGS tracking network.

Figure 3.1 shows the positional errors for GPS-only, GLONASS-only and combined GPS + GLONASS solutions. All solutions showed steady convergence, defined as a 10 cm threshold, for the horizontal components in 15 minutes. The GPS + GLONASS solution showed improvement with a convergence period of 10 and 15 minutes, for the horizontal and vertical components, respectively.

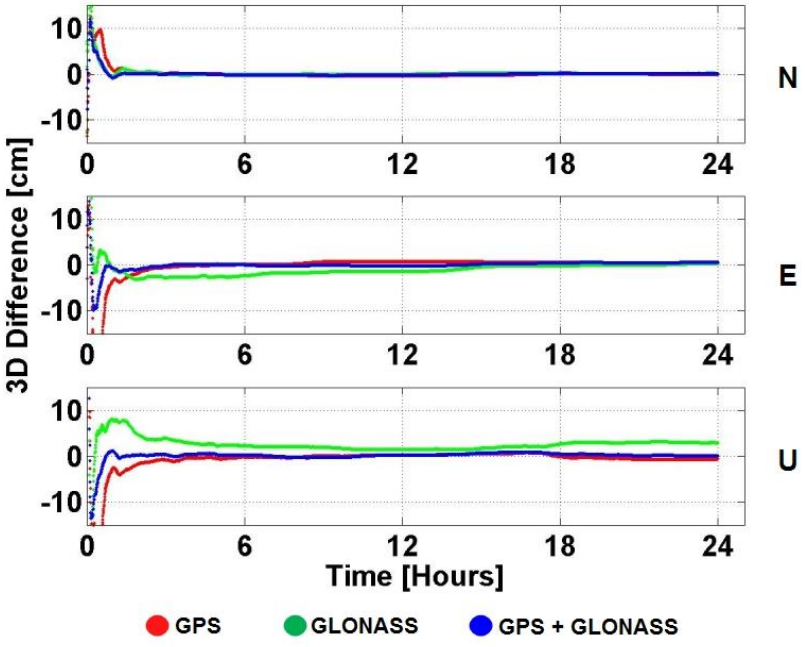

Figure 3.1: 3D difference in position errors for GPS, GLONASS and GPS + GLONASS solutions for station NRC1 24 hour dataset for DOY196 in 2013 in static processing mode

Table 3.2 shows the statistical results for the station NRC1 for GPS-only, GLONASS-only and GPS + GLONASS PPP solutions over a 24 hour period for the north, east and up components. The rms of the combined GPS + GLONASS PPP solution was 0.7, 0.4 and 1 mm in the east, north and up components, respectively, which was comparable to the GPS-only PPP with an rms of 0.6,

0.8 and 1 mm in the north, east and up components respectively. The horizontal component for the GPS + GLONASS PPP and GPS-only PPP were 0.8 and 1 mm, respectively. As shown in Table 3.3, the GLONASS-only PPP horizontal component was 1.7 mm, indicating that the GPS + GLONASS as well as GPS-only PPP results were better than that of GLONASS-only PPP though the difference was only in millimetres. The GPS + GLONASS PPP solution, from the statistics presented, shows an improved accuracy which is better than GPS-only and GLONASS-only PPP.

Statistic (mm)	GNSS processed	E (mm)	N (mm)	U (mm)
Std dev	GPS	0.7	0.5	1
	GLONASS	1.4	0.4	1
	GPS+GLONASS	0.7	0.3	0.8
rms	GPS	0.8	0.6	1
	GLONASS	1.6	0.5	2
	GPS+GLONASS	0.7	0.4	1

Table 3.2: 2D and 3D component statistics for GPS-only, GLONASS-only and GPS + GLONASS PPP by York GNSS PPP for station NRC1 24 hour dataset for DOY 196, processed in static mode. All units are in millimetres.

Statistic	GNSS processed	
2D rms	GPS	1
	GLONASS	1.7
	GPS+GLONASS	0.8
3D rms	GPS	1.4
	GLONASS	2.6
	GPS+GLONASS	1.3

Table 3.3: 2D and 3D component statistics for GPS-only, GLONASS-only and GPS + GLONASS PPP by York GNSS PPP for station NRC1 24 hour dataset for DOY 196, processed in static mode. All units are in millimetres.

Figure 3.2 and 3.3 illustrate the time series of the residuals for the ionosphere-free pseudorange and carrier-phase observations for GPS and GLONASS in GNSS PPP. Different satellites are represented by different colours.

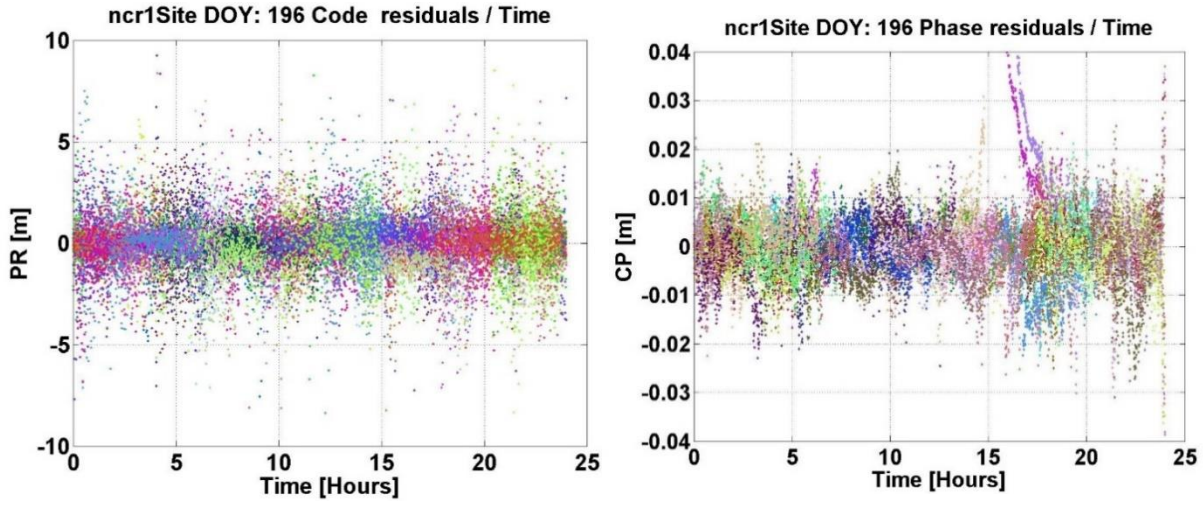

Figure 3.2: GPS-only time series for station NRC1 24 hour dataset for DOY196 during GPS week 1749 showing pseudorange (PR) and carrier-phase (CP) residuals in static processing mode

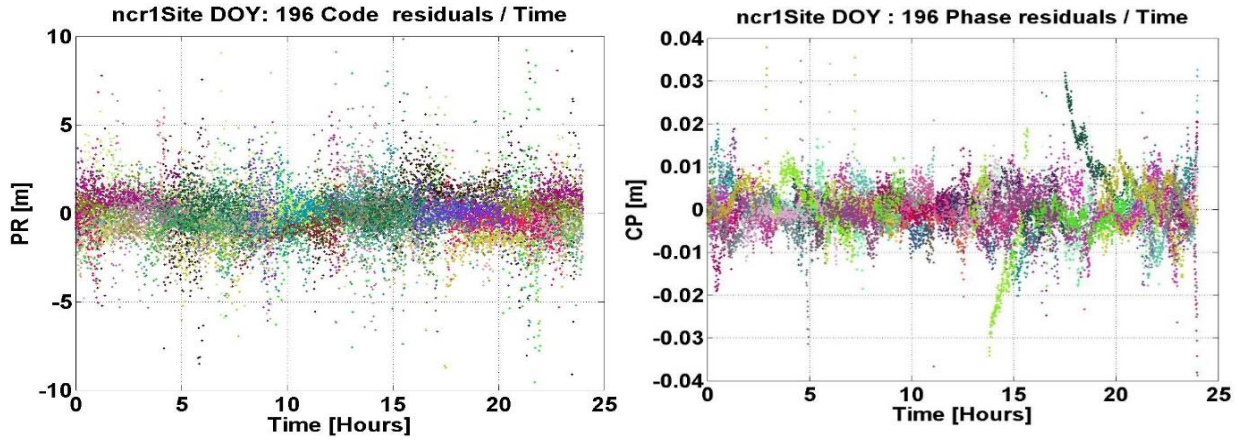

Figure 3.3: GLONASS-only time series for station NRC1 24 hour dataset for DOY196 during GPS week 1749 showing pseudorange (PR) and carrier-phase (CP) residuals in static processing mode

Comparing the GPS pseudorange residuals to that of GLONASS, the GLONASS pseudorange residuals are much noisier and vary between individual satellite residuals. The GLONASS ionosphere-free code observations have larger residual errors than the GPS ionosphere-free code observations. Potential reasons for this phenomenon involves the fact that the GLONASS observations are de-weighted because they are generally much noisier than GPS observations. Secondly, the inter-channel biases significantly affect the GLONASS ionosphere-free code observations due to each GLONASS satellite transmitting at a different frequency (Cai and Gao, 2013). The biases become apparent in the residuals if not estimated and calibrated out.

With respect to the relation between satellite elevation and the residuals, Figures 3.4 and 3.5 show how the pseudorange and carrier-phase ionospheric-free observations are dependent on the satellite elevation. It can be seen that both the pseudorange and carrier-phase residuals decrease as a function of increasing satellite elevation angle. The dependence of the residuals with increasing satellite elevation angle is similar for both GPS and GLONASS residuals. The presence of any bias is inherent in the residuals.

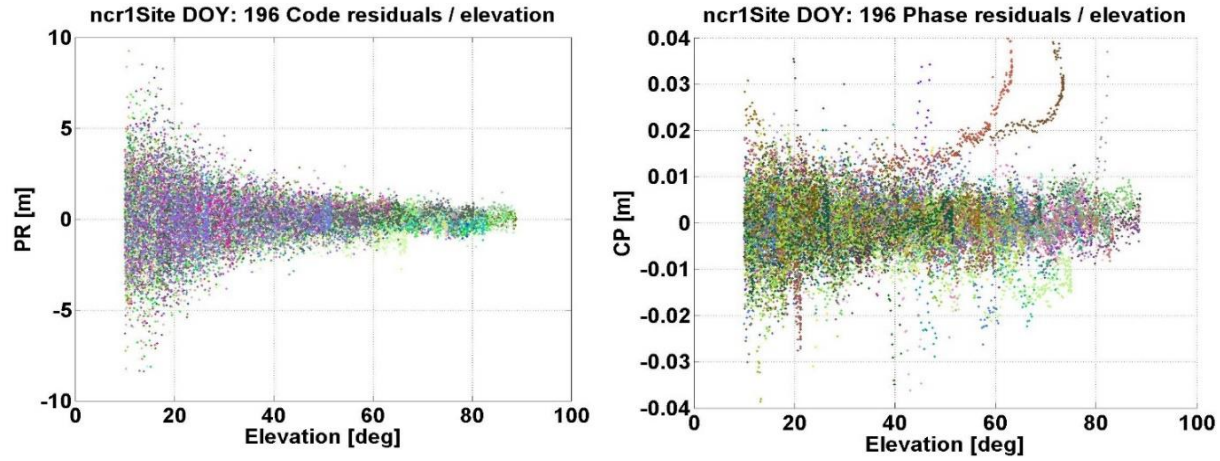

Figure 3.4: GPS residuals as a function of satellite elevation for station NRC124 hour dataset for DOY196 during GPS week 1749 in static processing mode.

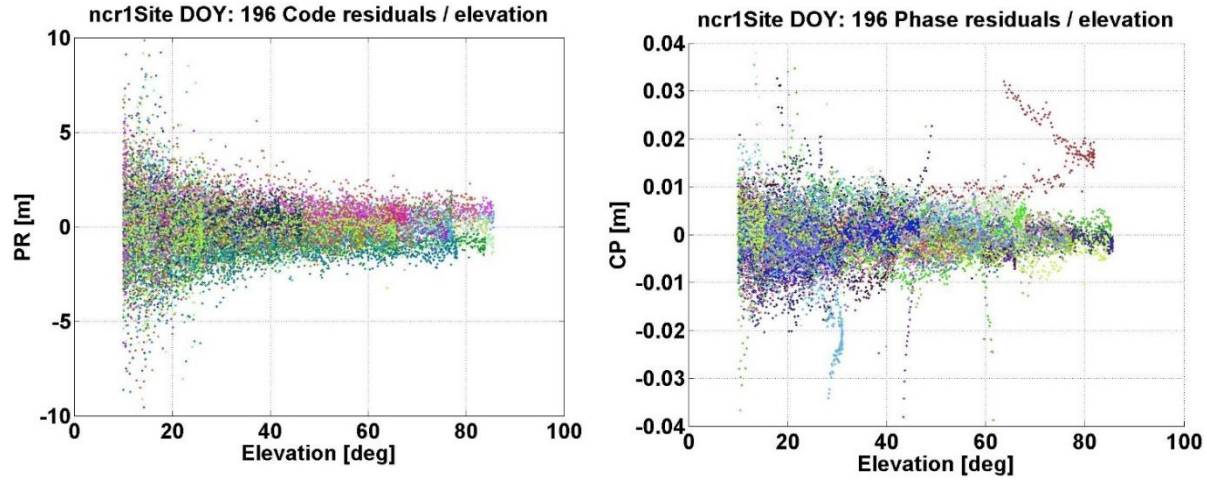

Figure 3.5: GLONASS residuals as a function of satellite elevation for station NRC124 hour dataset for DOY196 during GPS week 1749 in static processing mode.

3.2 Estimation and calibration of ICBs

With GLONASS at full operational capability in 2011, the concept of GLONASS PPP and GPS + GLONASS PPP has become a subject of interest as the addition of GLONASS presents more signals, better geometry of satellites and an improvement in the solution quality (Cai, 2009; Wang *et al*., 2012; Cai and Gao, 2013; Choy *et al*., 2013). The ICBs originate from the complex signal structure of GLONASS that is based on FDMA (Takac, 2009; Schaer, 2012; Kozlov, 2000; Povalyaev, 1997). Comparing GLONASS receiver types from different manufacturers, significant differences in the ICBs are noticeable and needs to be accounted for (Wanninger, 2011).

Wanninger (2012) analyzed the GLONASS inter-frequency carrier-phase biases and postulated that, for a given brand of receiver, the biases can be categorized with reference to the linear relation of the bias with respect to the GLONASS frequency number. Using short baseline data, Al-Shaery *et al*. (2012) estimated the pseudorange ICBs and indicated that these ICBs can reach up to several metres, and as such, cannot be ignored. Chuang *et al*. (2013) also estimated the pseudorange ICBs using solutions in standard point positioning in GPS + GLONASS processing, concluding that the ICBs are stable over time to the centimetre level and that there is a strong correlation between receiver firmware version and the ICBs. Banville (2013) estimated the pseudorange and carrier-phase ICBs with the purpose of resolving GLONASS ambiguities with mixed receiver types and firmware versions. By observing adjacent frequency numbers of two selected reference GLONASS satellites, it was concluded that the ambiguities can naturally converge to integer values, improving the resolution of the ambiguities.

GNSS pseudorange and carrier-phase observations, with the inclusion of GNSS biases, can be described in equations 3.1 and 3.2:

$$P_{L_i}^{GNSS} = \rho^i + c(\partial t^s - \partial t_r) + d_{ion,L_i} + d_{trop} + b_{Pr_i}^{L_i} + b_P^{L_i,s_j} + d_{multi\left(P_{L_i}\right)} + \varepsilon\left(P_{L_i}^{GNSS}\right) \quad (3.1)$$

$$\Phi_{L_i}^{GNSS} = \rho^i + c(\partial t^s - \partial t_r) + d_{trop} - d_{ion,L_i} + b_{\Phi r_i}^{L_i} + b_\Phi^{L_i,s_j} + \lambda_{L_i}, N_{L_i} + d_{multi\left(\Phi_{L_i}\right)} + \varepsilon\left(\Phi_{L_i}^{GNSS}\right) \quad (3.2)$$

The ionosphere-free combination observations, for GPS and GLONASS, can also be written as equations 3.3 to 3.6:

$$P_{ion,i}^{GPS,j} = c(\partial t^s - \partial t_r) + m_i^j T_i^w + \varepsilon(P_{ion,i}^{GPS,j}) \quad (3.3)$$

$$\Phi_{ion,i}^{GPS,j} = c(\partial t^s - \partial t_r) + m_i^j T_i^w + \lambda_{L_i} N_{L_i} + \varepsilon(\Phi_{ion,i}^{GPS,j}) \quad (3.4)$$

$$P_{ion,i}^{GLO,j} = c(\partial t^s - \partial t_r) + m_i^j T_i^w + b_{r_i}^{GLO_{L_i}} + b^{GLO_{L_i,s_j}} + \varepsilon(P_{ion,i}^{GLO,j}) \quad (3.5)$$

$$\Phi_{ion,i}^{GLO,j} = c(\partial t^s - \partial t_r) + m_i^j T_i^w + b_{r_i}^{GLO_{L_i}} + b^{GLO_{L_i,s_j}} + \lambda_{L_i} N_{L_i} + \varepsilon(\Phi_{ion,i}^{GLO,j}) \quad (3.6)$$

where

$P_{L_i}^{GNSS}, P_{ion,i}^{GPS,j}, P_{ion,i}^{GLO,j}$ - GNSS, GPS iono-free, GLONASS iono-free pseudorange measurement on L1 or L2 respectively (m)

$\Phi_{L_i}^{GNSS}, \Phi_{ion,i}^{GPS,j}, \Phi_{ion,i}^{GLO,j}$ - GNSS, GPS iono-free, GLONASS iono-free carrier-phase measurement on L1 or L2 (m)

ρ^i - Geometric range (m)

c - Speed of light (m/s^{-1})

∂t^s - Satellite clock error (sec)

∂t_r - Receiver clock offset (sec)

d_{ion,L_i} - Ionospheric delay (m)

d_{trop} - Tropospheric delay (m)

m_i^j - Tropospheric mapping function

T_i^w - Zenith tropospheric delay (m)

$b_{r_i}^{L_i}$, $b_{r_i}^{GLO_{L_i}}$ - Receiver GNSS equipment bias, GLONASS receiver pseudorange bias, respectively (m)

b^{L_i,s_j}, $b^{GLO_{L_i,s_j}}$ - Satellite GNSS equipment bias, GLONASS satellite pseudorange bias, respectively (m)

λ_{L_i} - Wavelength of L1 or L2 carrier waves (m)

N_{L_i} - Unknown cycle ambiguity term on L1 or L2 carrier-phases (cycles)

$d_{multi(\Phi_{L_i})}$ - Carrier-phase multipath on L1 or L2 (m)

$d_{multi(P_{L_i})}$ - Pseudorange multipath (m)

$\varepsilon(P_{L_i}^{GNSS})$, $\varepsilon(\Phi_{L_i}^{GNSS})$,$\varepsilon(P_{ion,i}^{GPS,j})$, $\varepsilon(\Phi_{ion,i}^{GPS,j})$, $\varepsilon(P_{ion,i}^{GLO,j})$, $\varepsilon(\Phi_{ion,i}^{GLO,j})$ - Measurement noise (m)

The ICBs for GPS, in GPS + GLONASS PPP processing, are non-existent, due to the CDMA signal structure, each GPS satellite transmits at the same frequency with different code modulations. The GLONASS satellites however transmit the same code with different frequencies. However, in a float solution, where the ambiguities are not fixed, the GLONASS carrier-phase ICBs are ignored as they are absorbed by the float ambiguities which affects PPP convergence as

well as performance. GLONASS PPP fixed ambiguity resolution becomes more challenging in the presence of these ICBs. A strong correlation between the GLONASS receiver clock offset and the pseudorange ICBs exist due to the ICBs being absorbed by the clock biases in the IGS Analysis Centres clock products (Chuang et al., 2013). A constraint, shown in equation 3.7, is placed to separate the effect of the pseudorange ICBs from the receiver clock offset. The constraint is placed with the assumption that one of the GLONASS satellite is free from the effect of the ICBs. With that assumption, the algebraic sum of the ICBs per PRN averaged over all the GLONASS satellites, should equal zero:

$$\frac{1}{24}\sum_{sat_{GLO}=1}^{sat_{GLO}=24} b_r^{sat_{GLO,j}} = 0$$

$b_r^{sat_{GLO,j}}$ - estimated ICB (3.7)

Given that the ICBs are also affected by the satellite and the specific clock biases of the ACs, it becomes necessary to separate the clock biases, originating from the satellites and the ACs, from the ICBs. Since the effects of the clock biases are the same on all stations, the effect of the clock biases common to all the satellites and inherent in the ICBs, can be subtracted. Shown in equation 3.8 is the "refined" daily ICB that results (Chuang et al., 2013):

$$\bar{b}_r^{sat_{GLO}} = \hat{b}_r^{sat_{GLO}} - \frac{1}{n}\sum_{r=1}^{n} \hat{b}_r^{sat_{GLO}}$$

where (3.8)

$\bar{b}_r^{sat_{GLO}}$ - refined ICB

$\hat{b}_r^{sat_{GLO}}$ - ICB affected by the satellite and AC satellite clock biases

3.3 Receiver type, antenna type and ICBs

350 IGS stations were used in the estimation of the GLONASS pseudorange ICBs. One week data from DOY 195 to 201 in 2013, were selected. Figure 3.6 shows the time series of the pseudorange ICB estimations for sample stations from DOY 195 to 201. The magnitude of the pseudorange ICBs are in the metre level, respectively. Though Figure 3.6 illustrates the changes seen in the pseudorange ICBs, the ICBs remain constant over the 7 day period with an absolute mean ICB of 0.89 m. The pseudorange ICBs had an average standard deviation of 21cm, considering 4 stations for PRN 35, 36 and 37. The uncertainties are approximately 5% to 30% of the ICB estimates for the pseudoranges. It therefore implies that the effect of pseudorange ICBs on the measurements may not be easily calibrated even though there might not be any receiver firmware update or change in the receiver antenna type. Chuang *et al*., (2013) estimated the pseudorange ICBs of 133 stations with an average standard deviation of 0.4 m which confirms the difficulty in the calibration of the pseudorange ICBs, given the uncertainties of the estimates.

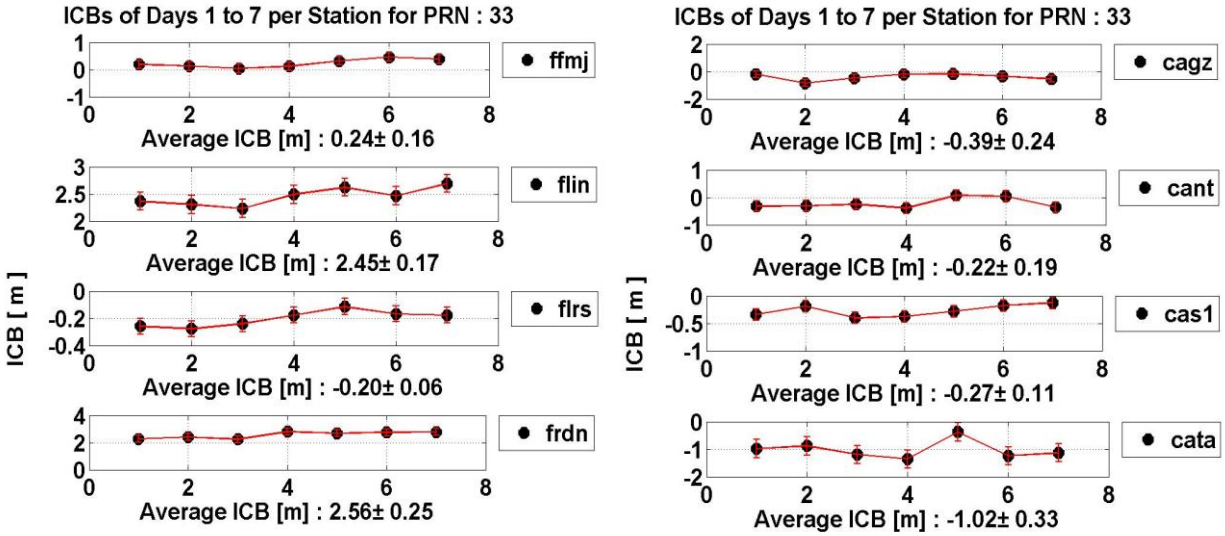
ICBs of Days 1 to 7 per Station for PRN : 33
ICB [m]
ffmj
Average ICB [m] : 0.24± 0.16
flin
Average ICB [m] : 2.45± 0.17
flrs
Average ICB [m] : -0.20± 0.06
frdn
Average ICB [m] : 2.56± 0.25
ICBs of Days 1 to 7 per Station for PRN : 33
ICB [m]
cagz
Average ICB [m] : -0.39± 0.24
cant
Average ICB [m] : -0.22± 0.19
cas1
Average ICB [m] : -0.27± 0.11
cata
Average ICB [m] : -1.02± 0.33

(a)

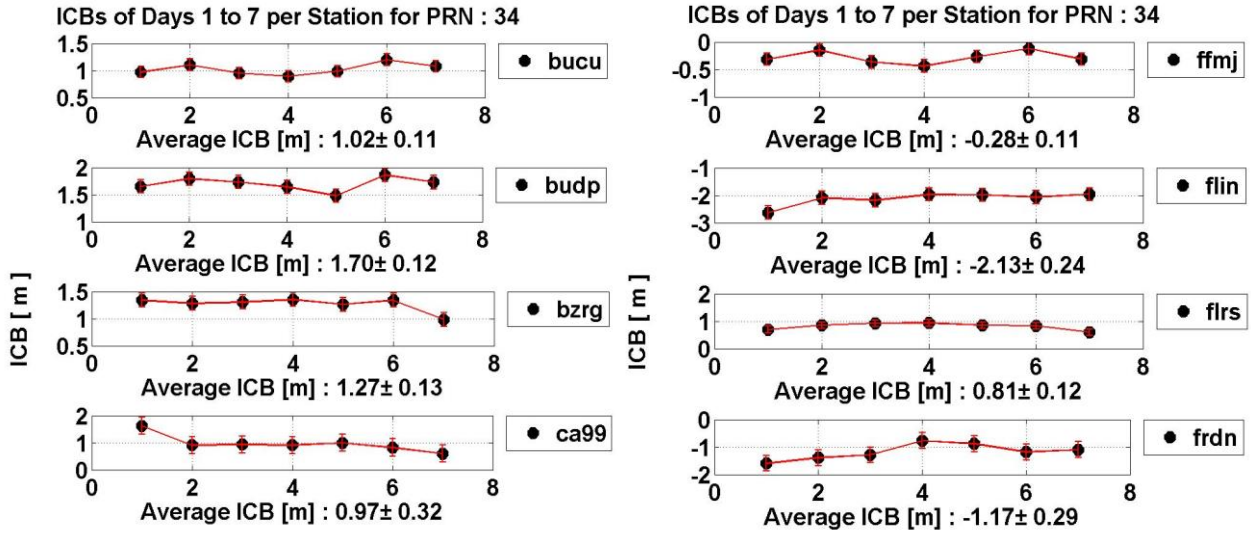
ICBs of Days 1 to 7 per Station for PRN : 34
ICB [m]
bucu
Average ICB [m] : 1.02± 0.11
budp
Average ICB [m] : 1.70± 0.12
bzrg
Average ICB [m] : 1.27± 0.13
ca99
Average ICB [m] : 0.97± 0.32
ICBs of Days 1 to 7 per Station for PRN : 34
ICB [m]
ffmj
Average ICB [m] : -0.28± 0.11
flin
Average ICB [m] : -2.13± 0.24
flrs
Average ICB [m] : 0.81± 0.12
frdn
Average ICB [m] : -1.17± 0.29

(b)

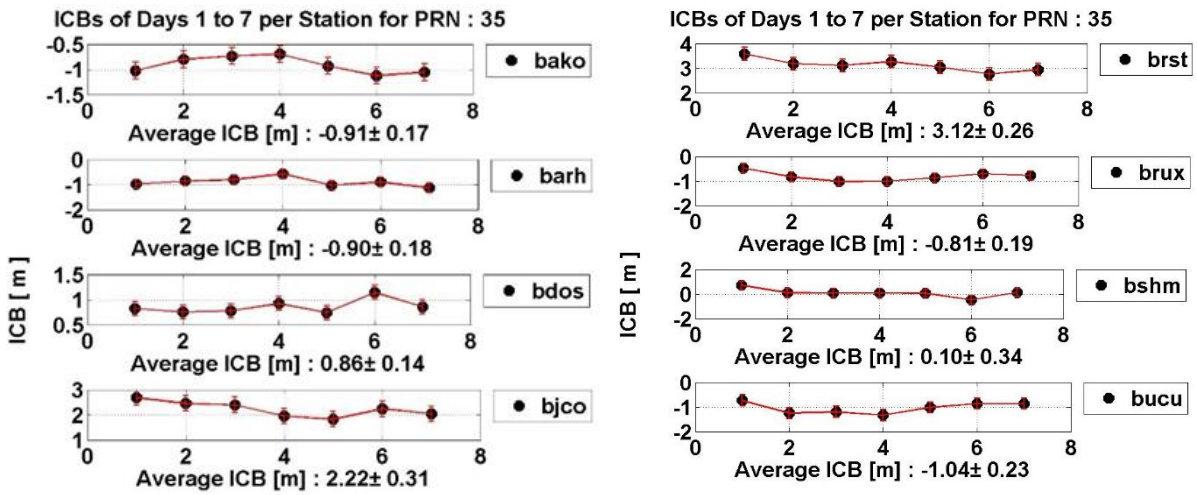

(c)

Figure 3.6: Pseudorange ICBs over a week period for sample stations a) PRN 33 (b) PRN 34 and (c) PRN 35

Table 3.4 shows the various receiver manufacturers, receiver type and number of stations falling under the receiver type category, which were used. This section investigates whether there is a correlation between the firmware versions of the receiver types and the pseudorange ICBs, with respect to the GLONASS frequency channel numbers.

To analyze the correlation between the receiver types, antenna types and the ICBs, IGS stations with 32 different receiver types from 8 manufacturers were used. 5 different scenarios corresponding to different possible receiver type, antenna type and firmware version combinations were analyzed.

Receiver manufacturer	Receiver type	Number of stations
JAVAD	JAVAD TRE_G3T DELTA	7
	JAVAD EGGDT	1
	JAVAD TRE_G3TH DELTA	24
	JAVAD TRE_G3TH SIGMA	31
AOA	AOA BENCHMARK ACT	1
	AOA SNR-8000 ACT	1
JPS	JPS E_GGD	6
	JPS EGGDT	9
	JPS LEGACY	10
LEICA	LEICA GR10	7
	LEICA GR 25	8
	LEICA GRX1200+GNSS	21
	LEICA GRX1200GGPRO	38
	LEICA GRX1200PRO	17
	LEICA GX1230+GNSS	1
	LEICA RS500	1
TPS	NET-G3A	15
	TPS E_GGD	3
	TPS GB-1000	1
	TPS LEGACY	2
	TPS NETG3	10
	TPS ODYSSEY_E	4
NOVATEL	NOV OEM4-G2	1
	NOV OEMV3	2
SEPT	SEPT POLARX2	4
	SEPT POLARX3ETR	3
	SEPT POLARX4	7
	SEPT POLARX4TR	1
TRIMBLE	TRIMBLE NETR5	19
	TRIMBLE NETR8	26
	TRIMBLE NETR9	59
	TRIMBLE NETRS	16
SUM		***356***

Table 3.4: Receiver manufacturers, receiver types and number of stations used for the estimation of the pseudorange ICBs

At least one of the varying components of the possible combinations had to be held fixed for the purpose of comparison. Table 3.5 highlights these different scenarios.

Scenario	Variability in antenna types	Variability in receiver types	Variability in firmware versions
1	Same antenna type	Different receiver types	Different firmware versions
2	Same antenna type	Same receiver type	Different firmware versions
3	Different antenna types	Same receiver type	Same firmware version
4	Different antenna types	Same receiver type	Different firmware versions
5	Same antenna type	Same receiver type	Same firmware version

Table 3.5: Various possible scenarios investigated in relation to the trend characteristics of the ICBs when considering different receiver-antenna-firmware version combinations

To investigate the characteristics of the ICBs with different receiver types and firmware versions, a common antenna type is held as a fixed parameter to all the stations being considered. Illustrated in Figure 3.7 are the ICB trend characteristics of stations ALGO, CAS1, CEDU, DUBO, GODZ, GOLD, HARV and HOB2. The antenna type common to all the stations, is AOAD/M_T. Table 3.6 however shows the different receiver types and firmware versions associated with the stations. There are linear and quadratic pseudorange ICB trends observed between the same

antenna type but different firmware versions and different receiver types, with respect to the GLONASS frequency numbers.

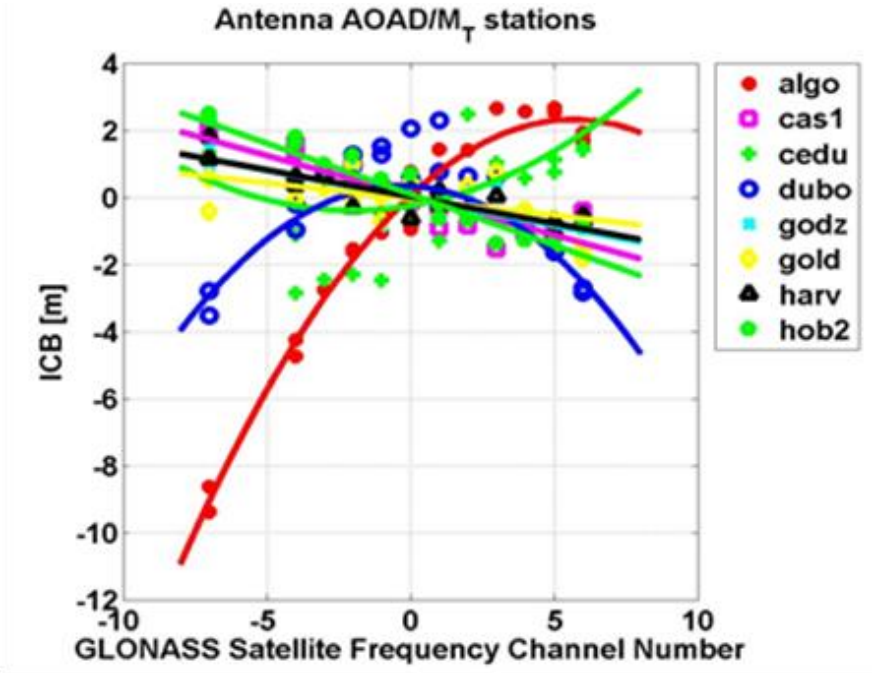

Figure 3.7: Pseudorange ICB trend characteristics of 8 stations with the same antenna type (AOAD/M_T) but different receiver type and firmware versions.

Site	Antenna	Receiver type	Firmware version
algo	AOAD/M_T	TPS NET-G3A	3.5
cas1		LEICA GRX1200GGPRO	8.20 / 3.019
cedu		TRIMBLE NETR8	4.48
dubo		TPS NETG3	3.5
godz		JPS EGGDT	2.70
gold		JPS EGGDT	2.70
harv		JAVAD TRE_G3TH DELTA	3.3.5
hob2		LEICA GRX1200GGPRO	8.01 / 3.019

Table 3.6: Receiver type and firmware versions of 8 stations used in the analysis of scenario 1. The antenna type was common for all the stations.

The second scenario investigates the characteristics of the ICBs with different firmware versions while holding the same receiver and antenna type fixed for all the stations. Figure 3.8 show the ICB trend characteristics of stations ATLI, BJFS, BRAZ, CUIB, DRAO, KARR, NAUS and POAL. The receiver and antenna type which are common to all the stations, are TRIMBLE NETR8 and TRM59800.00, respectively. Shown in Table 3.7 are the different firmware versions associated with the stations mounted with the same receiver and antenna type. Linear trends were observed for the pseudorange ICBs. However, there were variations in the linear trends for the pseudorange ICBs which ranged from a few centimetres to the metre level.

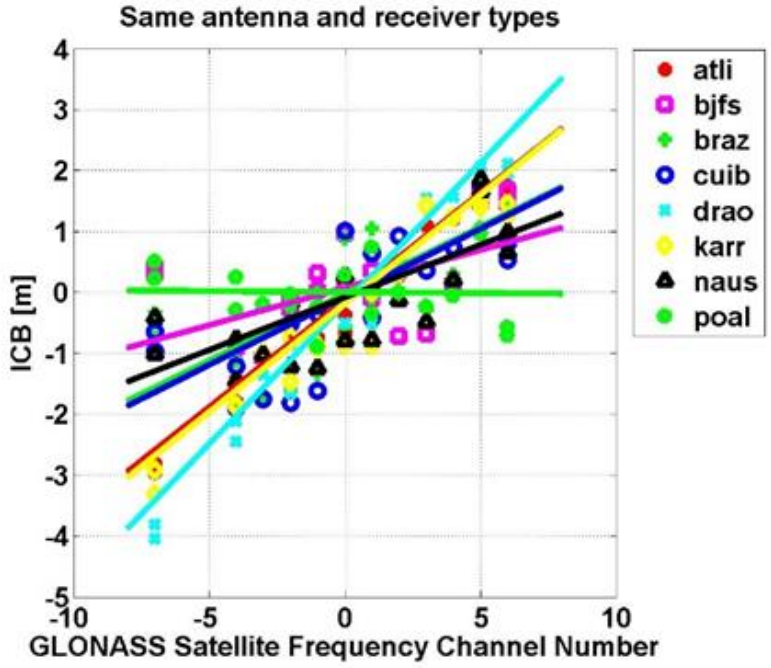

Figure 3.8: Pseudorange ICB trend characteristics of 8 stations with the same antenna and receiver type (TRM59800.00 and TRIMBLE NETR8, respectively) but different firmware versions.

Site	Antenna type	Receiver type	Firmware version
atli	TRM59800.00	TRIMBLE NETR8	4.48
bjfs			4.01
braz			4.7
cuib			4.7
drao			4.48
karr			4.48
naus			4.7
poal			4.7

Table 3.7: Firmware versions of 8 stations used in the analysis of scenario 2. The antenna and receiver types were common for all the stations.

Scenario 3 investigates the characteristics of the ICBs with different antenna types while holding the same receiver type and firmware version fixed for all the stations. Illustrated in Figure 3.9 are the ICB trend characteristics of stations ALON, JSLM, KABR, KATZ, MRAV, NZRT and YOSH. The receiver type and firmware version which are common to all the stations, are LEICA GRX1200PRO and 8.51, respectively. Table 3.8 shows the different antenna types which are associated with the stations. Linear trends were observed for the pseudorange ICBs. All the stations showed varying linear trends for the pseudorange ICBs with the exception of station NZRT which showed a quadratic trend.

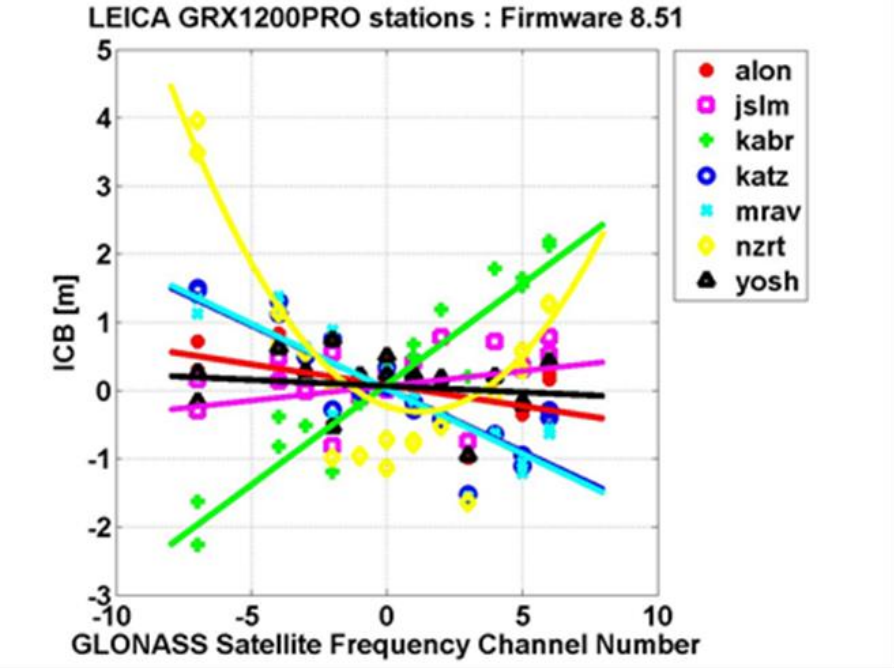

Figure 3.9: Pseudorange ICB trend characteristics of 7 stations with the same receiver type and firmware version (LEICA GRX1200PRO and 8.51, respectively) but different antenna types.

Receiver type	Firmware version	Site	Antenna type
LEICA GRX1200PRO	8.51	alon	LEIAT504_LEIS
		jslm	ASH701945B_M S
		kabr	ASH701945C_M S
		katz	TPSCR4_CONE
		mrav	LEIAT504GG_LEI
		nzrt	ASH700936B_M S
		yosh	LEIAT504_LEIS

Table 3.8: Antenna types of 7 stations used in the analysis of scenario 3. The receiver type and firmware version were common for all the stations

The fourth scenario investigates the characteristics of the ICBs with different firmware versions, different antenna types while holding the same receiver type fixed for all the stations. Figure 3.10 show the ICB trend characteristics of stations BZRG, CHAC, CONZ, GRAZ, KAT1, LAMA, LCK2 and LCKI. The receiver type which is common to all the stations, is LEICA GRX1200+GNSS. Shown in Table 3.9 are the different firmware versions and antenna types associated with the stations though they are mounted with the same receiver type. Linear trends were observed for the pseudorange ICBs for all the stations except for stations LCKI and LCK2, where both exhibited quadratic trends. This is potentially due to the fact that they were the only stations with same firmware versions.

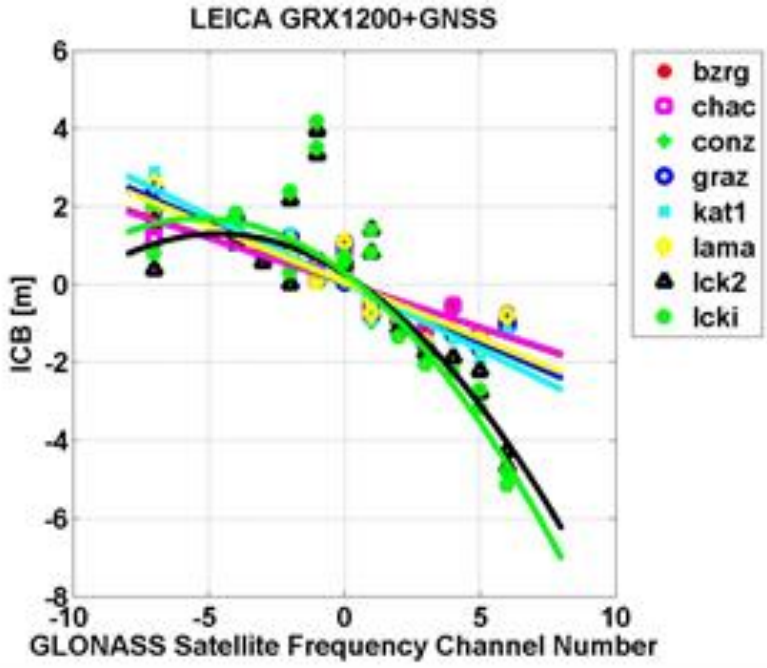

Figure 3.10: Pseudorange ICB trend characteristics of 8 stations with the same receiver type (LEICA GRX1200+GNSS) but different antenna types and firmware versions.

Site	Receiver type	Antenna type	Firmware version
brzg	LEICA GRX1200+GNSS	LEIAR25.R4	8.50/6.110
chac		LEIAS10	8.70/6.112
conz		LEIAR25.R3	8.71/6.112
graz		LEIAR25.R3	8.10 / 4.007
kat1		LEIAR25.R3	8.51/6.110
lama		LEIAT504GG	8.10/4.007
lck2		LEIAR25.R3	8.20/4.004
lck1		LEIAR25.R3	8.20/4.004

Table 3.9: Antenna types and firmware versions of 8 stations used in the analysis of scenario 2. The receiver type was common for all the stations

Scenarios 1 to 4 show that variations in the antenna-receiver-firmware combinations affect the ICB trend characteristics depending on the GLONASS frequency channel number. Scenario 5 involved the investigation of the characteristics of the ICBs with the same receiver type, antenna type and firmware versions. The expectation was to see similar trends for all stations. Figure 3.11 shows the ICB trend characteristics of stations BOAV, BOMJ, CATA, CEFE, IMPZ, POVE, SAVO and UFPR. Table 3.10 shows the antenna types which are associated with the stations. The receiver type, antenna type and firmware version which were common to all the stations, are TRIMBLE NETR5, TRM55971.00 and 3.84, respectively. All the stations show quadratic trends except for site CATA. However, site POVE has the same antenna type but an older model of it. It therefore may explain the variation in how convex the quadratic trend is, as compared to the others. Site CATA, though with the same antenna type as the others, shows a linear trend which was not expected.

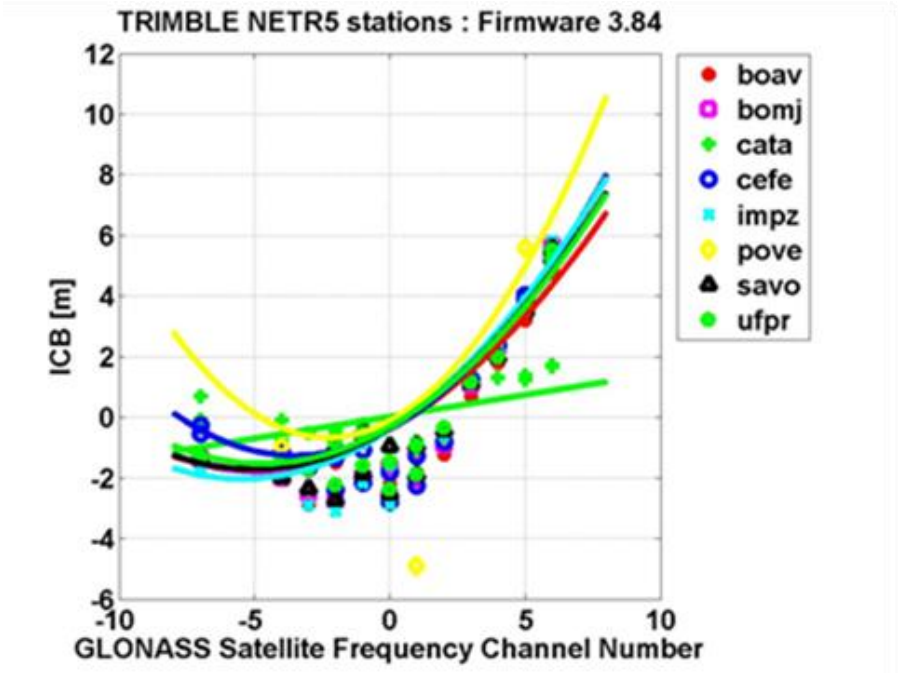

Figure 3.11: Pseudorange ICB trend characteristics of 8 stations with the same firmware versions, receiver and antenna types (TRIMBLE NETR5, TRM55971.00 and 3.84, respectively) but different antenna types and firmware versions.

Site	Receiver type	Antenna type	Firmware version
boav	Trimble NETR5	TRM55971.00	3.84
bomj		TRM55971.00	
cata		TRM55971.00	
cefe		TRM55971.00	
impz		TRM55971.00	
pove		TRM29659.00	
savo		TRM55971.00	
ufpr		TRM55971.00	

Table 3.10: Antenna types, firmware version and receiver type of 8 stations used in the analysis of scenario 5. The receiver, antenna types and firmware version were common for all the stations.

Similarly, considering the JAVAD TRE_G3T DELTA stations with firmware version 3.4.7, all the stations are equipped with the same antenna type, JAV_RINGANT_G3. Table 3.11 shows the stations which are mounted with the same antenna and receiver types with the same firmware versions. However, as Figure 3.12 illustrate, all the sites have similar ICB linear trends except RIO2 which shows a quadratic trend and a much more negative trend for the pseudorange ICBs.

The sites are widely distributed through the continents, from Asia, Europe, Africa, Oceania and South America. Though the years of the antennas of the sites vary, the variations in the trends are not profound with the exception of site RIO2. The site RIO2 is located in Tierra del Fuego, a region which has a sub-polar oceanic climate due to its proximity to the Antarctica. Though no current research has shown any correlation between the ICBs and climate or environmental factors, it could be a potential contributor to the variations in trends that has been observed. However, the more likely explanation could be because of gross errors in the metadata entry at the stations. The key note to all these scenarios is that the pseudorange ICBs are difficult to model or effectively mitigate when the hardware homogeneity, in terms of receiver-antenna-firmware version combination, of a station is compromised.

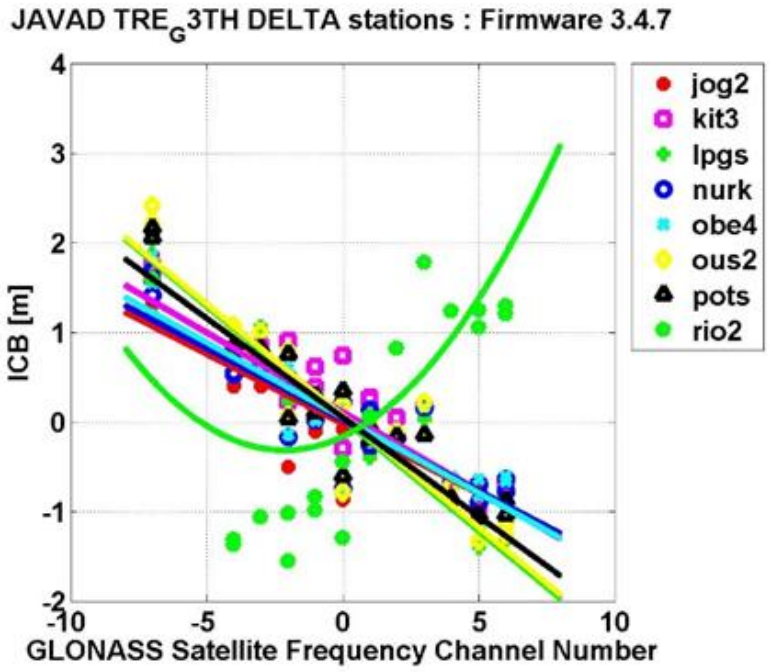

Figure 3.12: Pseudorange ICB trend characteristics of 8 stations with the same firmware versions, receiver and antenna types (JAVADTRE_G3T DELTA, JAV_RINGANT_G3 and 3.4.7, respectively) but different antenna types and firmware versions.

Site	Receiver type	Antenna type	Firmware version
jog2	JAVAD TRE_G3TH	JAV_RINGANT_G3TH DELTA	3.4.7
kit3			
lpgs			
nurk			
obe4			
ous2			
pots			
rio2			

Table 3.11: Pseudorange ICB trend characteristics of 8 stations with the same firmware versions, receiver and antenna types (JAVADTRE_G3T DELTA, JAV_RINGANT_G3 and 3.4.7, respectively) but different antenna types and firmware versions.

3.4 Pseudorange ICBs and impact on PPP convergence

3.4.1 GLONASS-only PPP after 20 minutes

The impact of the pseudorange ICBs on PPP convergence can be analyzed in the first few minutes of PPP processing when the pseudorange measurements dominate the solution before the carrier-phases take over. In determining the impact that the pseudorange ICB calibration has on PPP, initial convergence periods of 5, 10, 15 and 20 minutes were considered in GLONASS-only PPP and GPS + GLONASS PPP, using 350 IGS stations of 2500 datasets.

Figure 3.13 shows the effect of the pseudorange ICBs on the initial convergence of GLONASS-only PPP solutions in the first 5 minutes, before and after calibration. During the 5 minute convergence period, only the pseudorange measurements are used in the first few minutes before the carrier-phases dominate the solution. Without calibrating out the ICBs as shown in Figure 3.13(a), 1, 4, 16 and 17% of the stations had a horizontal error up to 25, 50, 75 and 100 cm, respectively. By calibrating the pseudorange ICBs, 1, 9, 23 and 32% of the stations had a horizontal error up to 25, 50, 75 and 100 cm, respectively. The vertical error, before calibration, as shown in Figure 3.13(b), had 1, 6, 15 and 13% of the stations with an error which equals or less than 25, 50, 75 and 100 cm, respectively. After calibration, 1, 5, 17, and 19% of the stations had a vertical error of 25, 50, 75 and 100 cm, respectively. In the horizontal component, after calibration, an improvement of 5% is observed considering a horizontal error of 50 cm. No improvement was observed for the vertical component considering a vertical error of 50 cm.

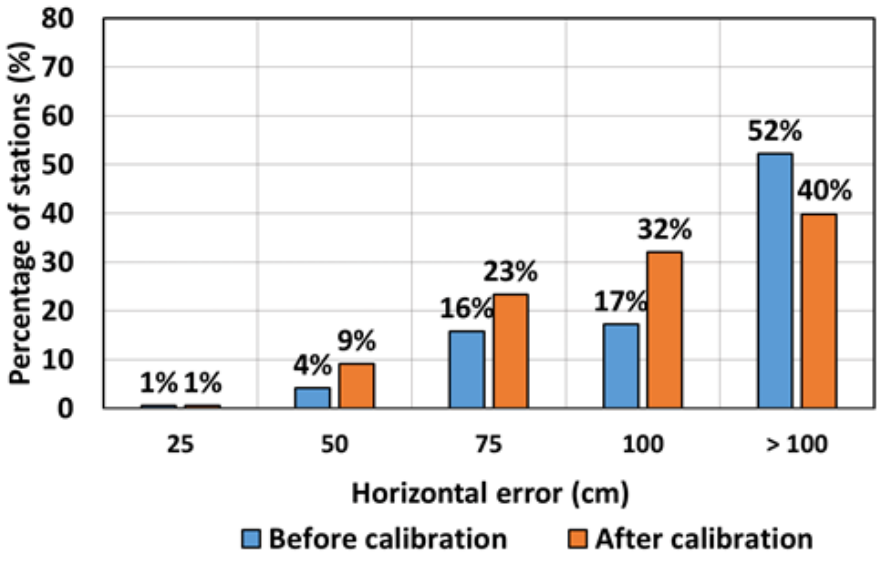

(a)

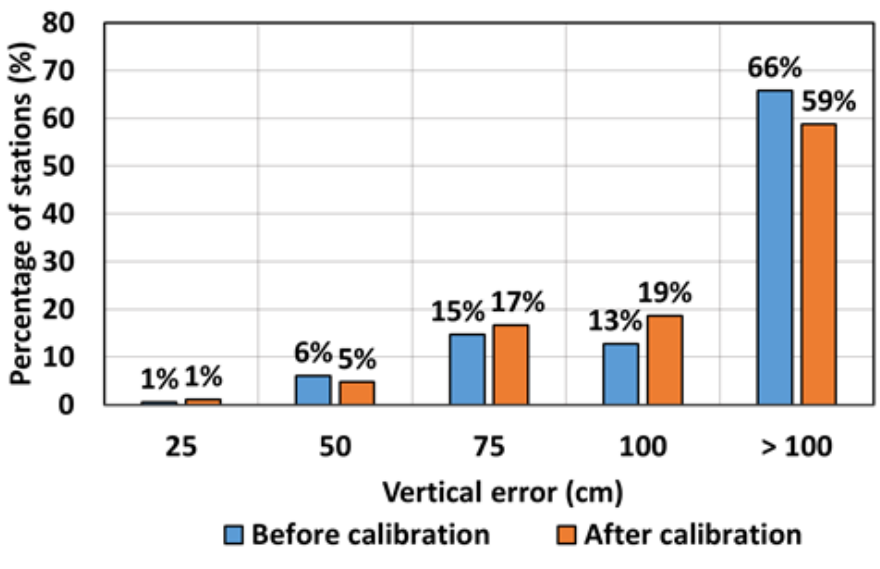

(b)

Figure 3.13: Horizontal and vertical error histogram of GLONASS PPP in the first 5 minutes of a 24 hour solution before and after pseudorange ICB calibration. (a) Horizontal error histogram before and after calibration (b) Vertical error histogram before and after calibration.

Considering a 10 minute convergence period as shown in Figure 3.14, 2, 16, 23 and 17% of the stations had a horizontal error which equals or less than 25, 50, 75 and 100 cm, respectively, without pseudorange ICB calibration. However, 3, 12, 21 and 15% of the stations had a vertical error that was less than or equal to 25, 50, 75 and 100 cm, respectively.

Upon calibration of the pseudorange ICBs, 1, 18, 35 and 21% of the stations had a horizontal error less than or equal to 25, 50, 75 and 100 cm, respectively. In the horizontal component, after calibration, an improvement of 2% is observed considering a horizontal error of 50 cm. The vertical component also improved insignificantly by 1% considering a vertical error of 50 cm.

A 15 minute convergence period was also considered where, 4, 20, 27 and 17% of the stations had a horizontal error which equals or less than 25, 50, 75 and 100 cm, respectively, without pseudorange ICB calibration. 3, 19, 22, and 18% of the stations also had a vertical error that was less than or equal to 25, 50, 75 and 100 cm, respectively. By calibrating out the pseudorange ICBs, 1, 30, 38, and 14% of the stations had a horizontal error less than or equal to 25, 50, 75 and 100 cm, respectively. 3, 20, 27 and 21% of the stations had a vertical error less than or equal to 25, 50, 75 and 100 cm, respectively. In the horizontal component, after calibration, an improvement of 10% is observed considering a horizontal error of 50 cm. The vertical component also improved by 1% considering a vertical error of 50 cm. Figures 3.15(a) and (b) illustrate the results before and after calibration of the pseudorange ICBs in the first 15 minutes.

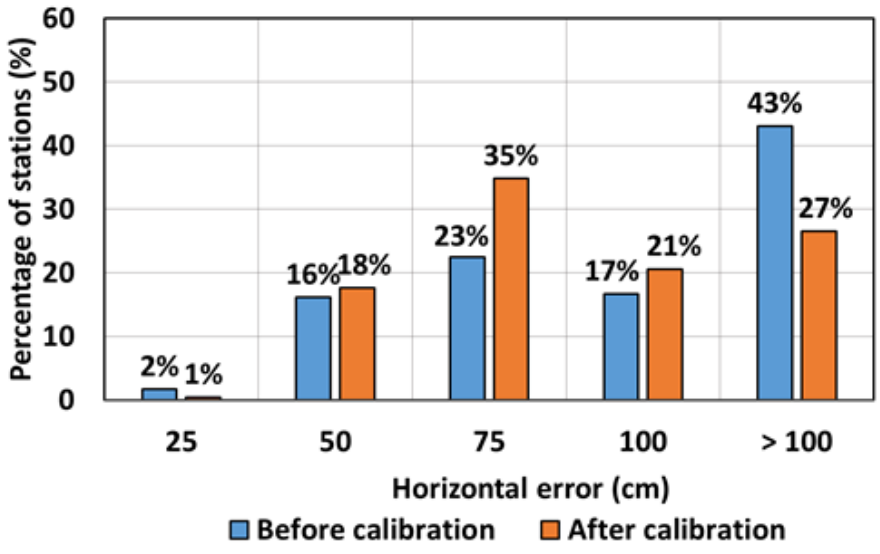

(a)

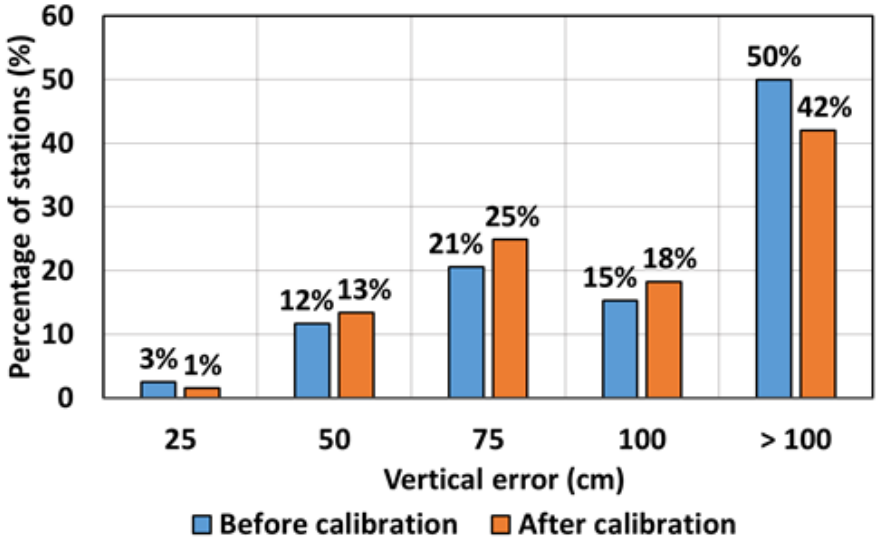

(b)

Figure 3.14: Horizontal and vertical error histogram of GLONASS PPP in the first 10 minutes of a 24 hour solution before and after pseudorange ICB calibration. (a) Horizontal error histogram before and after calibration (b) Vertical error histogram before and after calibration.

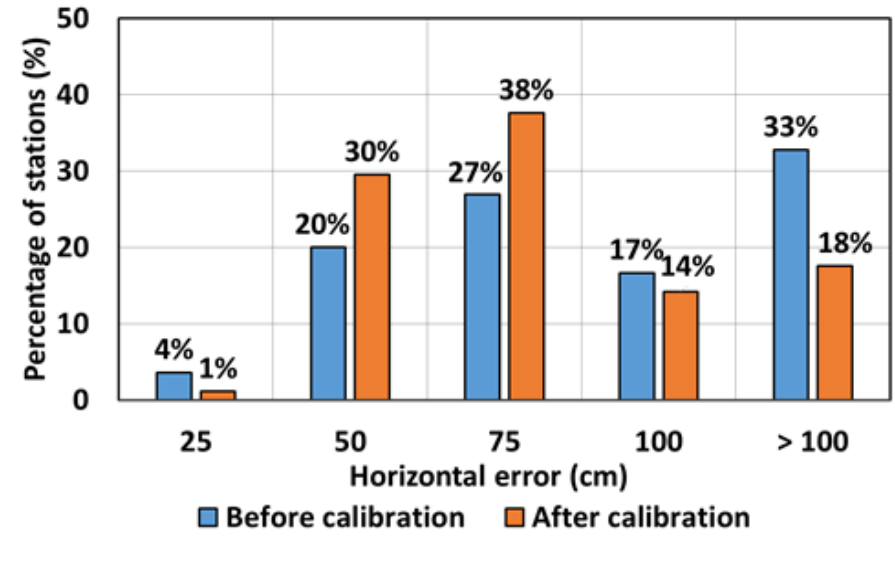

(a)

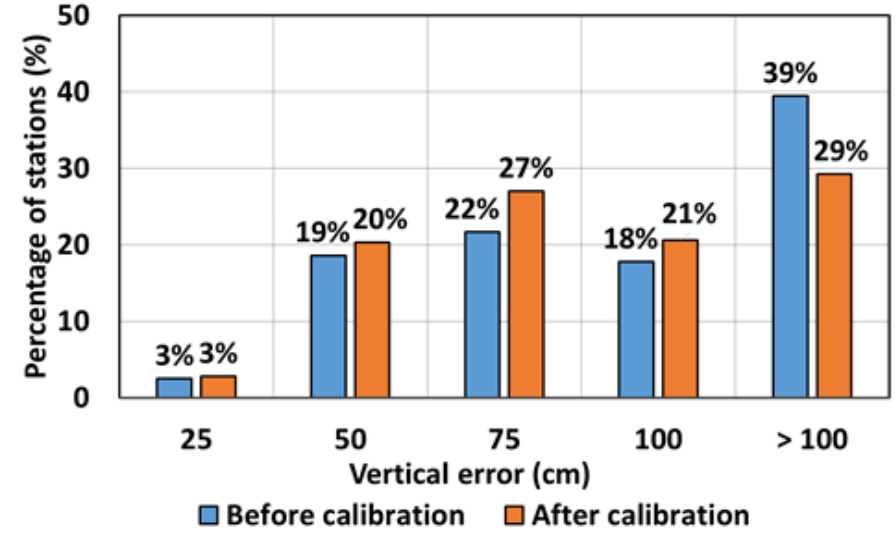

(b)

Figure 3.15: Horizontal and vertical error histogram of GLONASS PPP in the first 15 minutes of a 24 hour solution before and after pseudorange ICB calibration. (a) Horizontal error histogram before and after calibration (b) Vertical error histogram before and after calibration.

Figure 3.16 shows the effect of the pseudorange ICBs on the initial convergence of GLONASS PPP solutions in the first 20 minutes, before and after calibration. Without calibrating out the ICBs as shown in Figure 3.16(a), 1, 25, 27 and 16% of the stations had a horizontal error up to 25, 50, 75 and 100 cm, respectively. By calibrating out the pseudorange ICBs, 7, 44, 31 and 14% of the stations had a horizontal error of 25, 50, 75 and 100 cm, respectively. The vertical error, before calibration, as shown in Figure 3.16(b), had 1, 25, 22 and 17% of the stations with an error which is less than or equal to 25, 50, 75 and 100 cm, respectively. After calibration, 3, 26, 33 and 20% of the stations had a vertical error of 25, 50, 75 and 100 cm, respectively. In the horizontal component, after calibration, an improvement of 13% is observed considering a horizontal error of 50 cm. The vertical component also improved by 2 % considering a vertical error of 50 cm.

In summary, the results presented indicate that the GLONASS pseudorange ICBs impact the performance of GNSS PPP, especially in the first few minutes. GLONASS pseudorange ICBs can reach up to several metres, thus they cannot be ignored because they have an impact in the accuracy of PPP solutions. In the first 20 minutes, the horizontal and vertical components improved by an average of 19% and 1%, respectively, considering a horizontal and vertical error of 50 cm. The significance of these improvements become evident when resolving ambiguities within the first few minutes when the pseudorange measurements dominate the solution in GLONASS-only PPP processing.

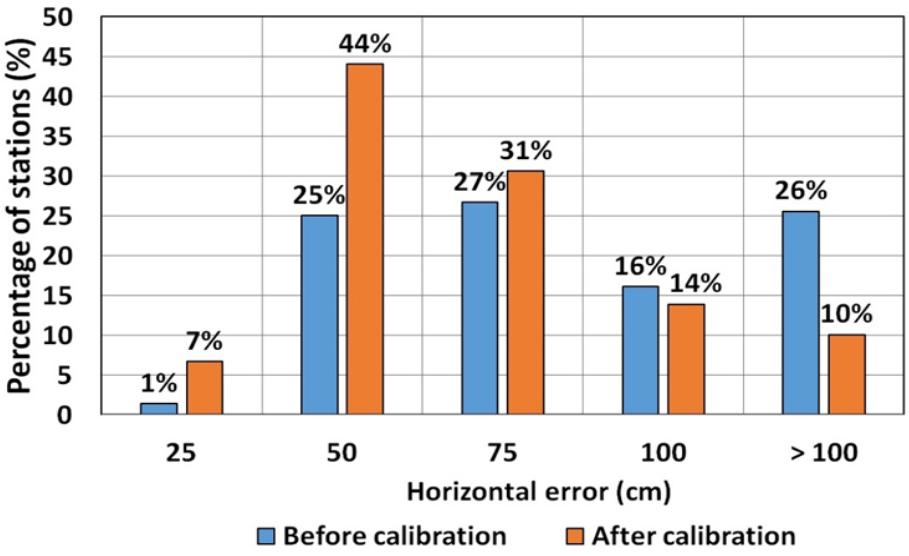

(a)

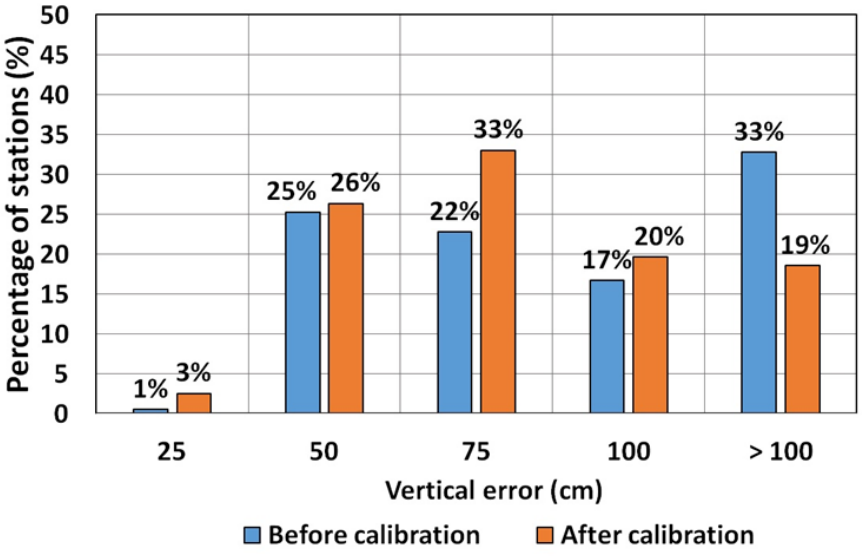

(b)

Figure 3.16: Horizontal and vertical error histogram of GLONASS PPP in the first 20 minutes of a 24 hour solution before and after pseudorange ICB calibration. (a) Horizontal error histogram before and after calibration (b) Vertical error histogram before and after calibration.

3.4.2 3D convergence analysis of GPS-only, GLONASS-only and GPS + GLONASS PPP after 15 minutes

A tight convergence constraint was placed in analyzing the effect of ICBs, before and after calibration in GPS + GLONASS PPP. A 20 cm convergence threshold in the first 15 minutes was chosen with the aim of investigating how the calibration of the ICBs can potentially assist in resolving ambiguities in the shortest possible time. Figure 3.17 shows the effect of the pseudorange ICBs on the initial convergence of GPS-only, GLONASS-only and GPS+GLONASS PPP solutions in the first 5 minutes, before and after calibration. 19 % of the solutions converged within 5 minutes for GPS PPP solutions with and without the ICB calibration. Without calibrating out the ICBs for GLONASS PPP, 7 % of the solutions converged. After calibration, there was a 3% improvement in the convergence rate. 22 and 26% of the solutions converged for GPS + GLONASS PPP before and after calibration. In general, the improvement seen in the first 5 minutes was less than 5% which was significantly low.

Figure 3.18 shows the effect of the pseudorange ICBs on the initial convergence of combined GNSS PPP solutions in the first 10 minutes, before and after calibration. 51% of the solutions converged within 10 minutes for GPS PPP solutions with and without the ICB calibration. Without calibrating out the ICBs for GLONASS PPP, 34% of the solutions converged. After calibration, there was a 7% improvement in the convergence rate. 57 and 61% of the solutions converged for GPS + GLONASS PPP before and after calibration. In general, the improvement seen in the first 10 minutes was about 6%.

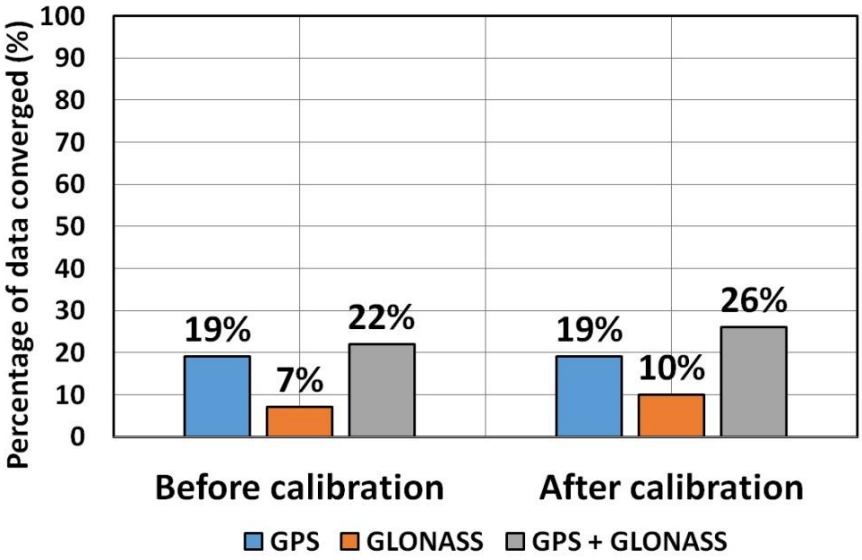

Figure 3.17: Histogram showing convergence of GPS-only, GLONASS-only and GPS + GLONASS PPP in the first 5 minutes of 24 hour solutions for 350 IGS stations before and after pseudorange ICB calibration. Datasets were processed in static mode.

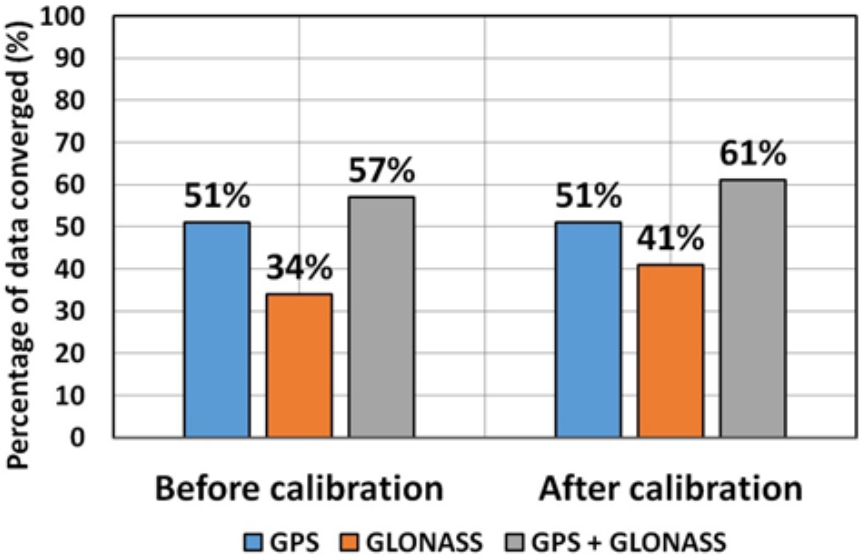

Figure 3.18: Histogram showing convergence of GPS-only, GLONASS-only and GPS + GLONASS PPP in the first 10 minutes of 24 hour solutions for 350 IGS stations before and after pseudorange ICB calibration. Datasets were processed in static mode.

Figure 3.19 shows the effect of the pseudorange ICBs in the first 15 minutes, before and after calibration. 69 % of the solutions converged within 15 minutes for GPS PPP solutions with and without the ICB calibration. Without calibrating out the ICBs for GLONASS PPP 54 % of the solutions converged. After calibration, there was a 6% improvement in the convergence rate. 78 and 82% of the solutions converged for GPS + GLONASS PPP before and after calibration. In general, the improvement seen in the first 15 minutes was 4%.

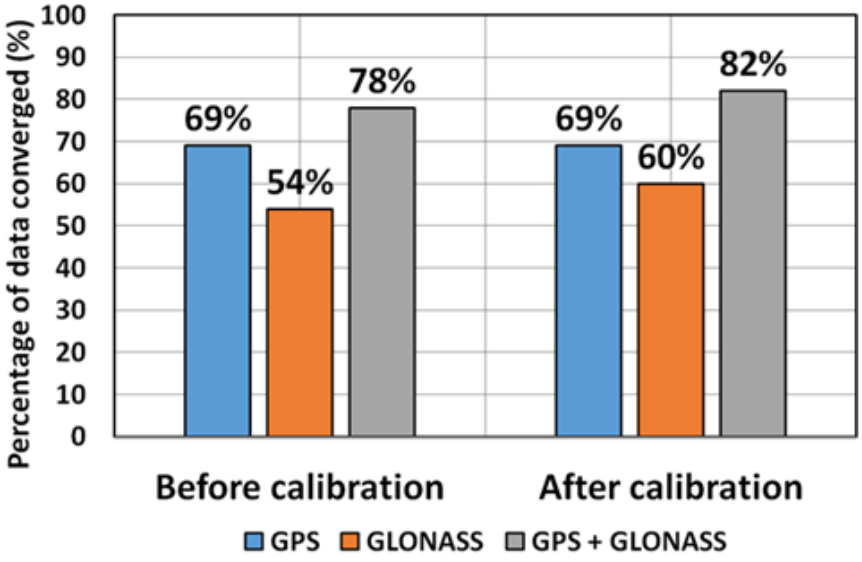

Figure 3.19: Histogram showing convergence of GPS-only, GLONASS-only and GPS + GLONASS PPP in the first 15 minutes of 24 hour solutions for 350 IGS stations before and after pseudorange ICB calibration. Datasets were processed in static mode.

In summary, improving the convergence period of GNSS PPP is critical for various applications like precision agriculture, hydrographic surveying and remote sensing. Given that GLONASS observations are affected by inter-frequency biases, the effect of the pseudorange ICBs on convergence period was investigated in GLONASS-only PPP and GPS + GLONASS PPP

solutions. Time intervals of 5, 10 and 15 minutes were considered for the analysis because of the dominance of the pseudorange measurements within that time period. After calibration of the GLONASS pseudorange ICBs, there was an average improvement of 5% and 4% in the percentage of datasets that converged for GLONASS-only PPP and GPS + GLONASS PPP, respectively.

3.5 Effects of averaged and daily ICBs

The use of average ICB estimates over days to calibrate out the effect of these biases has proved beneficial, but not without some limitations. From the previous section, it has been observed that the uncertainties of the biases can be greater than the estimated ICBs given the observation data and the length of the days averaged. The quality of the measurements at a station is vital to the estimation of the ICBs. However, the alternative is to estimate the ICBs by taking into consideration, not only the quality of the observations, but the AC-satellite common mean error affecting the stations on a particular day. The error can be easily determined and calibrated out as shown in equation 3.8. However, it is interesting to note the characteristics of the AC-satellite common mean error with regards to pseudorange and carrier-phase measurements of 350 IGS stations, averaged over 7 days. Figure 3.20 illustrates the characteristics of the AC-satellite common mean error in relation to the GLONASS frequency channel number, of the pseudorange and carrier-phase measurements respectively. There is a correlation of the errors for the pseudorange measurements with the GLONASS frequency channel numbers which reflects the fact that the errors are similar on all the GLONASS satellites irrespective of the antipodal nature of the GLONASS satellite pairs.

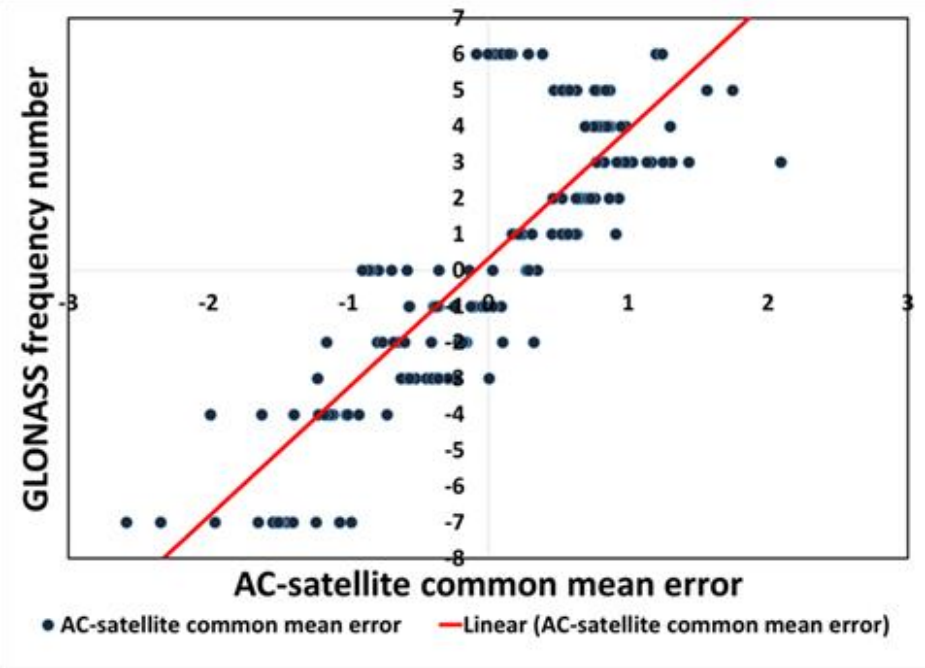

Figure 3.20: Correlation between the AC-satellite common mean errors and GLONASS satellite frequency number for pseudorange ICB calibration.

3.6 Summary

In this chapter, the GLONASS pseudorange ICBs were estimated for 350 IGS stations with varied receiver-antenna type combinations. The following conclusions could be drawn from the results presented; first, though the GLONASS pseudorange ICBs remain stable over time, the magnitude of the uncertainties is about 5% to 30% of the ICB estimate which makes it a challenge in accurately calibrating them out. It implies that there may be other biases inherent in the estimated ICBs that have not been accounted for. Second, there is a correlation between the GLONASS pseudorange ICBs of stations and various receiver types, antenna types and firmware versions. The more homogeneous a group of stations are, in terms of receiver type, antenna type

and firmware version, the more correlated the pseudorange ICBs are with the GLONASS frequency numbers. Different scenarios were presented to show how the correlations of a heterogeneous or homogeneous network of stations affect the calibration of the GLONASS pseudorange ICBs. Third, the impact of GLONASS pseudorange ICB calibration on GNSS PPP processing was investigated. The improvements seen in the horizontal and vertical components as well as convergence period, indicate that the presence of biases can significantly impact the performance of GNSS PPP processing. It is essential that the biases be mitigated, especially in the resolution of float ambiguities which is critical in the first few minutes of GNSS PPP solutions. Fourth, the AC-satellite common mean error was estimated which strongly correlated with the GLONASS frequency channel numbers. The correlation indicated an alternative way of estimating the daily GLONASS pseudorange ICBs, rather than averaging over days.

Chapter 4
Conclusions and Recommendations

With the emergence of GLONASS, GALILEO and BeiDou satellite constellations, PPP has or will achieve better solution quality and accuracy due to more available signals, better geometry of satellites. In challenging scenarios, for instance urban areas, deep pit mines and canyons, the GNSS signals become compromised as the signal reception is affected due to bad line of sight and multipath interference. With the expanding multi-satellite constellations, there is the possibility of choice, in preferring the best and strong signals over the weak ones, in order to maintain better solution quality. The availability of more multi-constellational satellites and signals means the ability to achieve better positional accuracy without the worry of satellite-signal interruptions.

However, the interoperability among the GNSS constellations present challenges that have to be dealt with. There are clear and discernible differences between the satellite constellations with regards to their signal structures. The question of interchangeability is raised due to these differences in the signals. As a product of the complexity of the signal structure, from different satellite constellations, there are biases to be considered if multi-GNSS PPP should reach optimal accuracy.

As a means of addressing the above problems, it was the primary objective of this research to commence the development of the complete multi-GNSS PPP software architecture, with the aim of estimating or modelling all significant GNSS biases. This approach is not only a step closer

in achieving signal interchangeability among the GNSS constellations, but also improving the solution integrity, quality and accuracy of multi-GNSS PPP processing.

Also presented in this study is the estimation and calibration of GLONASS pseudorange ICBs based on receiver and antenna types, through the developing a GNSS (GPS and GLONASS) PPP software which meets scientific standards, compared to existing PPP services.

The York GNSS PPP software processor was developed in ANSI C++ language on the Microsoft.NET platform, with over 100 functions grouped in classes. Using MATLAB for statistical analysis, a total of over 27,000 lines of C++ and MATLAB lines codes were written by the author. The goal of the object-oriented structure of the processor was to maintain a robust and scalable software framework, with the concept of adding more GNSS satellite constellations in the near future.

4.1 Conclusions

4.1.1 Performance of GNSS PPP

. In ascertaining that the York GNSS PPP processor met scientific standards, it was compared to four online PPP services. Employing combined GPS and GLONASS PPP processing of 40 stations over a week data, the results showed that the York GNSS PPP processor differed in millimetres from the online PPP services.

To further assess the performance of the York GNSS PPP software package, 350 stations distributed globally, one week data, were processed in GPS-only, GLONASS-only and combined GPS and GLONASS PPP processing modes. The overall rms was 1, 1 and 3 mm in the north, east

and up components, respectively, for GPS-only PPP; 2, 2 and 3 mm in the north, east and up components, respectively, for GLONASS-only PPP; 1, 1 and 2 mm in the north, east and up components, respectively, for combined GPS and GLONASS PPP

4.1.2 GLONASS pseudorange ICBs in relation to PPP

With the possibility of a few GPS satellites being tracked, GLONASS observations become necessary in combined GPS and GLONASS PPP. However, each GLONASS satellite transmits with a different frequency that introduces inter-frequency biases. The concentration on the estimation and calibration of pseudorange ICBs and its effects on GNSS PPP is needed with regards to combined GPS and GLONASS PPP. The overall rms of GLONASS PPP before and after the pseudorange ICB calibration were analyzed considering the convergence periods of 5, 10, 15, and 20 minutes. Table 4.1 shows the rms of 350 IGS stations used in static GLONASS PPP processing for the first 20 minutes. There was a 17% and 19% improvement in the rms of the horizontal and vertical components, respectively, after calibration of the ICBs. The 3D component also improved by 20%.

25% of the stations processed had a horizontal and vertical error that was less or equal to 50 cm before the pseudorange ICB calibration with 20 minutes convergence. However, after calibrating out the pseudorange ICBs, the percentage of stations that had horizontal and vertical errors less or equal to 50 cm improved by 19% and 1%, respectively. By calibrating out the pseudorange ICBs, the horizontal accuracy of GLONASS-only PPP is significantly improved in the first few minutes of a 24 hour solution, but not in terms of vertical accuracy.

	Component	max	mean	rms
Before	Horizontal	61	16	58
	Vertical	58	11	68
	3D	72	20	96
After	Horizontal	31	10	48
	Vertical	73	11	55
	3D	79	16	77

Table 4.1: 20 minutes solution produced by York GNSS PPP from 24 hour datasets from 350 sites for DOY 195-201, processed in static mode for a total sample size of 2500. All units are in centimetres.

4.1.3 Characteristics and effects of GLONASS pseudorange ICBs

350 receiver stations, from 32 receiver manufacturers capable of processing GPS and GLONASS, were used in the estimation and calibrations of the GLONASS pseudorange ICBs. The conclusions involve the fact that the GLONASS ICBs are stable over time. The stability of the pseudorange ICBs provide an advantage in calibrating them out as it can be certain that there is not much variation from day-to-day. There is also a strong correlation between the ICBs, the same receiver type and firmware versions. However, there is little correlation between different receiver firmware versions and the pseudorange ICBs. There is, however, a correlation between the different antenna types and the GLONASS inter-frequency channel numbers. There were trend patterns, both linear and quadratic, that exist between the pseudorange ICBs and the GLONASS channel numbers, in relation to the receiver types, receiver firmware versions and the antenna types. Small variations in the order of a few millimetres, were observed in the ICBs with

heterogeneous combination of receiver-antenna combinations as well as firmware versions. Given that each GLONASS satellite transmits at a different frequency, the magnitude of the ICBs vary from satellite to satellite.

Organizations, such as IGS, are recommended to provide the ICB products for calibration based on each GLONASS PRN and frequency, as well as the receiver type, antenna type and firmware version. As a novel alternative approach, the AC-satellite common errors can be made into a product and subtracted from the daily ICB estimations in the least-squares adjustment process. As presented in this work, there is a correlation between AC-satellite common mean errors and the GLONASS satellite frequency numbers. The correlation implies that the same common satellite error can be subtracted from the daily ICB estimates for two antipodal GLONASS satellites to obtained refined ICB estimates.

4.2 Recommendations for future research

This study is a commencement to a grand idea of involving all available GNSS satellite constellations, conducting experiments with the aim of improving or solving current and pertinent research problems affecting the GNSS community. Some recommendations are therefore made in this section for potential future contributions.

4.2.1 Multi-GNSS PPP processing

GPS, GLONASS, GALILEO and BeiDou offers many advantages to the PPP end user. These advantages range from increased number of visible satellites, stronger signals and redundant observations, to improved solution position accuracy, reliability, integrity and availability. This

research has already broken ground in the implementation of a “complete” GNSS PPP software architecture. The near future would see the expansion of the York GNSS PPP processor into a full functioning software package capable of processing all available satellite constellations. However, there are existing problems to consider when it comes to GNSS interoperability. These limiting issues include solving for the system time offsets between the GNSS constellations which presents itself as a bias to be dealt with. Other biases exist, both from the GNSS satellite constellations and the user receiver ends, which has to be solved. The issue of dealing with equipment biases, is one of the primary near future goals to be solved to further improve inter-compatibility between the GNSS satellite constellations.

4.2.2 Real-time GNSS PPP processing

Network RTK undoubtedly provides the best accuracy in positioning and is currently available and used in a broad range of applications. However, it is a disadvantage in building and maintaining the reference station network. The requirement and need to maintain communication between the stationary reference station and the roving receiver, can also become a problem. As convenient as network RTK is, there are scenarios where a reference station or mobile network may not be visible. Due to such cases, the use of real-time GNSS PPP is fast developing and serves as a potential alternative to network RTK with low cost maintenance. Two main problems are presented with the use of GNSS PPP in real-time. The first issue has to do with the fact that GNSS PPP, in general, depends on the use of satellite clock and orbit information to achieve accurate solutions. The predicted satellite orbit and clock products for real-time positioning reduces the

accuracy of the solution as compared to post-processing. It is a problem which is going to be compounded in the near future when all GNSS satellite constellations are considered, given inter-satellite constellation biases that exists between them. The second issue relates to latency and convergence period, which depends on the broadcast and quality of the satellite information, respectively.

Work has already began in the expansion of the York GNSS PPP processor to handle real-time data processing options. Through the NTRIP casters, the real-time precise satellite orbits and clock corrections would be transmitted together with atmospheric corrections.

4.2.3 GNSS Ambiguity Resolution

Over the past few years, much research has gone into integer ambiguity resolution of carrier-phase observations. Ambiguity resolution in GNSS PPP processing has become a focal point in research due to the many challenges presented because of the expanding satellite constellations and the complexity of the signal structures. Non-integer biases are usually mitigated significantly in double-differencing processing but are a major challenge in GNSS PPP, considering that un-differenced carrier-phase observations are used. The problem exists because of the fractional cycle biases in the GNSS observations that are absorbed into the un-differenced float ambiguity estimates, preventing the estimates to naturally converge to integers. One of the primary goals in the near future is the estimation of the GNSS biases affecting the carrier-phase measurements coming from different satellite constellations. The aim will be to isolate these biases

in processing through modelling and calibration, leading to shorter convergence periods, near-integer realistic float ambiguities.

References

Al-Shaery A, S Zhang, C Rizos (2012). “An enhanced calibration method of GLONASS inter-channel bias for GNSS RTK.” GPS Solutions, April 2013, Volume 17, Issue 2, pp 165-173.

Astronomical Institute of University of Bern (2007). “Bernese GPS Software Version 5.0”. University of Bern, Astronomical Institute, Stampfli Publications, pp. 475-552.

Banville S (2013). “GLONASS ambiguity resolution of mixed receiver types without external calibration.” GPS Solutions, July 2013, Volume 17, Issue 3, pp 275-282.

Bisnath S and Y Gao (2009). "Current State of Precise Point Positioning and Future Prospects and Limitations." International Association of Geodesy Symposia – "Observing our Changing Earth", 133, pp. 615-623.

Bisnath S and R Langley (2001). “Pseudorange Multipath Mitigation By Means of Multipath Monitoring and De-Weighting”, IEEE 4th International Symposium on Kinematic Systems in Geodesy, Geomatics and Navigation, pp. 392-400

Boehm J, B Werl and H Schuh (2007). “Troposphere mapping functions for GPS and very long baseline interferometry from European Centre for Medium-Range Weather Forecasts operational analysis data”, Journal of Geodesy, vol. 81, no. 6. pp 246-257.

Cai C (2009). “Precise Point Positioning Using Dual-Frequency GPS and GLONASS Measurements.” Calgary: UCGE Reports No. 20291, pp. 40-52.

Cai C and Y Gao (2013). “Modeling and assessment of combined GPS/GLONASS precise point positioning.” GPS Solutions, pp. 223-236.

Caissy M, L Agrotis, G Weber, M Hernandez-Pajares, U Hugentobler (2012). “The International GNSS Real-Time Service.” GPS World, pp 52-58.

Chen, D S (1994). “Development of a Fast Ambiguity Search Filtering (FASF) method for GPS Carrier Phase Ambiguity Resolution.” Doctoral Thesis, University of Calgary, Schulich School of Engineering, Department of Geomatics Engineering, Calgary, Alberta, Canada, UCGE Reports No. 20071, pp 43-58.

Chen, J, P Xiao, Y Zhang and B Wu (2013). “GPS/GLONASS System Bias Estimation and Application in GPS/GLONASS Combined Positioning.” China Satellite Navigation Conference (CSNC) 2013 Proceedings, pp. 323-333.

Chen K and Y Gao (2005). "Real-Time Precise Point Positioning Using Single Frequency Data," Proceedings of the 18th International Technical Meeting of the Satellite Division of The Institute of Navigation (ION GNSS 2005), Long Beach, CA, September 2005, pp. 1514-1523.

Choy S, S Zhang, F Lahaye and P Héroux (2013). “A comparison between GPS-only and combined GPS+GLONASS Precise Point Positioning.” Journal of Spatial Science, Volume 58, Issue 2, pp. 169-190.

Chuang S, Y Wenting, S Weiwei, L Yidong, Y Yibin and Z Rui (2013). “GLONASS pseudorange inter-channel biases and their effects on combined GPS/GLONASS precise point positioning.” GPS Solutions, pp. 1-13.

Collins J P, F Lahaye, P Héroux and S. Bisnath (2008). “Precise Point Positioning with ambiguity resolution using the decoupled clock model”, Proceedings of the Institute of Navigation International Technical Meeting ION GNSS, 16-19 September, pp. 1315-1322.

Collins P, S Bisnath, F Lahaye and P Héroux (2010). “ Undifferenced GPS Ambiguity Resolution Using the Decoupled Clock Model and Ambiguity Datum Fixing”, ION GNSS, Vol. 57, No. 2, pp. 123-135.

Daly P and I Kitching (1990). “Characterization of NAVSTAR GPS and GLONASS on-board clocks”, IEEE Aerospace and Electronics Systems Magazine, July 1990, pp. 3–9.

Dawoud S (2012). “GNSS principles and comparison”, Potsdam University, Potsdam, Germany, pp. 6-10.

Dou J and K O'keefe (2013). "Augmenting GPS RTK with Regional BeiDou in North America, "Proceedings of the 26th International Technical Meeting of The Satellite Division of the Institute of Navigation (ION GNSS+ 2013), Nashville, TN, September 2013, pp. 3205-3213.

El-Rabbany A (2002). “Introduction to GPS: The Global Positioning System.” 1st edition, Norwood: Artech House, Inc. pp. 78-82.

Erickson, C (1992). “Investigations of C/A Code and Carrier Measurements and Techniques for Rapid Static GPS Surveys.” Masters Thesis, University of Calgary, Shulich School of Engineering, Department of Geomatics Engineering, Calgary, Alberta, Canada, UCGE Reports No. 20044, pp. 131-160.

European Space Agency (2014). Navigation Support Office: http://dgn7.esoc.esa.int/activities/igs-activities/orbits-clocks/ . Accessed: August, 2014.

European Space Agency. (2011). ESA Galileo navigation: http://www.esa.int/esaNA/GGG0H750NDC_galileo_0.html . Accessed: August, 2014.

Ge M, G Gendt, M Rothacher, C Shi, and J Liu (2008). "Resolution of GPS Carrier-Phase Ambiguities in Precise Point Positioning (PPP) with Daily Observations." J Geodesy, 82 (7): pp. 389-399.

Geng J, X Meng, AH Dodson, FN Teferle (2010). "Integer Ambiguity Resolution in Precise Point Positioning: Method Comparison." Journal of Geodesy, 84(9): pp. 569-581.

GMV (2013). "MAGIC GNSS Precise Point Positioning", http://magicgnss.gmv.com/ppp/ . Accessed: August, 2014.

Grinter T and C Roberts (2013). "Real Time Precise Point Positioning: Are We There Yet?" International Global Navigation Satellite Systems Society Symposium 2013, pp. 16.

Group of Astronomy and GEomatics (GAGE) of the Technical University of Catalonia (2010). http://gage14.upc.es/gLAB/HTML/LaunchHTML.html . Accessed: August, 2014.

Gurtner W (1993). "RINEX: The Receiver Independent Exchange Format Version 2". University of Berne, Astronomical Institute, Berne, pp. 6-30.

Hefty J and L Gerhatova (2012). "Effects of non-modeled signal biases in multi-GNSS Precise Point Positioning." Geophysical Research, pp 1-13.

Héroux P, Y Gao, J Kouba, F Lahaye, Y Mireault, P Collins, K Macleod, P Tetreault and K Chen (2004). "Products and Applications for Precise Point Positioning - Moving Towards Real-Time." Proceedings of the 17th International Technical Meeting of the Satellite Division of The Institute of Navigation (ION GNSS 2004), Long Beach, CA, September 2004, pp. 1832-1843.

Hofmann-Wellenhof B, and H Lichtenegger (2008). "Global Navigation Satellite Systems." NewYork: SpringerWien, pp. 33-58.

Hofmann-Wellenhoff B, H Lichtenegger and J Collins (2001). "Global Positioning System: Theory and Practice", 5th Edition, Berlin: Springer-Verlag, pp. 23-41.

Hofmann-Wellenhof B, H Lichtenegger and E Wasle (2007). “GNSS – Global Navigation Satellite Systems: GPS, GLONASS, Galileo, and more.” Springer; 1st edition, December 2007, pp. 80-92.

IGS (2013). IGS Products: http://igscb.jpl.nasa.gov/components/prods.html. Accessed: August, 2014.

International GNSS Service. (2014): http://igs.org/mgex/ , Accessed: September, 2014.

Jin R, S Jin, G Feng (2012). “M_DCB: Matlab code for estimating GNSS satellite and receiver differential code biases” GPS Solutions, June 2012, Volume 16, Issue 3, pp 541-548.

Jung J, P Enge and B Pervan (2000). “Optimization of cascade integer resolution with three civil GPS frequencies.” Proceedings of the 13th International Technical Meeting of the Satellite Division of the Institute of Navigation (ION GPS 2000), Salt Lake City, UT, September 2000, pp. 2191-2200.

Kouba J and P Héroux (2001). “Precise Point Positioning Using IGS Orbit and Clock Products”, GPS Solutions, Vol. 5, No. 2, pp. 12-28.

Kouba, J (2009). “A guide to using International GNSS Service (IGS) products.” Ottawa, Canada. http://igscb.jpl.nasa.gov/components/usage.htm. Date Accessed: August 19, 2014.

Kozlov D, M Tkachenko and A Tochilin (2000). “Statistical Characterization of Hardware Biases in GPS+GLONASS Receivers.” Proceedings of the 13th International Technical Meeting of the Satellite Division of The Institute of Navigation (ION GPS 2000), Salt Lake City, UT, September 2000, pp. 817-826.

Laurichesse D, F Mercier, JP Berthias, P Broca and L Cerri (2009). "Integer Ambiguity Resolution on Undifferenced GPS Phase Measurements and Its Application to PPP and Satellite Precise Orbit Determination", NAVIGATION, Journal of The Institute of Navigation, Vol. 56, No. 2, Summer 2009, pp. 135-149.

Leandro R F (2009). “Precise point positioning a new approach for positioning, atmospheric studies, and signal analysis.” Fredericton, New Brunswick, Canada, Technical Report No. 267, http://www.gmat.unsw.edu.au/snap/gps/glossary. Accessed: August, 2014.

Leandro R F, M C Santos and R B Langley (2010). “Analyzing GNSS data in precise point positioning software”, GPS Solutions, Vol. 15, No. 1. pp 1-13

Leandro R F and M C Santos (2006). “Wide area based Precise Point Positioning”, ION GNSS 2006, Fort Worth, Texas, pp. 2272-2278.

Leick A (2004). “GPS Satellite Surveying”, 3rd edition, New Jersey: John Wiley & Sons Inc., pp. 92-129.

Li P and X Zhang (2013). "Integrating GPS and GLONASS to Accelerate Convergence and Initialization Times of Precise Point Positioning." GPS Solutions, July 2014, Volume 18, Issue 3, pp 461-471.

Li T and J Wang (2013). “Ambiguity resolution and validation in precise point positioning.” http://www.gmat.unsw.edu.au/snap/publications/lit&wang2012d.pdf, pp. 1-8.

Liu H, Z Chen, W Ye and H Wang (2014). “GNSS carrier phase ambiguity resolution based on integrity restriction in ambiguity domain.” Advances in Space Research, Volume 53, pp. 1207-1218.

Mader G L (1999). “GPS Antenna Calibration at the National Geodetic Survey”, GPS Solutions, Vol. 3, No. 1, pp. 50-58.

Medzida M, K Krdzalić, E Donlagic and A Bilajbegovic (2013). “Possibilities and benefit of the online GNSS PPP free services for GNSS applications- the accuracy and reliability”, UN/Croatia Workshop on GNSS Application, Baska Croatia, pp. 10-15.

Montenbruck O, A Hauschild and P Steigenberger (2014). "Differential Code Bias Estimation Using Multi-GNSS Observations and Global Ionosphere Maps," Proceedings of the 2014 International Technical Meeting of The Institute of Navigation, San Diego, California, January 2014, pp. 802-812.

NRCan (2010). About Us, http://www.nrcan-rncan.gc.ca/com/index-eng.php. Accessed: August, 2014.

Oleynik E G, V V Mitrikas, S G Revnivykh, A I Serdukov, E N Dutov, V F Shiriaev (2006). “High-Accurate GLONASS Orbit and Clock Determination for the Assessment of System Performance.” Proceedings of the 19th International Technical Meeting of the Satellite Division of The Institute of Navigation (ION GNSS 2006), Fort Worth, TX, September 2006, pp. 2065-2079.

Povalyaev A (1997). “Using Single Differences for Relative Positioning in GLONASS.” 10th Int. Tech. Meeting of the Satellite Division of the U.S. Inst. of Navigation GPS ION'97, Kansas City, Missouri, 16-19 September, pp.929-934.

Reshetnev Company (2010). 50 years on Earth and in space. Zheleznogorsk: JSC ISS, http://www.iss-reshetnev.com/images/File/magazin/2009/m8-screen_en.pdf.Accessed: September, 2014.

RTCM Special Committee No. 104. (2001). "RTCM Recommended Standards for Differential GNSS". Alexandria, Virginia: Radio Technical Commission for Maritime Services, pp. 12-16.

Schaer S (2012). "Key Issues, Recommendations, Action Items." IGS Workshop on GNSS Biases, January 2012, pp. 1-8.

Schaer S, W Gurtner and J Feltens (1998). "IONEX: The IONosphere Map EXchange Format Version 1". Darmstadt: ESA/ESOC, pp. 3-14.

Schmid R (2011). "Upcoming switch to IGS08/igs08.atx - Details on igs08.atx". IGSMAIL-6355, http://igs.org/pipermail/igsmail/2011/006347.html. Accessed: September 2014

Seepersad G (2012). "Reduction of initial convergence period in GPS PPP data processing." York University, Toronto, Canada, pp. 42-50.

Shen X and Y Gao (2006). "Analyzing the Impacts of Galileo and Modernized GPS on Precise Point Positioning." Proceedings: ION-NTM-2006, Institute of Navigation, Monterey, California, January, pp. 837-846.

Shi J and Y Gao (2010). "Analysis of the Integer Property of Ambiguity and Characteristics of Code and Phase Clocks in PPP using a Decoupled Clock Model", Proceedings of the 23rd International Technical Meeting of The Satellite Division of the Institute of Navigation, Portland, OR, pp. 2553-2564.

Spofford P R and B W Remondi (1994). "The National Geodetic Survey Standard GPS Format SP3. (SP3-a format)", IGS website: http://igscb.jpl.nasa.gov/igscb/data/format/sp3_docu.txt. Accessed: September 2014.

Takac F (2009). "What are the challenges associated with GLONASS (FDMA) ambiguity resolution and how are they addressed?" GNSS Solutions column, Inside GNSS, March, pp. 24-28.

Teunissen, P J (2003). "Towards a unified theory of GNSS ambiguity resolution." Journal of Global Positioning Systems, Volume 2, pp. 1-12.

Teunissen, P J and S Verhagen (2009b). "The GNSS ambiguity ratio-test revisited: a better way of using it." Survey Review, 41(312), pp. 138-151.

Teunissen, P J and S Verhagen (2009a). “GNSS carrier phase ambiguity resolution: challenges and open problems.” International Association of Geodesy Symposia, Observing our Changing Earth. Springer-Verlag, Berlin, Heidelberg, pp. 785-792.

Teunnissen J P and D Odijik (1999). “The Reliability of GPS Ambiguity Resolution.” GPS Solutions, Volume 2, Issue 3, pp. 63-69.

Tu R, M Ge, H Zhang, G Huang (2013). “The realization and convergence analysis of combined PPP based on raw observation.” Advances in space research, pp. 211-221.

Wang Q and Y Chen (2012). “Analysis and Modeling of PPP Residuals from GPS and GLONASS.” China Satellite Navigation Conference (CSNC) 2012 Proceedings, pp. 301-308.

Wanninger L (2011). “Carrier-phase inter-frequency biases of GLONASS receivers.” Journal of Geodesy, pp. 1-10.

Wanninger L (2012). “Carrier-Phase Inter-Frequency Biases of GLONASS Receivers.” Journal of Geodesy, Vol. 86, No. 2, February 1, 2012, pp. 139-148.

Weber R and J Slater (2001). “The International GLONASS Service – Pilot Project” GPS Solutions, Vol. 4, Issue 4, April, 2001, pp. 61-67.

Wells D, N Beck, D Delikaraoglou, A Kleusberg, E J Krakiwsky, G Lachapelle, R B Langley, M Nakiboglu, K Schwarz, J M Tranquilla, P Vanicek (1986). “Guide to GPS positioning.” Fredericton, New Bruinswick, Canada: Canadian GPS Associates, pp. 9.00-9.15.

Werner W and J Winkel (2003). “TCAR and MCAR Options with GALILEO and GPS.” Proceedings of the 16th International Technical Meeting of the Satellite Division of The Institute of Navigation (ION GPS/GNSS 2003), Portland, OR, September 2003, pp. 790-800.

Willis P, G Beutler, W Gurtner, G Hein, R E Neilan, C Noll and J Slater (1999). "IGEX: International GLONASS Experiment", Advanced Space Research, volume 23, No. 4, pp 659-663.

Zhu S Y, F-H Massmann, Y Yu and C Reigber (2002). “Satellite antenna phase centre offsets and scale errors in GPS solutions”, Journal of Geodesy, Vol. 76, pp. 668-672.

Zumberge J F, M B Heflin D C Jefferson, M M Watkins and F H Webb (1997). "Precise point positioning for the efficient and robust analysis of GPS data from large networks", J. Geophys. Res., volume 102, No. B3, pp 5005-5017.

Appendices

Appendix A: Flowchart of GNSS RINEX readers design and operation

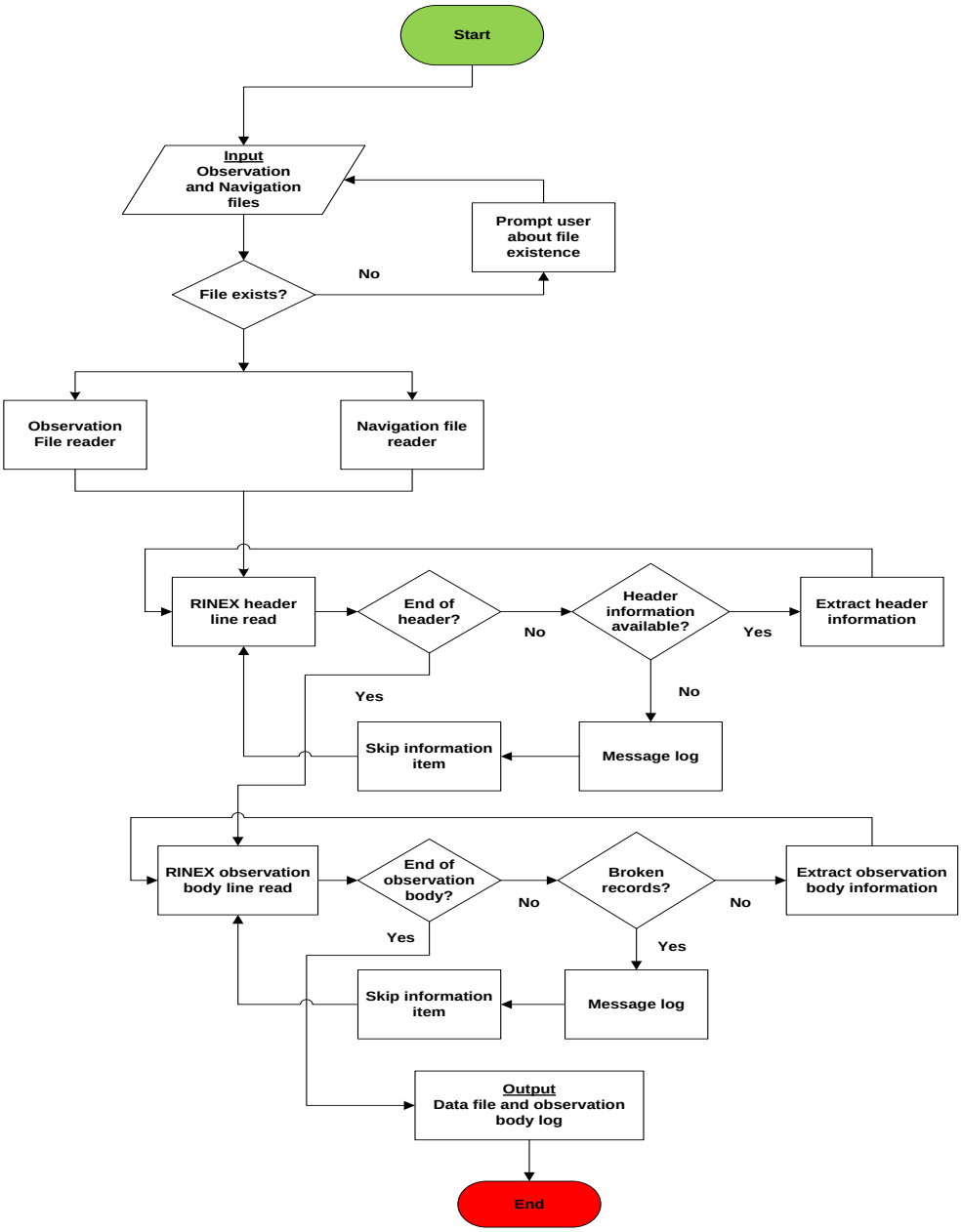

Appendix B: Structure of GNSS RINEX reader for different GNSSs

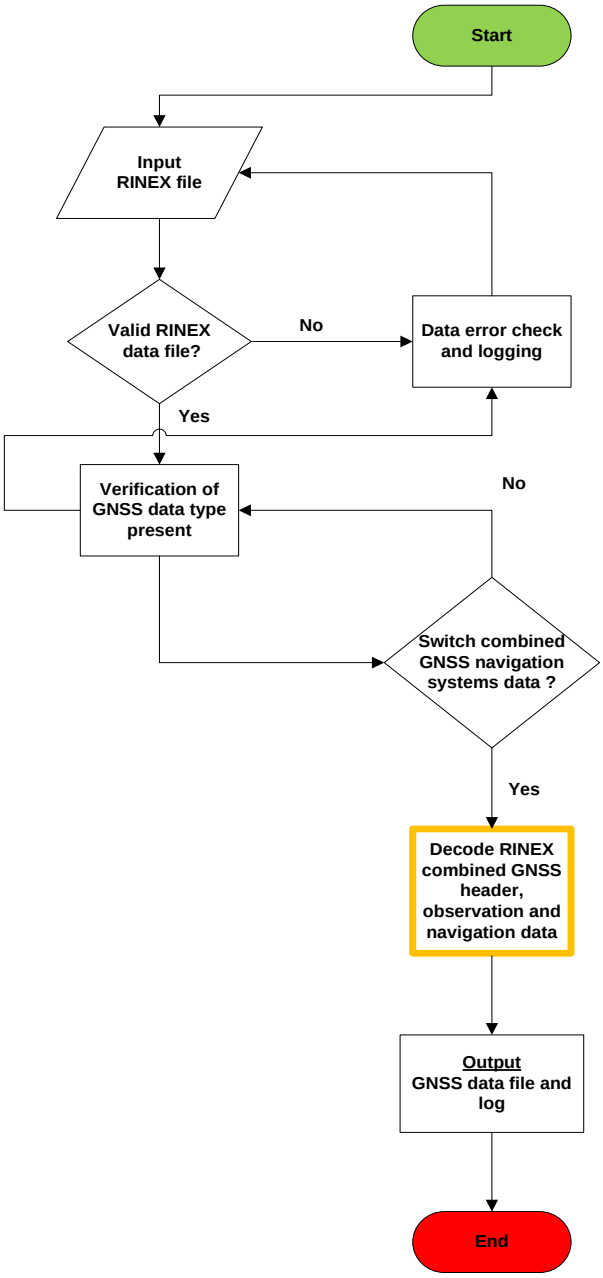

Appendix C: Structure of decoders for RINEX combined GNSS data files

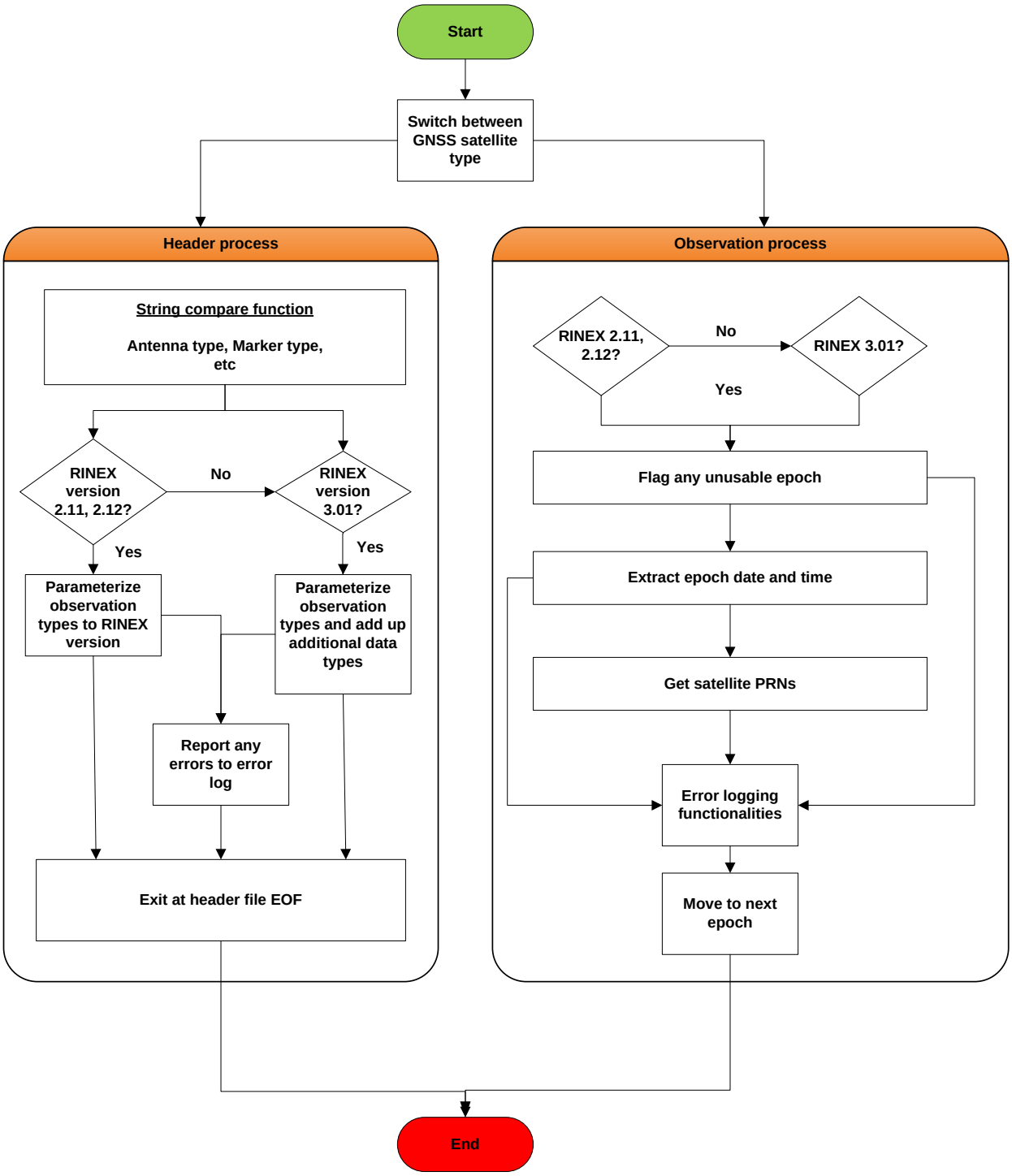

Appendix D: Functions included in the GNSS RINEX reader class

Function *FileType*: This function identifies the input file type. It runs various checks to ascertain the validity of the input file, as well as the observation types in it. In the case of invalidity, it runs diagnostics to determine the causes and reports to error logs. The following figure illustrates the structure of this function.

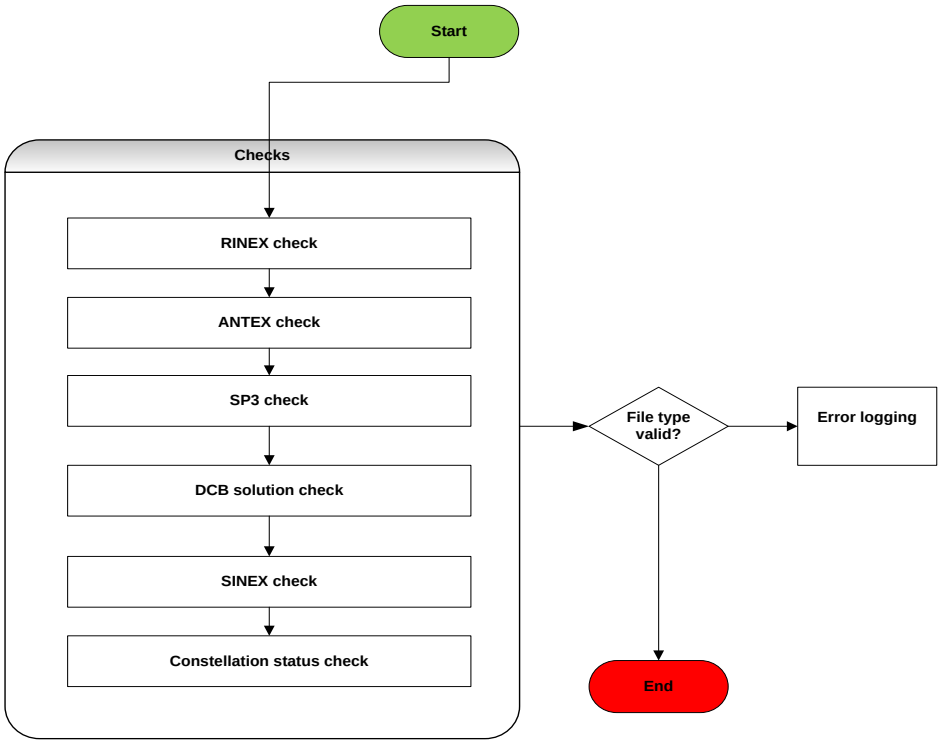

Function *readRINEXObsHeader:* This function reads a RINEX observation header. It has a detailed structure to both save and read the data based on the RINEX versions (2.11, 2.12 and 3.01). Error logging functionalities are included.

Function *readRINEXObsEpoch:* This function reads a RINEX observation epoch. It has a detailed data structure based on the observable types and the ability to change processing directions (either forward or backward). Error logging functionalities are included.

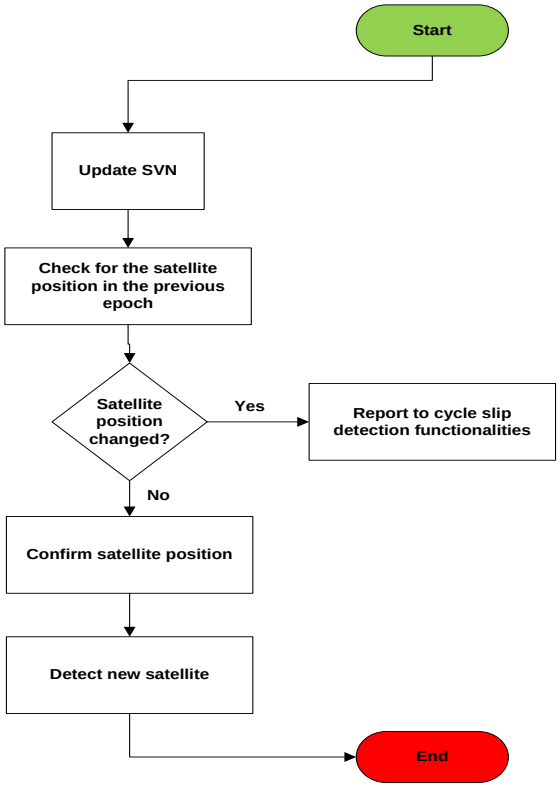

Function *readRinexNavFile*: This function reads a RINEX navigation file based a given filename(s). There are developed structures for the saving of the read data which are parsed to the output functionalities.

Appendix E: RTCM reader design

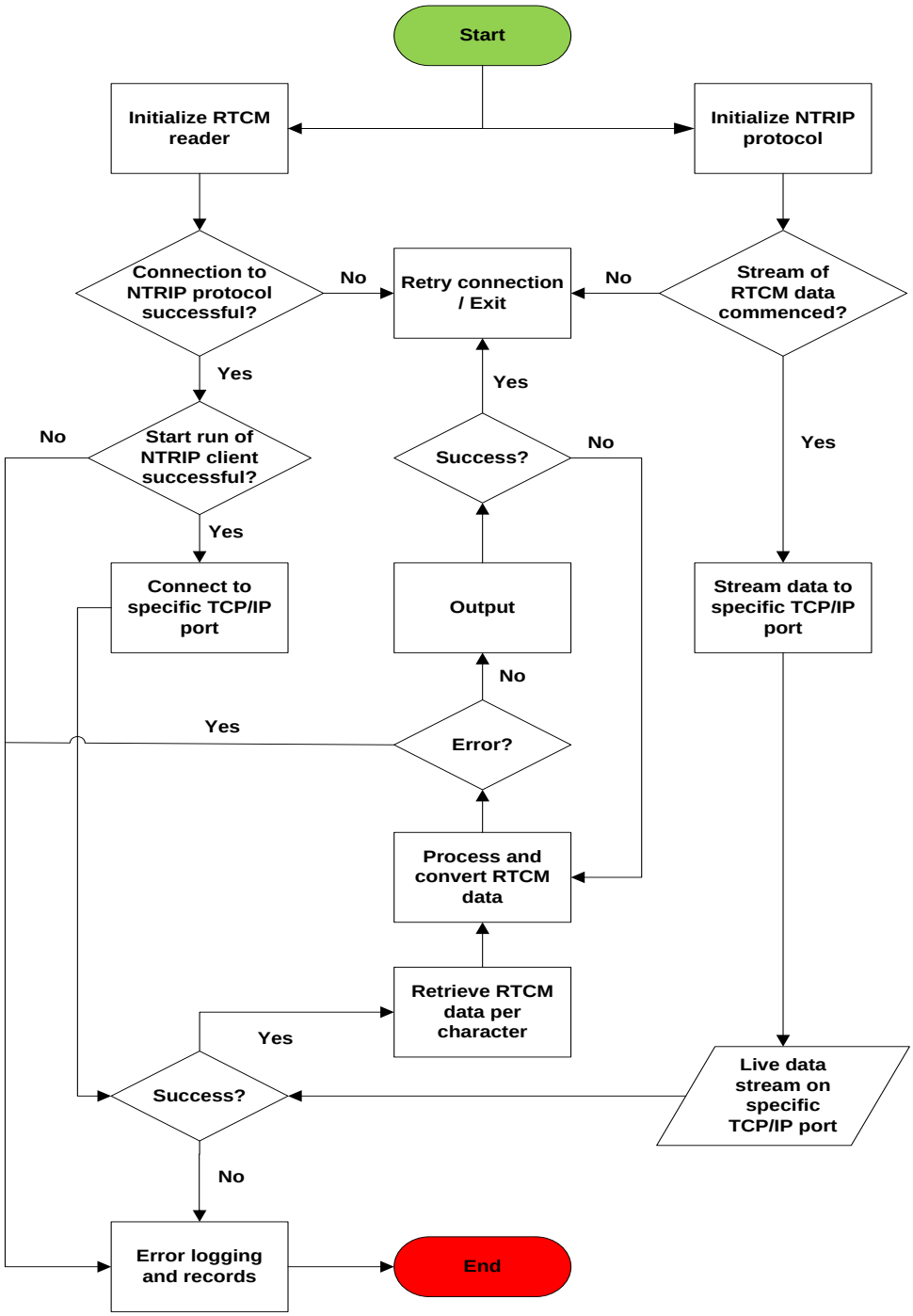

Appendix F: General structure of the GNSS RINEX clock reader

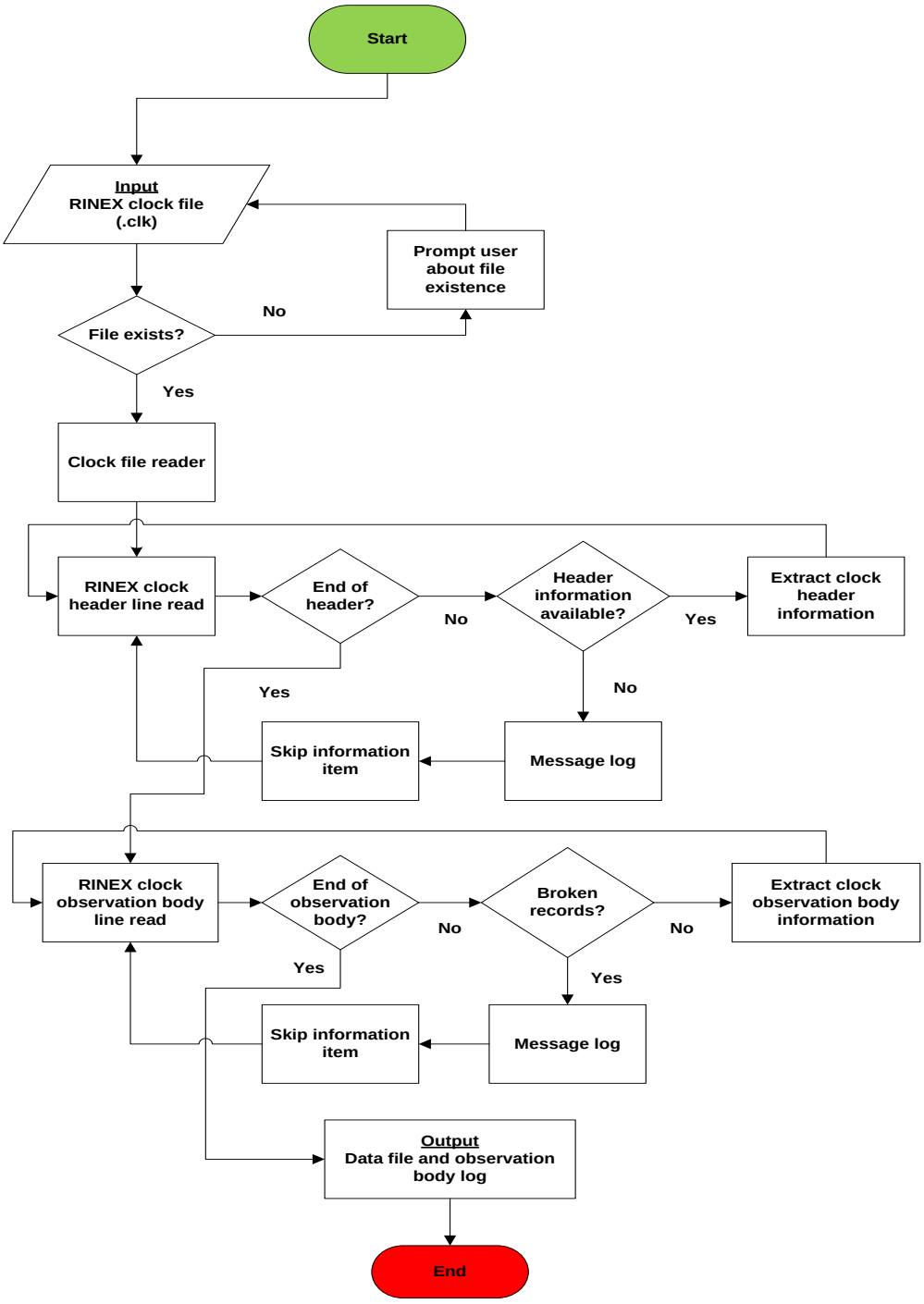

Appendix G: General structure of the GNSS RINEX IONEX reader

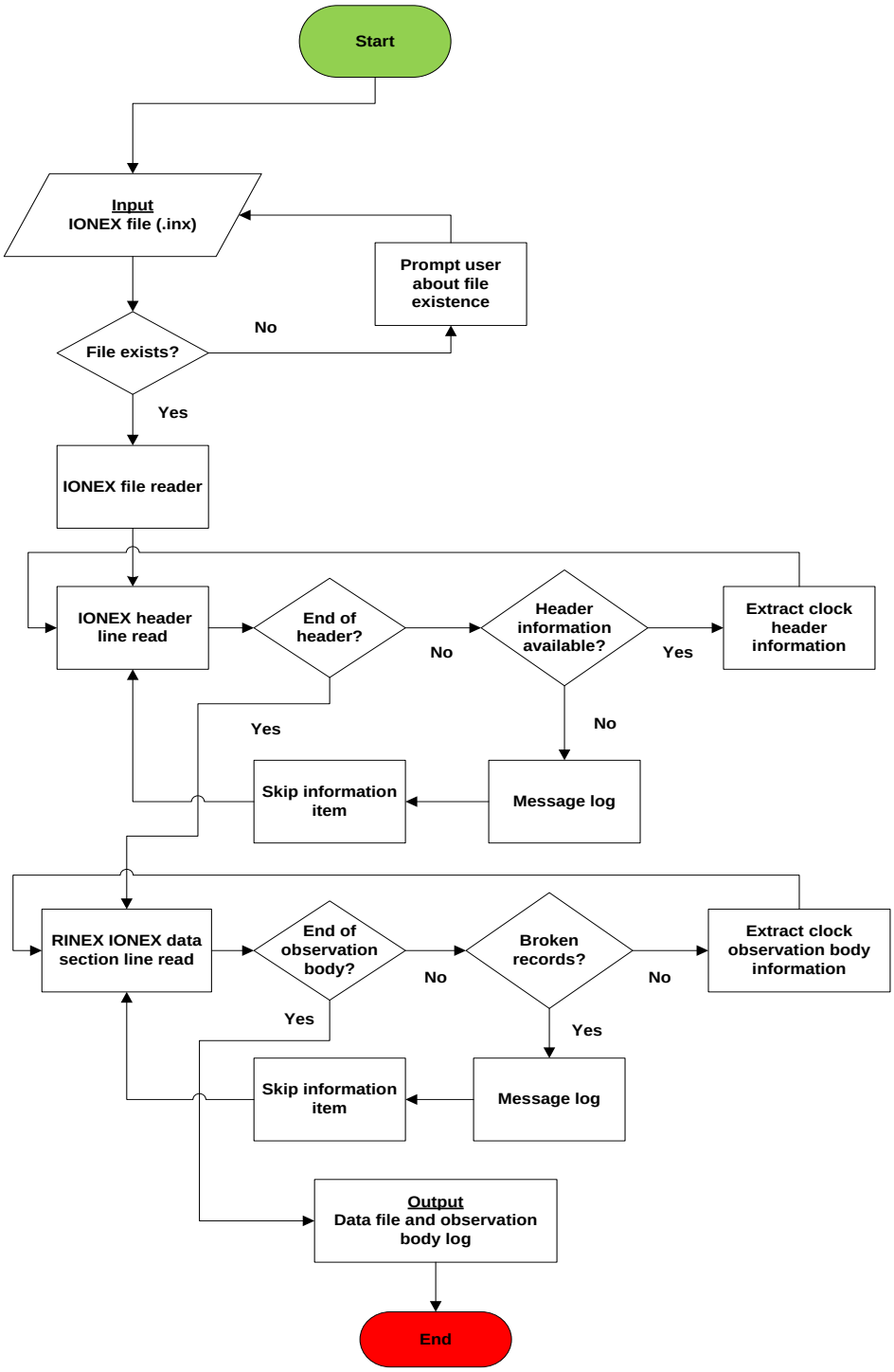

Appendix H: General structure of the GNSS RINEX ANTEX reader

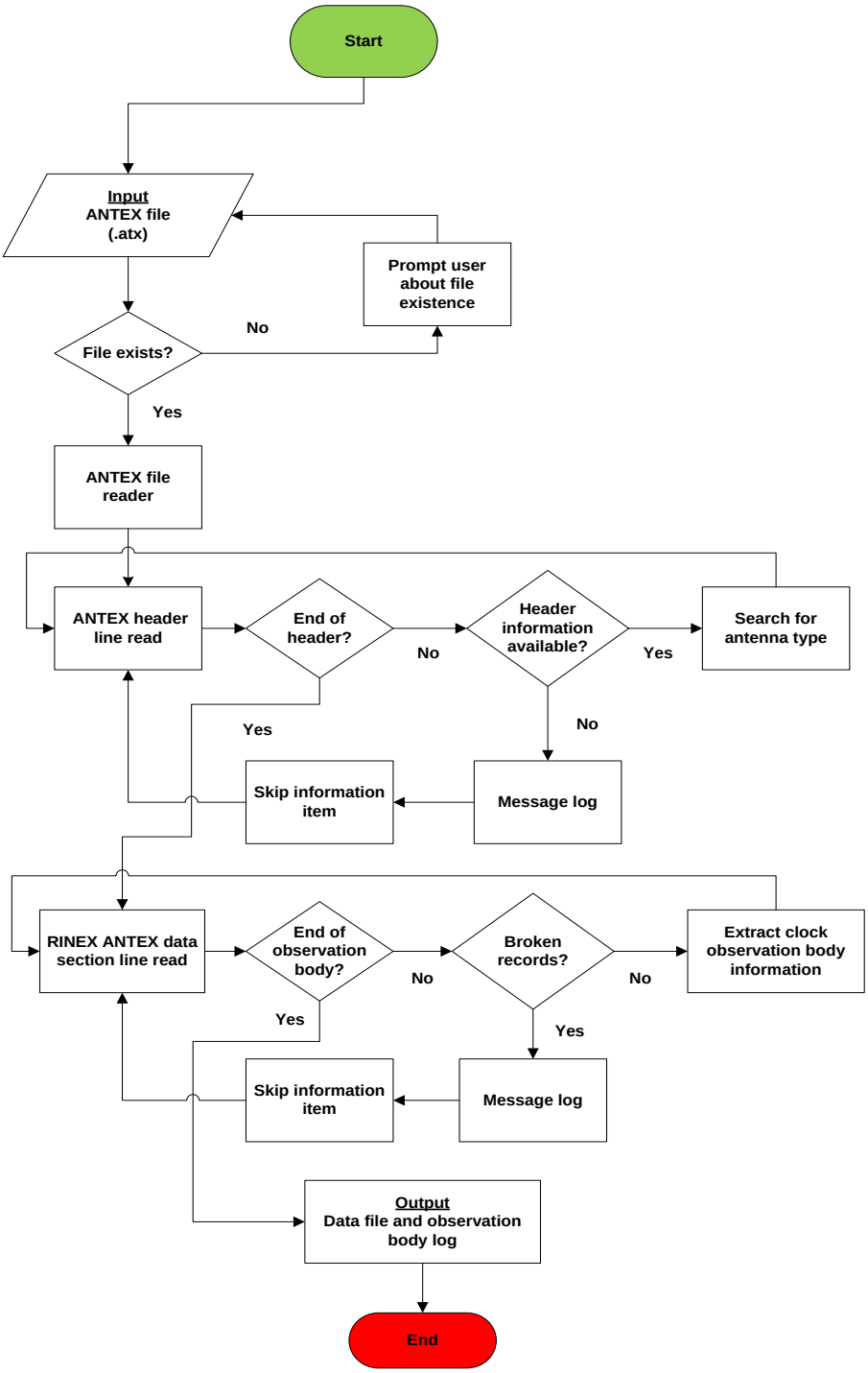

Appendix I: General structure of the GNSS RINEX precise satellite orbits and clocks reader

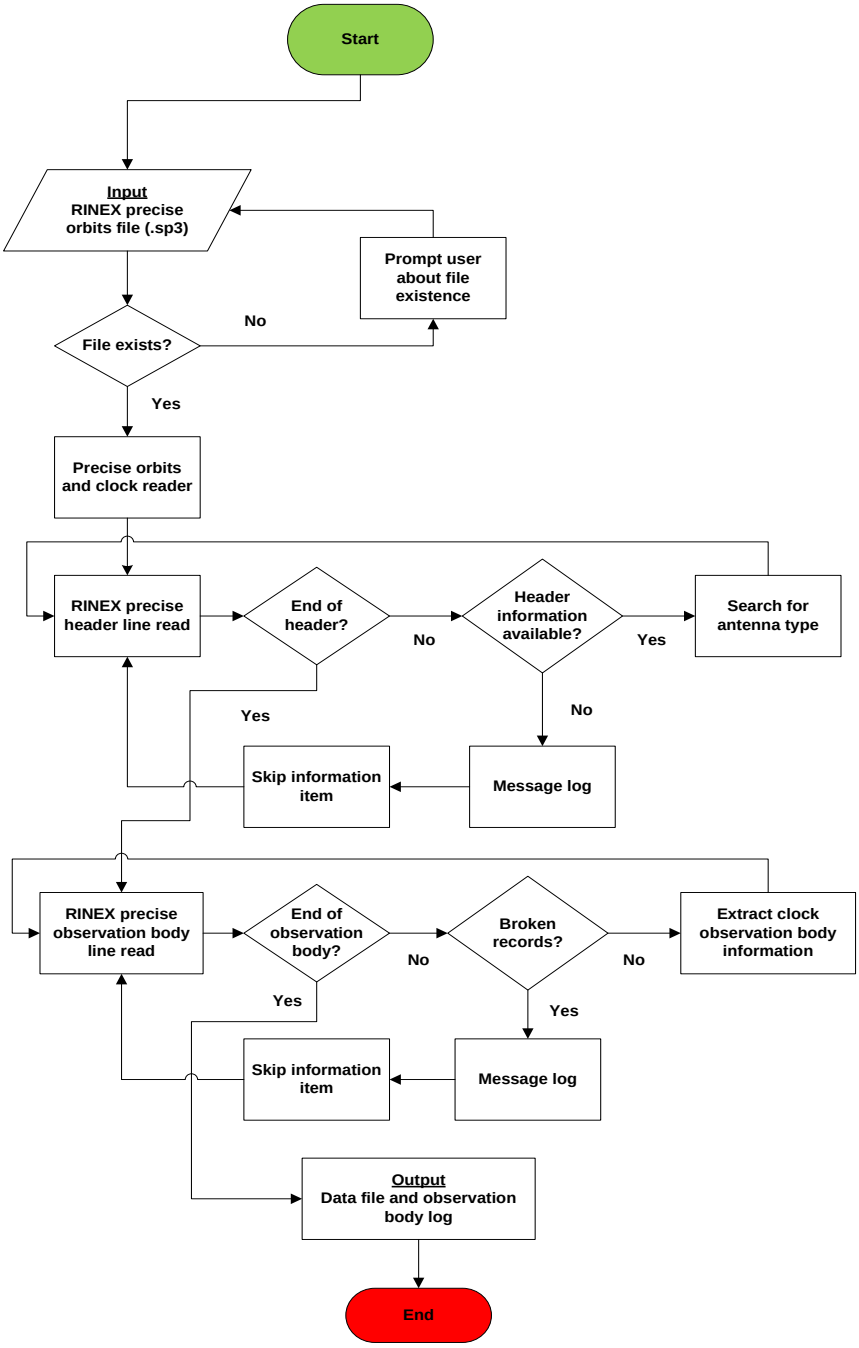

Appendix J: General structure of the GNSS RINEX ocean loading reader

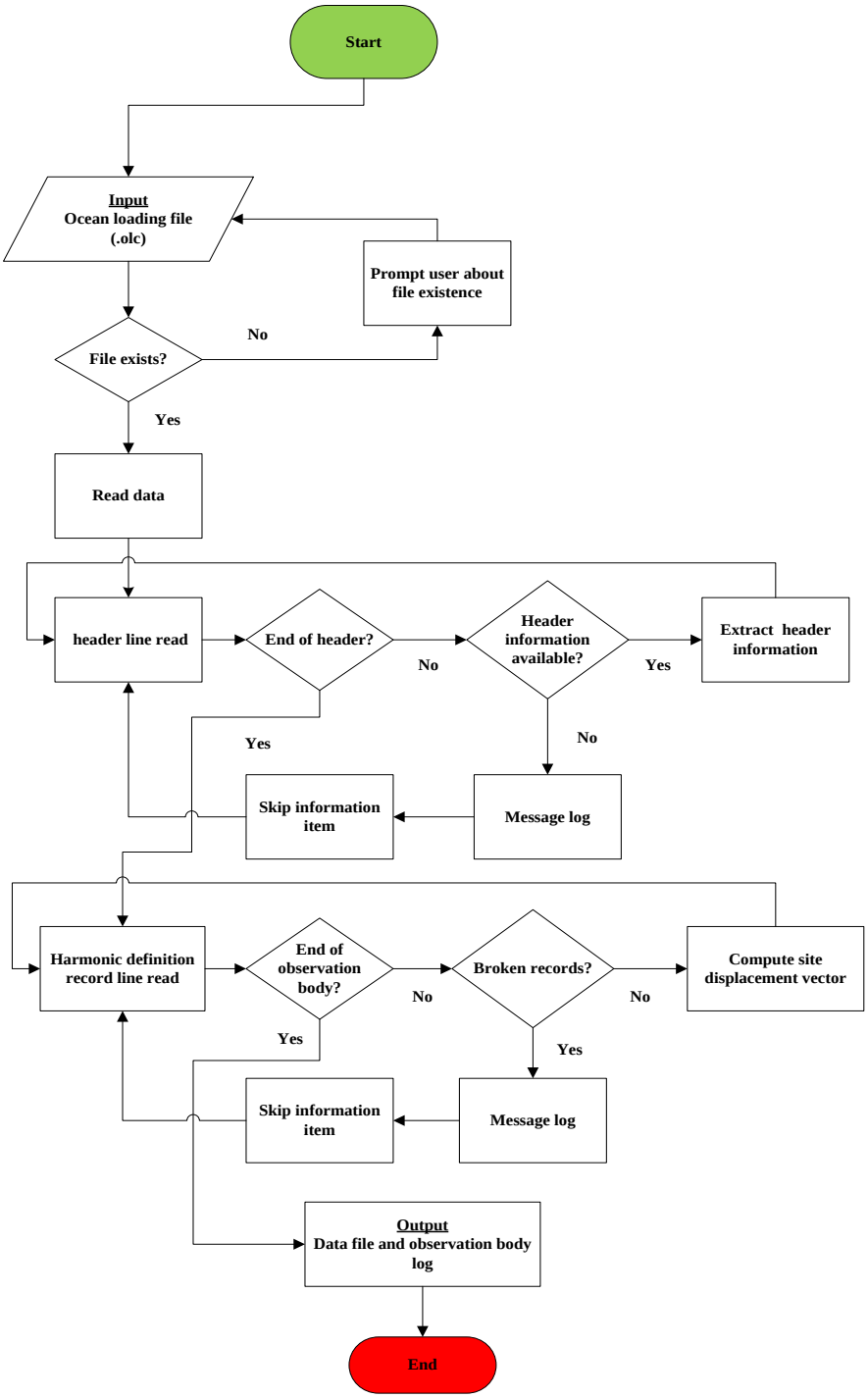

Appendix K: Class Atmospheric Refraction

Function *ionoKlobucharModel:* This function computes the ionospheric correction using the Klobuchar model. The flowchart below illustrates the structure of the function.

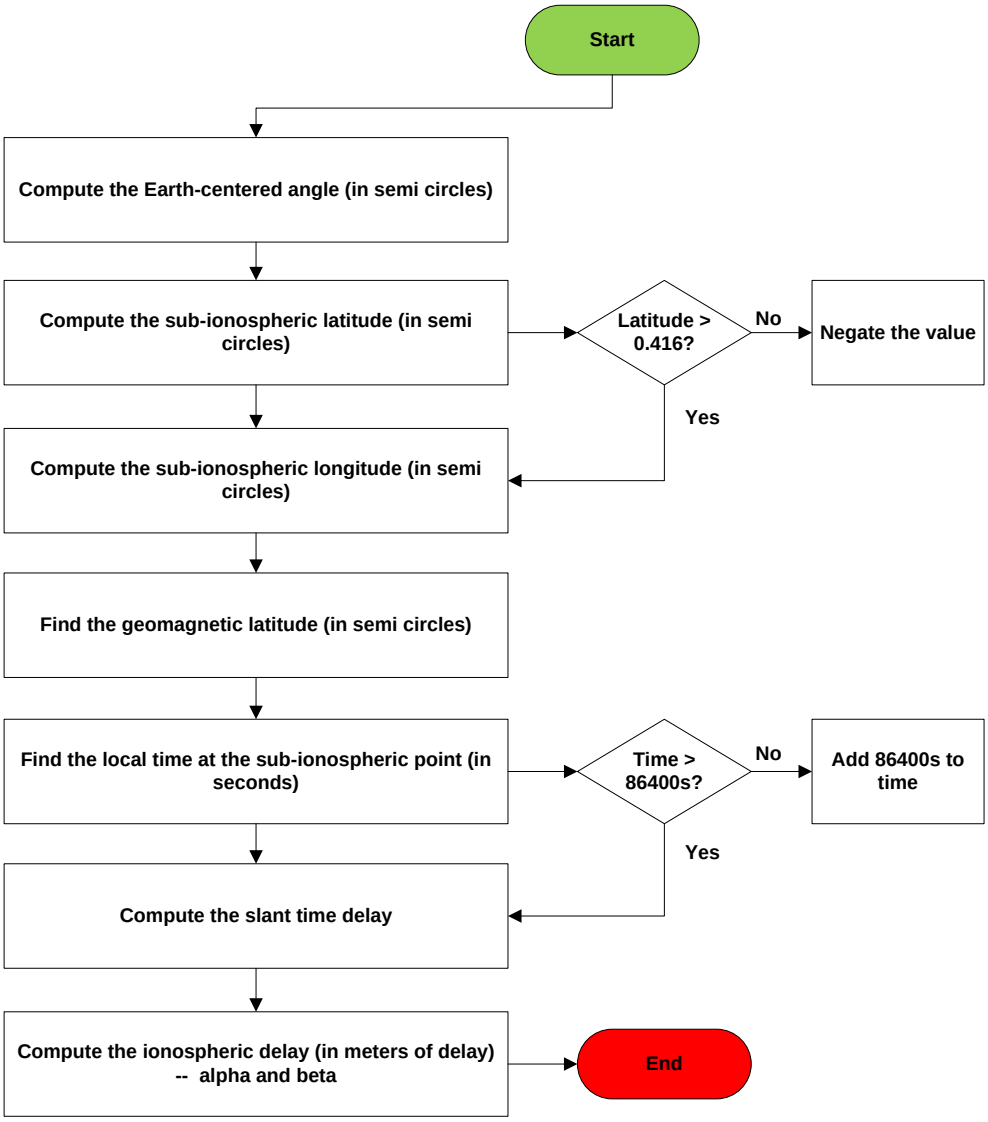

Function *tropoCorrectionModel:* This function computes nominal zenith path delay values and mapping function values used to obtain the tropospheric correction depending on the input options. Essential parameters which serve as input to this function are the 3D position vector of the station, elevation of the station-satellite pair, wet mapping function (relates to the vertical delay with slant delay), zenith tropospheric delay and the tropospheric slant correction. The flowchart illustrates the structure of the function.

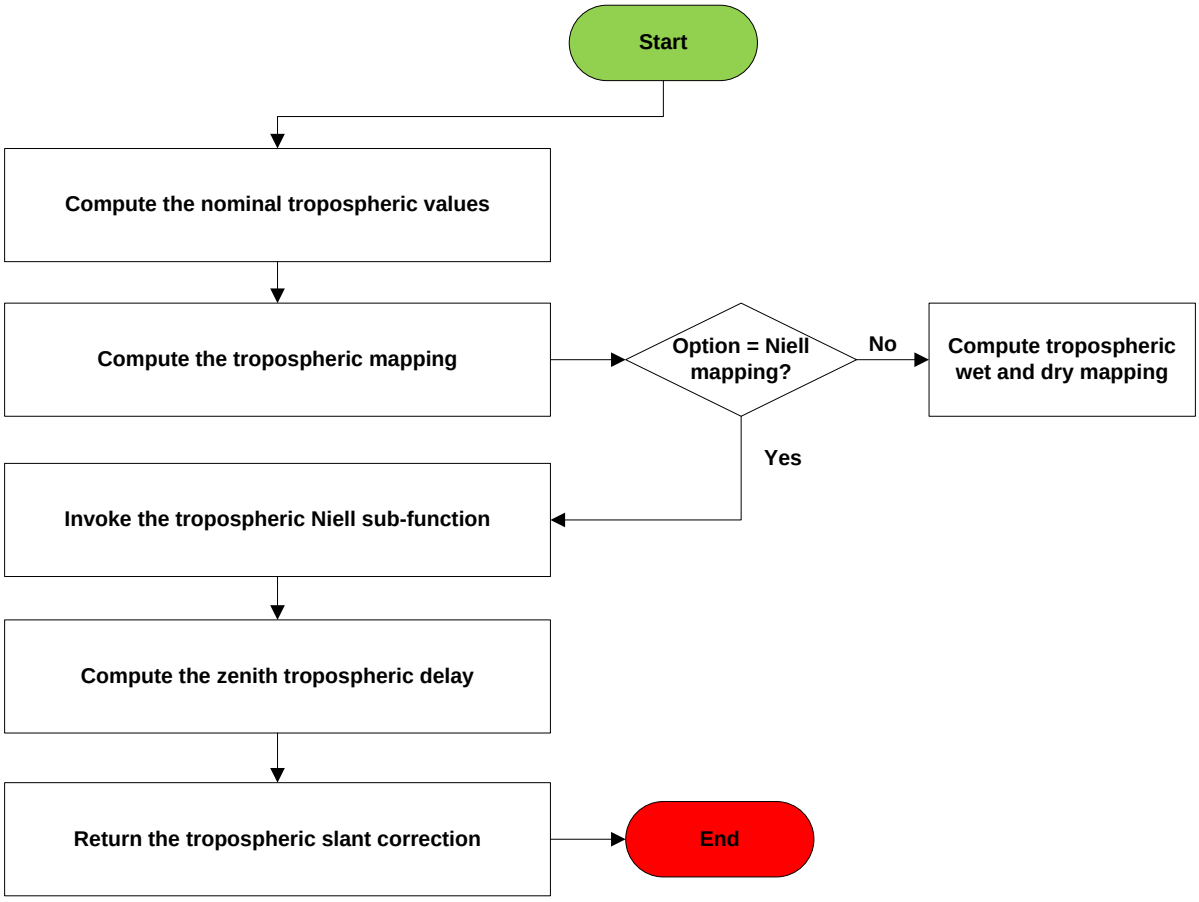

Appendix L: Antenna types and GLONASS pseudorange ICBs

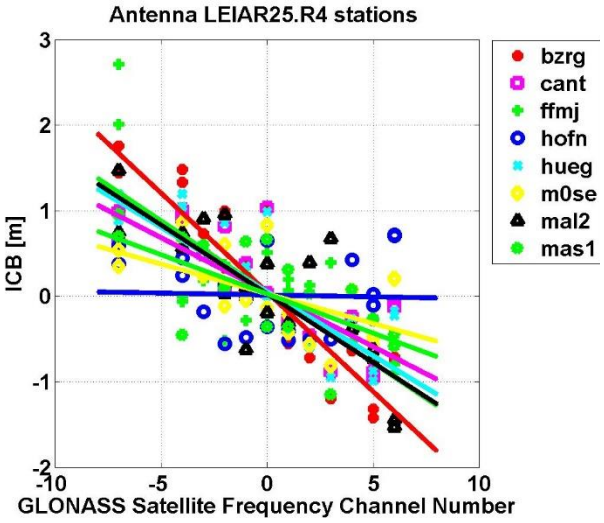

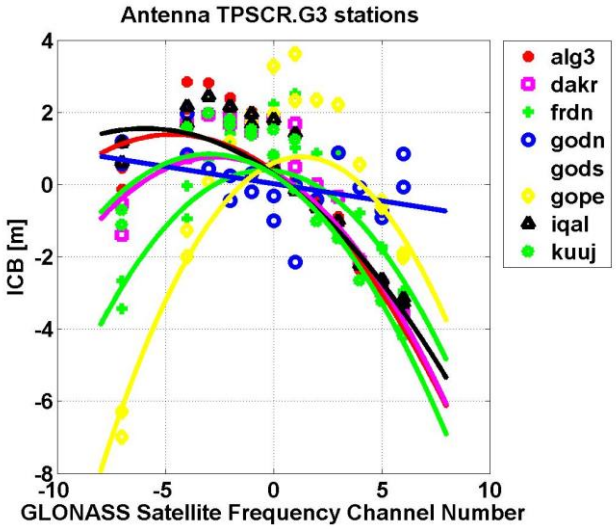

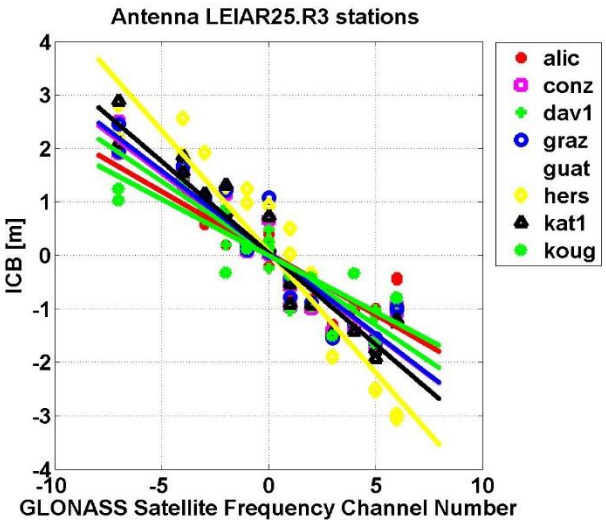

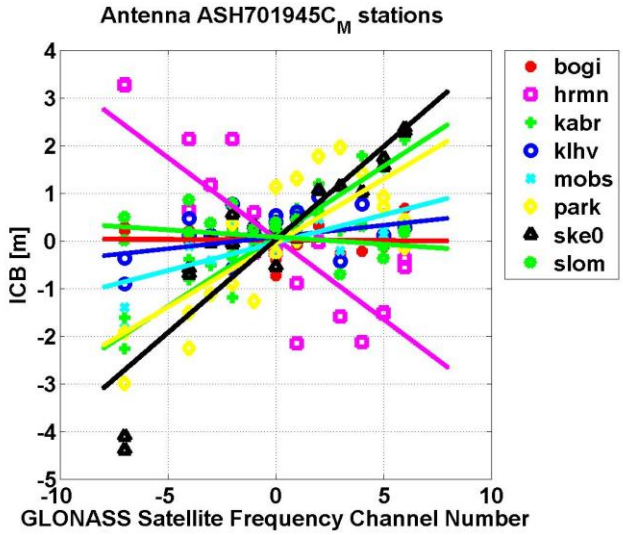

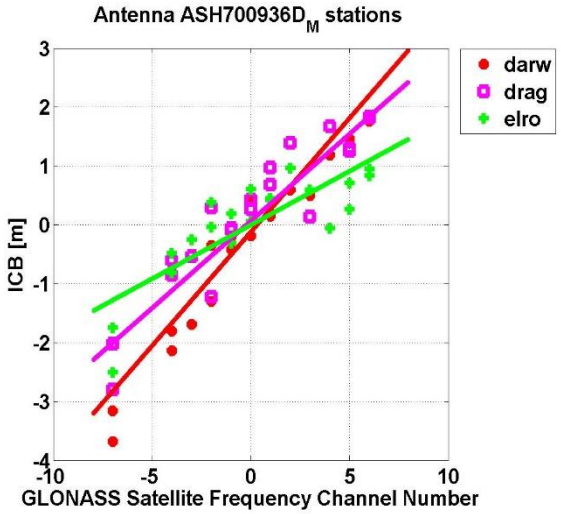
Antenna ASH700936D_M stations
darw
drag
elro
ICB [m]
GLONASS Satellite Frequency Channel Number

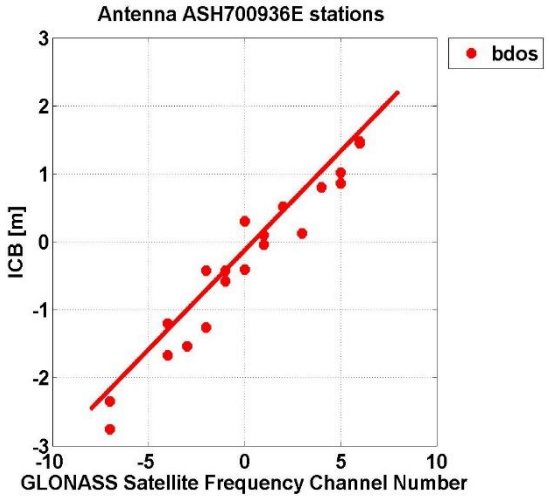
Antenna ASH700936E stations
bdos
ICB [m]
GLONASS Satellite Frequency Channel Number

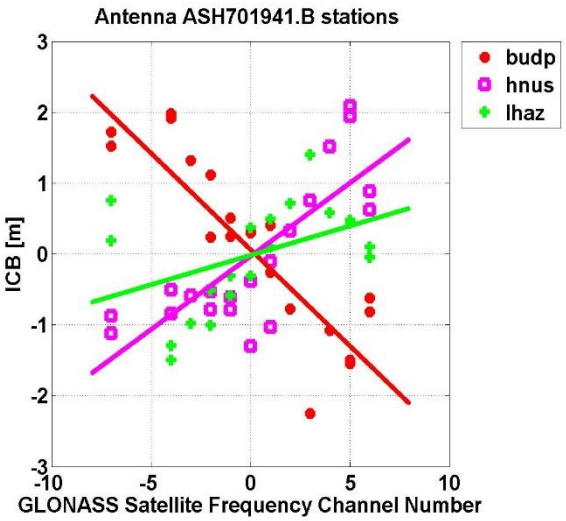
Antenna ASH701941.B stations
budp
hnus
lhaz
ICB [m]
GLONASS Satellite Frequency Channel Number

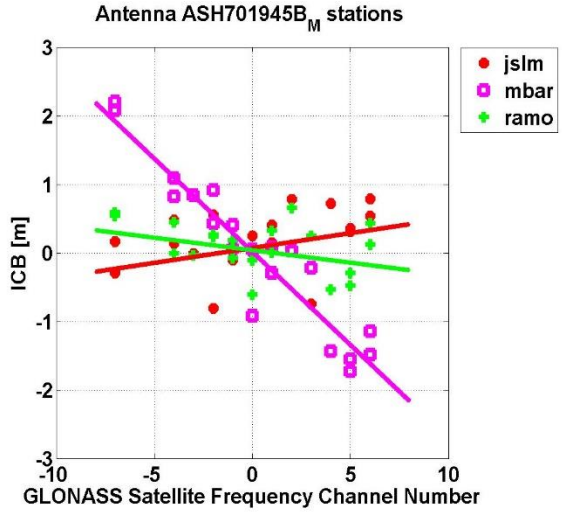
Antenna ASH701945B_M stations
jslm
mbar
ramo
ICB [m]
GLONASS Satellite Frequency Channel Number

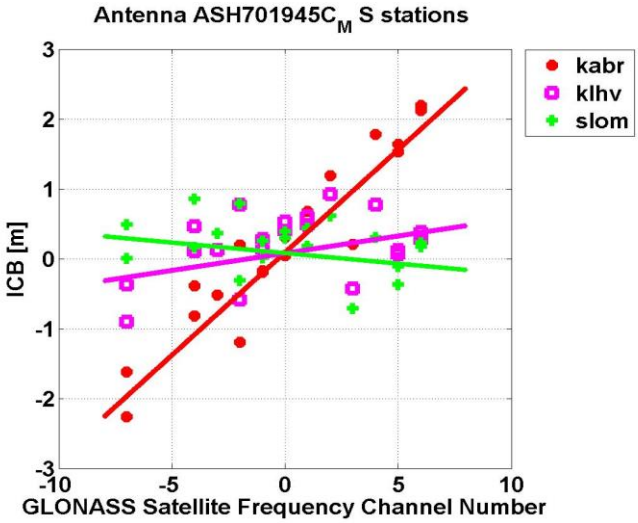
Antenna ASH701945C_M S stations
ICB [m]
GLONASS Satellite Frequency Channel Number
kabr
klhv
slom

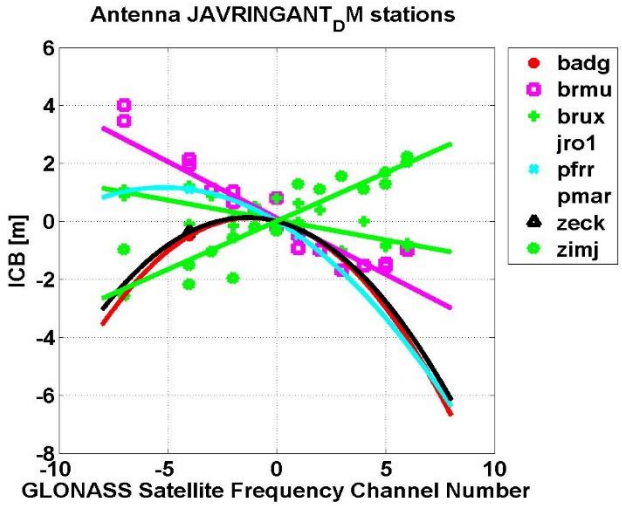
Antenna JAVRINGANT_DM stations
ICB [m]
GLONASS Satellite Frequency Channel Number
badg
brmu
brux
jro1
pfrr
pmar
zeck
zimj

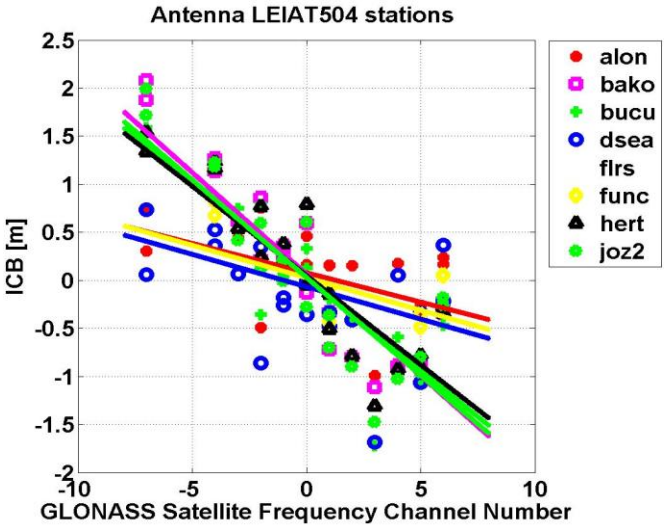
Antenna LEIAT504 stations
ICB [m]
GLONASS Satellite Frequency Channel Number
alon
bako
bucu
dsea
flrs
func
hert
joz2

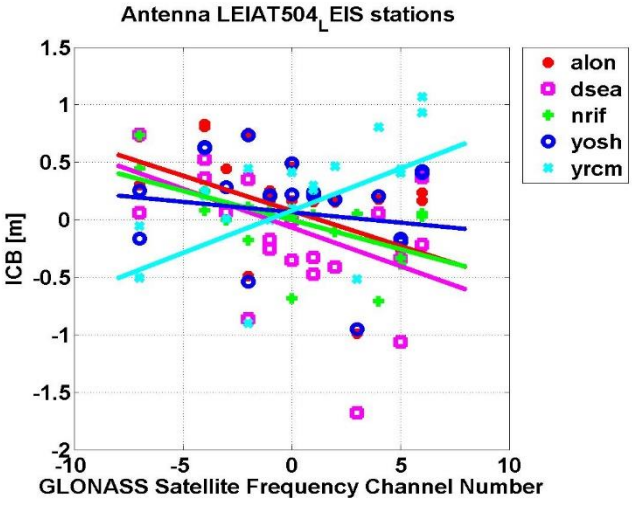
Antenna LEIAT504_L EIS stations
ICB [m]
GLONASS Satellite Frequency Channel Number
alon
dsea
nrif
yosh
yrcm

Appendix M: GLONASS pseudorange ICBs as a function of receiver firmware versions

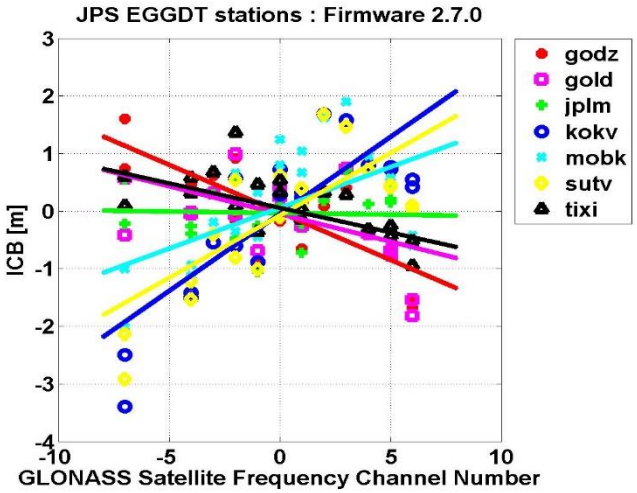

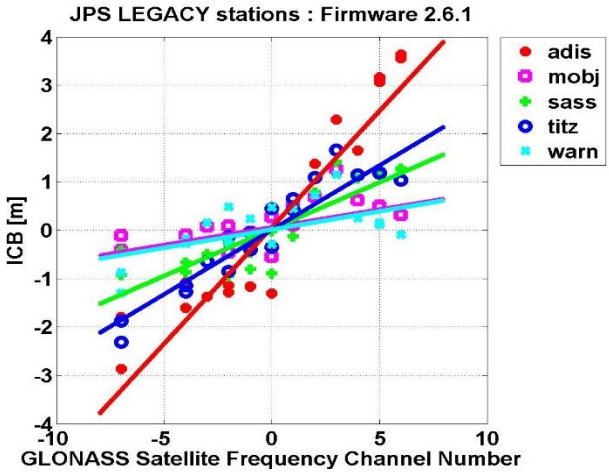

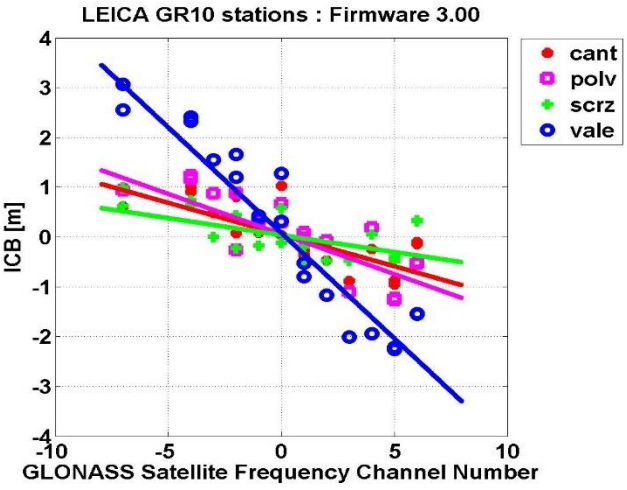

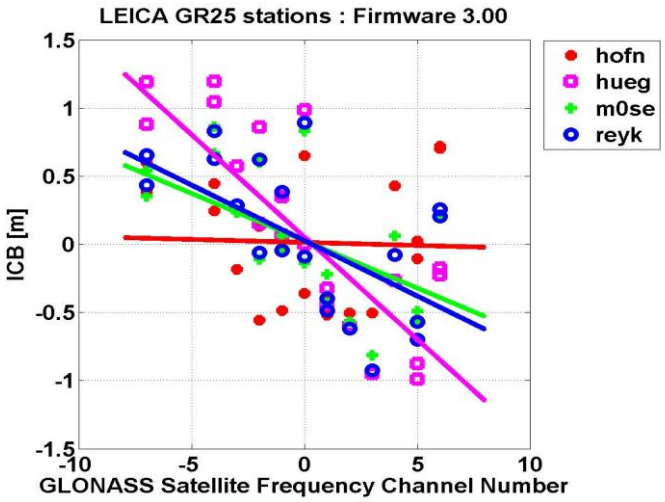

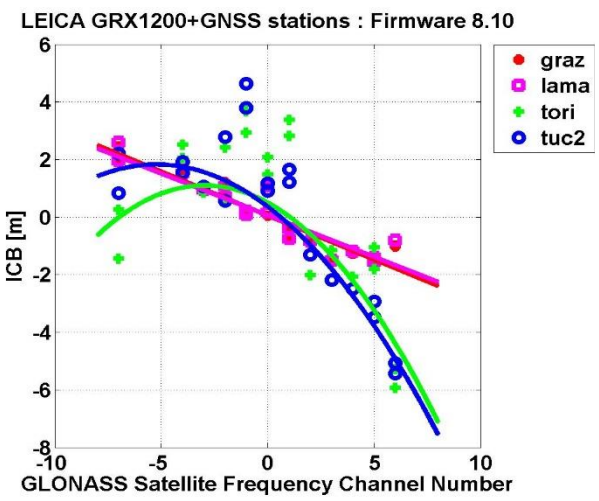
LEICA GRX1200+GNSS stations : Firmware 8.10
graz
lama
tori
tuc2
ICB [m]
GLONASS Satellite Frequency Channel Number

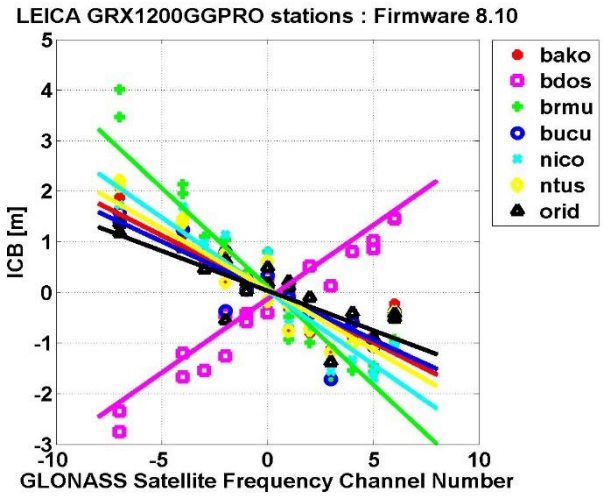
LEICA GRX1200GGPRO stations : Firmware 8.10
bako
bdos
brmu
bucu
nico
ntus
orid
ICB [m]
GLONASS Satellite Frequency Channel Number

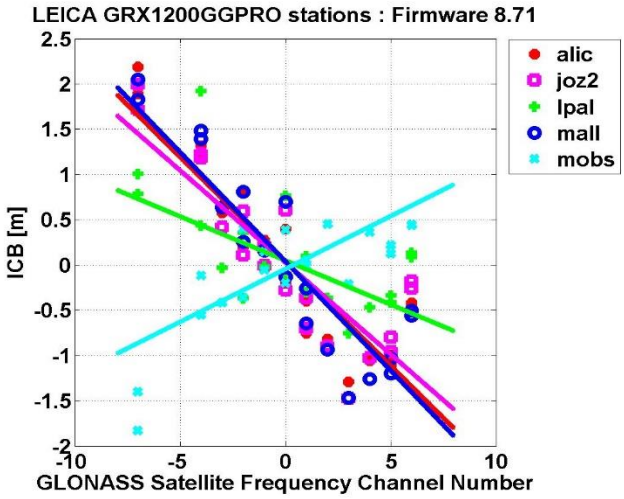
LEICA GRX1200GGPRO stations : Firmware 8.71
alic
joz2
lpal
mall
mobs
ICB [m]
GLONASS Satellite Frequency Channel Number

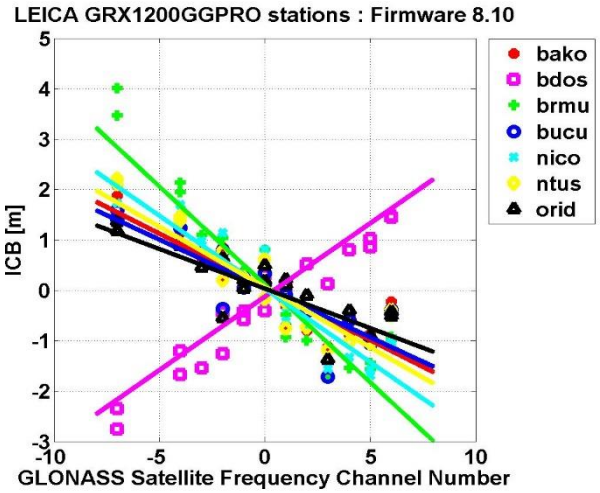
LEICA GRX1200GGPRO stations : Firmware 8.10
bako
bdos
brmu
bucu
nico
ntus
orid
ICB [m]
GLONASS Satellite Frequency Channel Number

Appendix N: GLONASS pseudorange ICBs from DOY 195 to 201 in 2013 for PRN 33 to 56 at sample stations

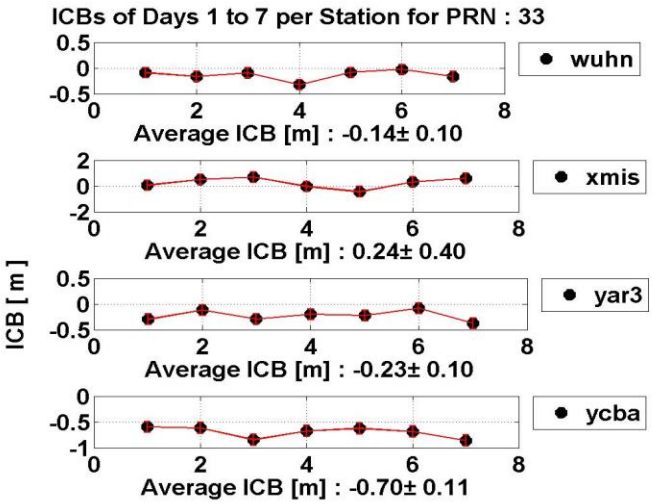

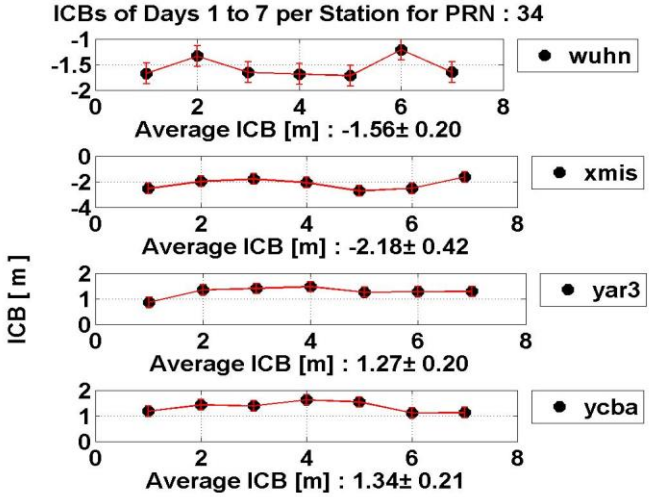

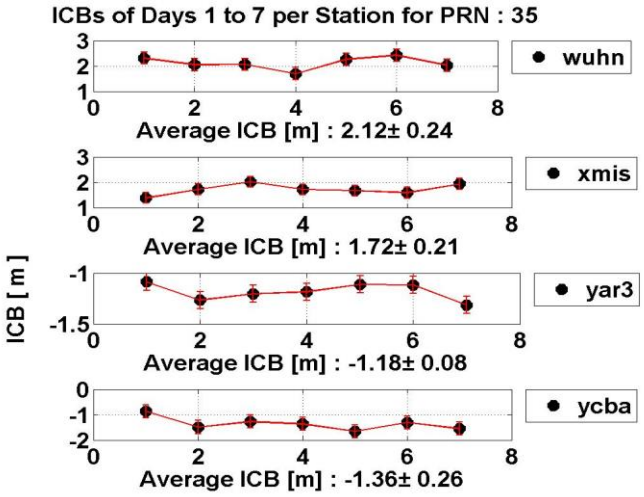

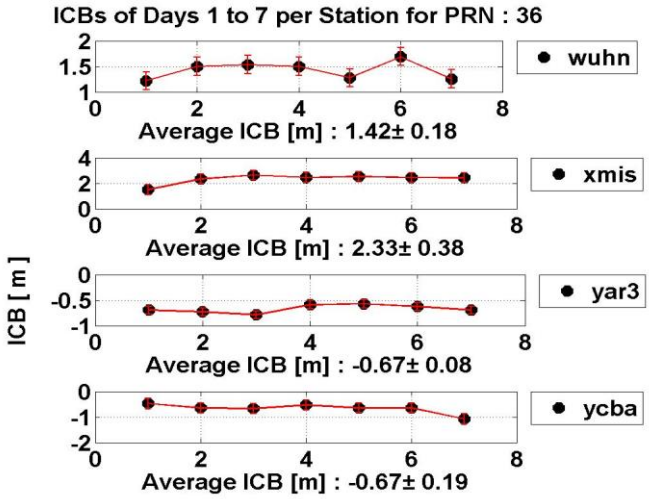

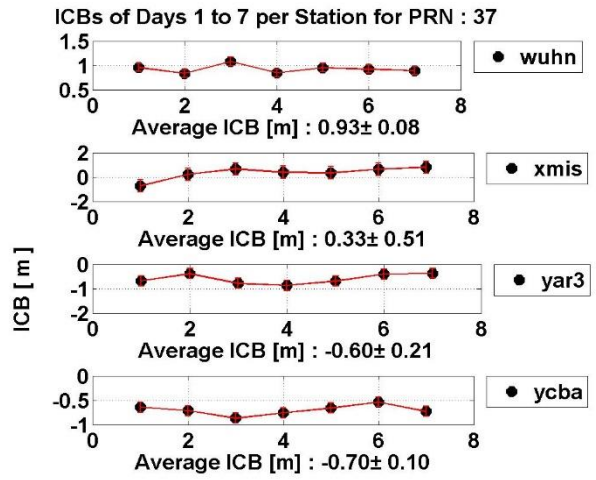
ICBs of Days 1 to 7 per Station for PRN : 37
ICB [m]
wuhn
Average ICB [m] : 0.93± 0.08
xmis
Average ICB [m] : 0.33± 0.51
yar3
Average ICB [m] : -0.60± 0.21
ycba
Average ICB [m] : -0.70± 0.10

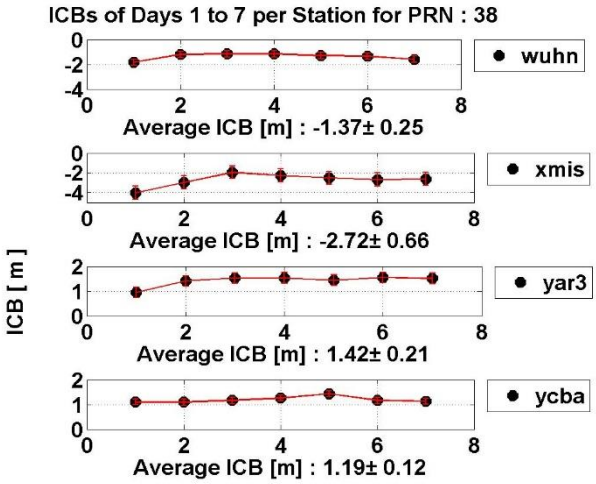
ICBs of Days 1 to 7 per Station for PRN : 38
ICB [m]
wuhn
Average ICB [m] : -1.37± 0.25
xmis
Average ICB [m] : -2.72± 0.66
yar3
Average ICB [m] : 1.42± 0.21
ycba
Average ICB [m] : 1.19± 0.12

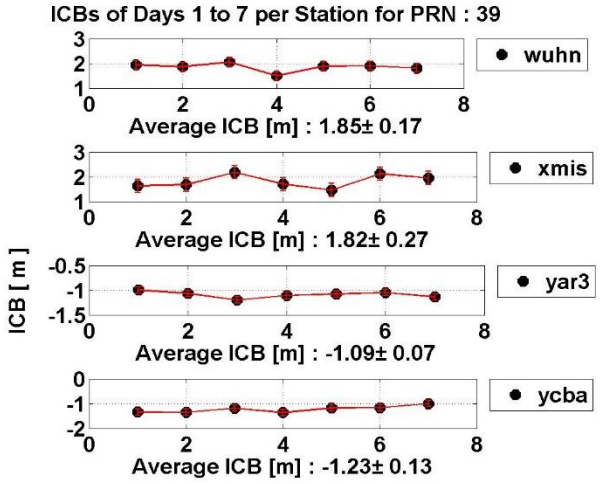
ICBs of Days 1 to 7 per Station for PRN : 39
ICB [m]
wuhn
Average ICB [m] : 1.85± 0.17
xmis
Average ICB [m] : 1.82± 0.27
yar3
Average ICB [m] : -1.09± 0.07
ycba
Average ICB [m] : -1.23± 0.13

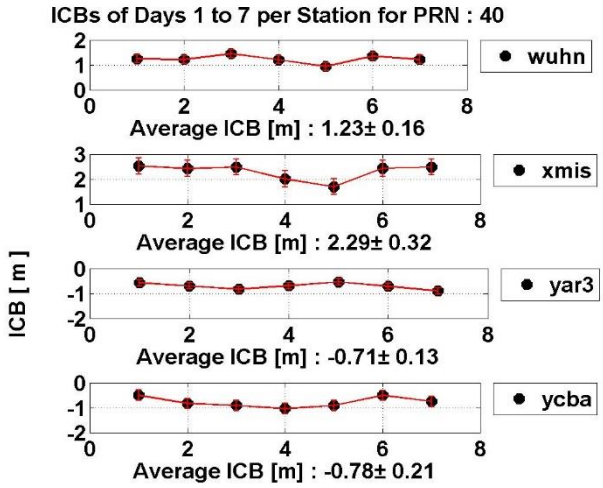
ICBs of Days 1 to 7 per Station for PRN : 40
ICB [m]
wuhn
Average ICB [m] : 1.23± 0.16
xmis
Average ICB [m] : 2.29± 0.32
yar3
Average ICB [m] : -0.71± 0.13
ycba
Average ICB [m] : -0.78± 0.21

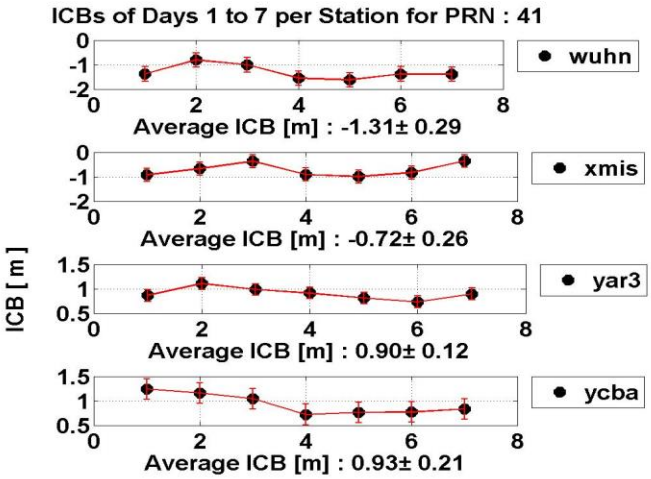
ICBs of Days 1 to 7 per Station for PRN : 41
ICB [m]
wuhn
Average ICB [m] : -1.31± 0.29
xmis
Average ICB [m] : -0.72± 0.26
yar3
Average ICB [m] : 0.90± 0.12
ycba
Average ICB [m] : 0.93± 0.21

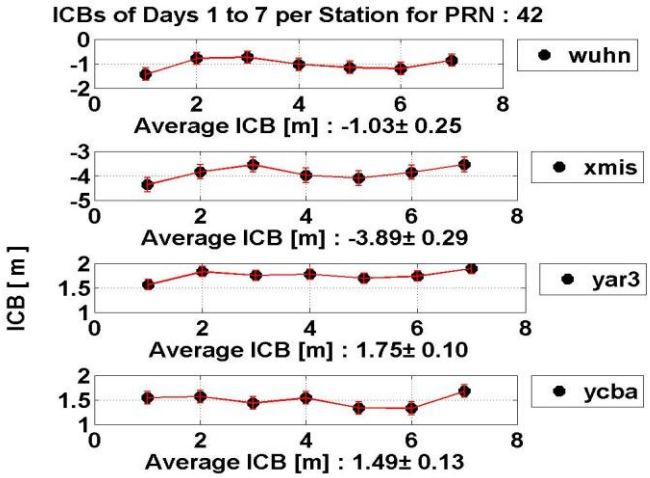
ICBs of Days 1 to 7 per Station for PRN : 42
ICB [m]
wuhn
Average ICB [m] : -1.03± 0.25
xmis
Average ICB [m] : -3.89± 0.29
yar3
Average ICB [m] : 1.75± 0.10
ycba
Average ICB [m] : 1.49± 0.13

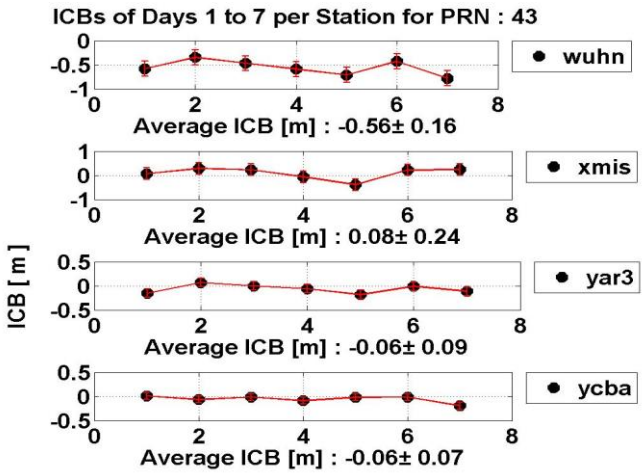
ICBs of Days 1 to 7 per Station for PRN : 43
ICB [m]
wuhn
Average ICB [m] : -0.56± 0.16
xmis
Average ICB [m] : 0.08± 0.24
yar3
Average ICB [m] : -0.06± 0.09
ycba
Average ICB [m] : -0.06± 0.07

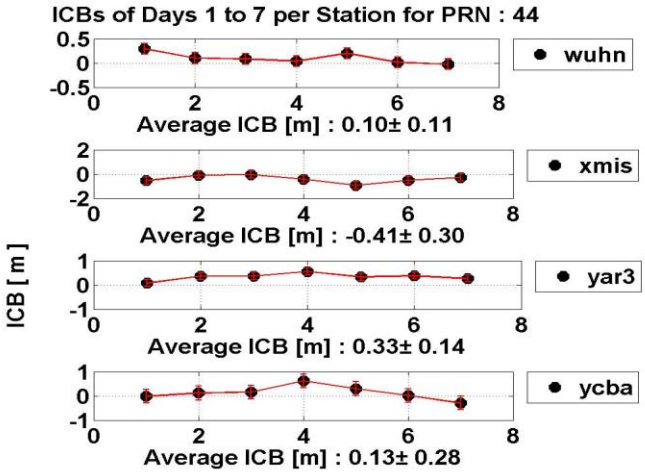
ICBs of Days 1 to 7 per Station for PRN : 44
ICB [m]
wuhn
Average ICB [m] : 0.10± 0.11
xmis
Average ICB [m] : -0.41± 0.30
yar3
Average ICB [m] : 0.33± 0.14
ycba
Average ICB [m] : 0.13± 0.28

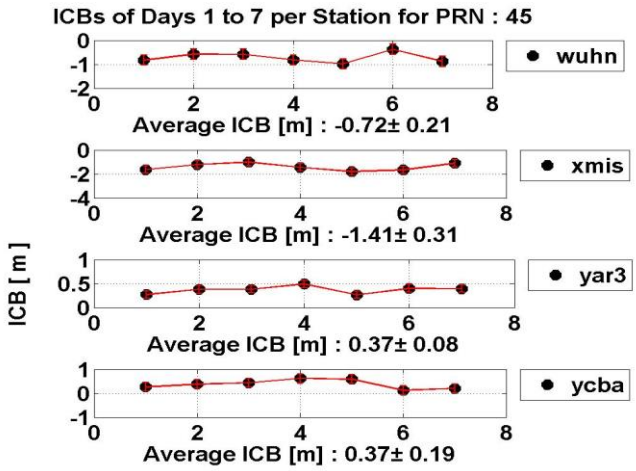
ICBs of Days 1 to 7 per Station for PRN : 45
ICB [m]
wuhn
Average ICB [m] : -0.72± 0.21
xmis
Average ICB [m] : -1.41± 0.31
yar3
Average ICB [m] : 0.37± 0.08
ycba
Average ICB [m] : 0.37± 0.19

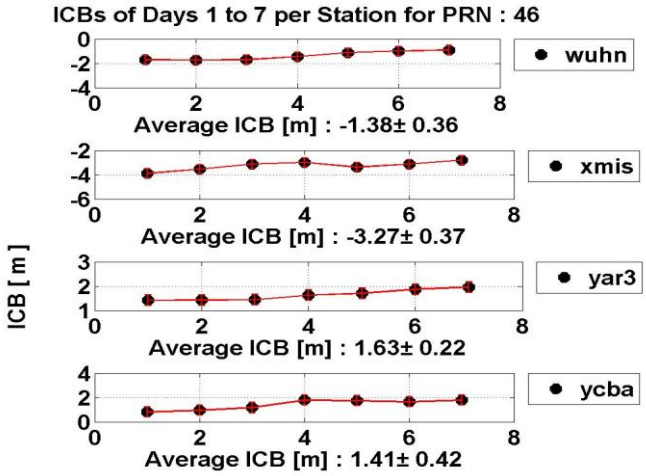
ICBs of Days 1 to 7 per Station for PRN : 46
ICB [m]
wuhn
Average ICB [m] : -1.38± 0.36
xmis
Average ICB [m] : -3.27± 0.37
yar3
Average ICB [m] : 1.63± 0.22
ycba
Average ICB [m] : 1.41± 0.42

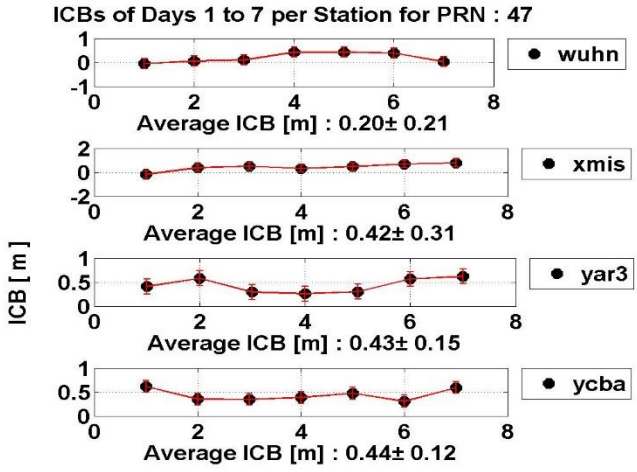
ICBs of Days 1 to 7 per Station for PRN : 47
ICB [m]
wuhn
Average ICB [m] : 0.20± 0.21
xmis
Average ICB [m] : 0.42± 0.31
yar3
Average ICB [m] : 0.43± 0.15
ycba
Average ICB [m] : 0.44± 0.12

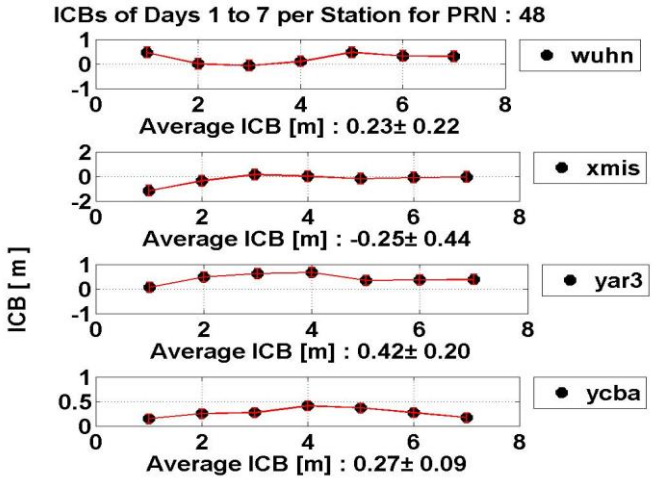
ICBs of Days 1 to 7 per Station for PRN : 48
ICB [m]
wuhn
Average ICB [m] : 0.23± 0.22
xmis
Average ICB [m] : -0.25± 0.44
yar3
Average ICB [m] : 0.42± 0.20
ycba
Average ICB [m] : 0.27± 0.09

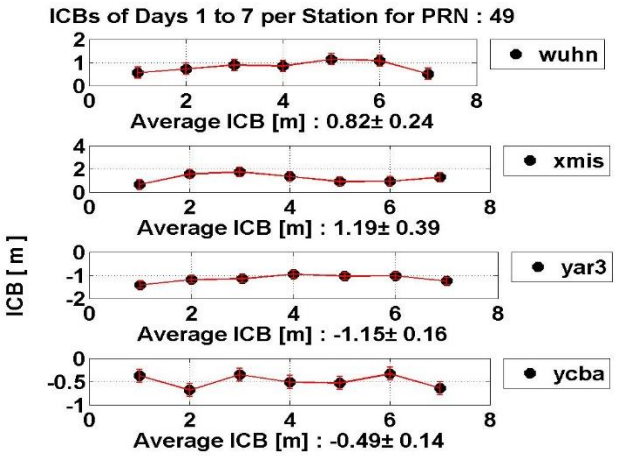
ICBs of Days 1 to 7 per Station for PRN : 49
ICB [m]
wuhn
Average ICB [m] : 0.82± 0.24
xmis
Average ICB [m] : 1.19± 0.39
yar3
Average ICB [m] : -1.15± 0.16
ycba
Average ICB [m] : -0.49± 0.14

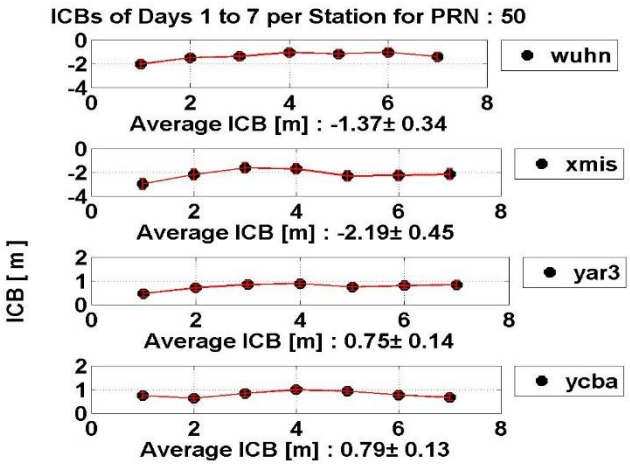
ICBs of Days 1 to 7 per Station for PRN : 50
ICB [m]
wuhn
Average ICB [m] : -1.37± 0.34
xmis
Average ICB [m] : -2.19± 0.45
yar3
Average ICB [m] : 0.75± 0.14
ycba
Average ICB [m] : 0.79± 0.13

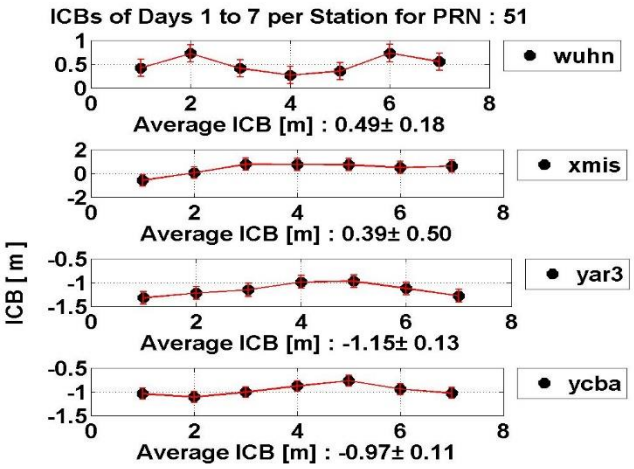
ICBs of Days 1 to 7 per Station for PRN : 51
ICB [m]
wuhn
Average ICB [m] : 0.49± 0.18
xmis
Average ICB [m] : 0.39± 0.50
yar3
Average ICB [m] : -1.15± 0.13
ycba
Average ICB [m] : -0.97± 0.11

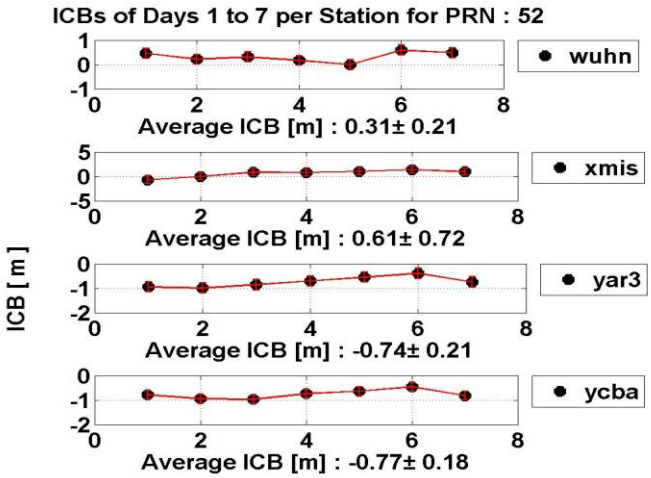
ICBs of Days 1 to 7 per Station for PRN : 52
ICB [m]
wuhn
Average ICB [m] : 0.31± 0.21
xmis
Average ICB [m] : 0.61± 0.72
yar3
Average ICB [m] : -0.74± 0.21
ycba
Average ICB [m] : -0.77± 0.18

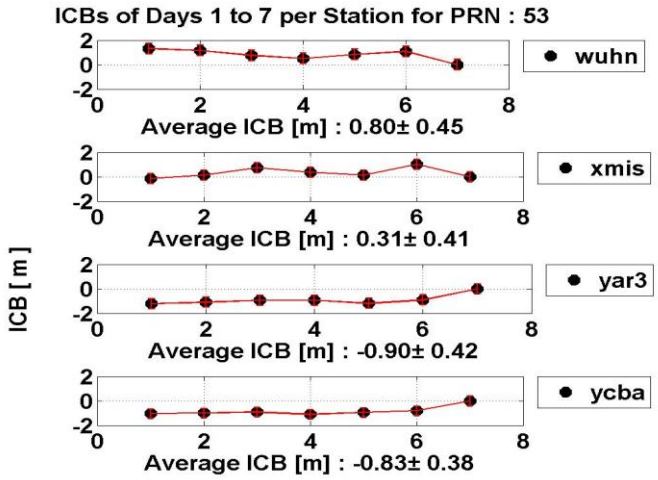
ICBs of Days 1 to 7 per Station for PRN : 53
ICB [m]
wuhn
Average ICB [m] : 0.80± 0.45
xmis
Average ICB [m] : 0.31± 0.41
yar3
Average ICB [m] : -0.90± 0.42
ycba
Average ICB [m] : -0.83± 0.38

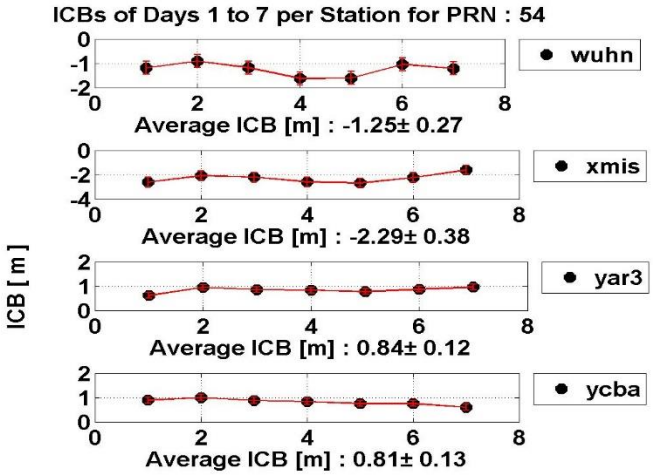
ICBs of Days 1 to 7 per Station for PRN : 54
ICB [m]
wuhn
Average ICB [m] : -1.25± 0.27
xmis
Average ICB [m] : -2.29± 0.38
yar3
Average ICB [m] : 0.84± 0.12
ycba
Average ICB [m] : 0.81± 0.13

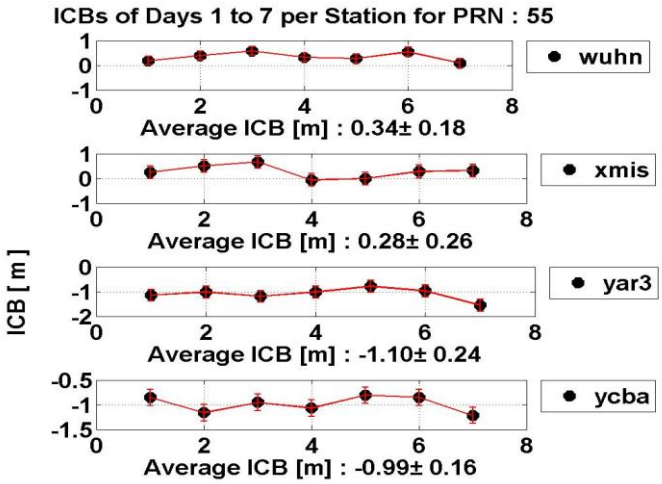
ICBs of Days 1 to 7 per Station for PRN : 55
ICB [m]
wuhn
Average ICB [m] : 0.34± 0.18
xmis
Average ICB [m] : 0.28± 0.26
yar3
Average ICB [m] : -1.10± 0.24
ycba
Average ICB [m] : -0.99± 0.16

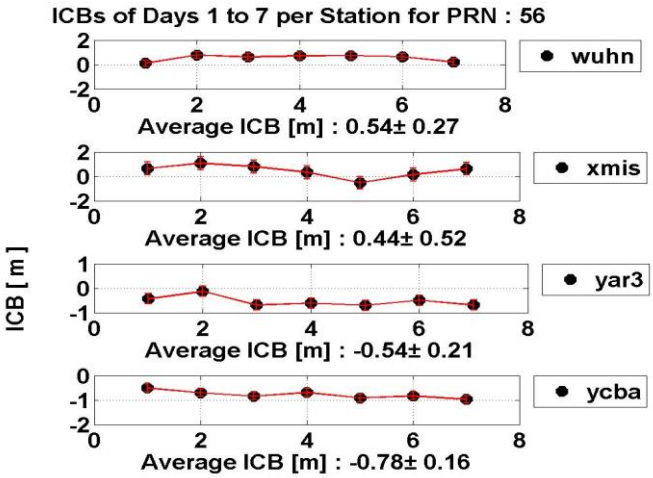
ICBs of Days 1 to 7 per Station for PRN : 56
ICB [m]
wuhn
Average ICB [m] : 0.54± 0.27
xmis
Average ICB [m] : 0.44± 0.52
yar3
Average ICB [m] : -0.54± 0.21
ycba
Average ICB [m] : -0.78± 0.16